Quantum-Classical Correspondence and Entanglement in Periodically Driven Spin Systems

by

Meenu Kumari

A thesis
presented to the University of Waterloo
in fulfillment of the
thesis requirement for the degree of
Doctor of Philosophy
in
Physics (Quantum Information)

Waterloo, Ontario, Canada, 2019

Examining Committee Membership

The following served on the Examining Committee for this thesis. The decision of the Examining Committee is by majority vote.

External Examiner:	Karl-Peter Marzlin Professor, Dept. of Physics, St. Francis Xavier University
Supervisor(s):	Shohini Ghose Professor, Dept. of Physics and Computer Sci., Wilfrid Laurier University Robert B. Mann Professor, Dept. of Physics and Astronomy, University of Waterloo
Internal Member:	Norbert Lütkenhaus Professor, Dept. of Physics and Astronomy, University of Waterloo
Internal-External Member:	Achim Kempf Professor, Dept. of Applied Mathematics, University of Waterloo
Other Member(s):	Eduardo Martín-Martínez Asst. Professor, Dept. of Applied Mathematics, University of Waterloo

This thesis consists of material all of which I authored or co-authored: see Statement of Contributions included in the thesis. This is a true copy of the thesis, including any required final revisions, as accepted by my examiners.

I understand that my thesis may be made electronically available to the public.

Statement of Contributions

This thesis is based on the following publications and forthcoming articles:

- Chapters 2 and 3 are based on
  - M. Kumari and S. Ghose, *Quantum-classical correspondence in the vicinity of periodic orbits*, Phys. Rev. E **97**, 052209 (2018).

- Chapter 4 is based on
  - M. Kumari and S. Ghose, *Untangling entanglement and chaos*, Phys. Rev. A **99**, 042311 (2019).

- Chapter 5 is based on
  - M. Kumari, S. Ghose, and R. B. Mann, *Sufficient condition for nonexistence of symmetric extension of qudits using Bell inequalities*, Phys. Rev. A, **96**, 012128 (2017)
  - M. Kumari, R. B. Mann, and S. Ghose, *Quantum kicked top as a generator of nonlocality, In preparation, 2019.*

Abstract

This dissertation sets out to examine some fundamental open questions in quantum physics regarding quantum-classical correspondence in regular versus chaotic systems. Specifically, we study these questions using approaches in quantum information science in an experimentally realized textbook model of quantum chaos - the quantum kicked top (QKT).

The effect of classical chaos on the generation of entanglement in spin systems has been a field of active research for a couple of decades. Whether high entanglement in these systems is a hallmark of chaos or not remains a widely debated topic. We explain the connection between entanglement and chaos in spin systems and resolve previous conflicting results. The previous studies have mostly drawn conclusions from numerical work on a few initial states in regular versus chaotic regions. We instead focus on stable and unstable periodic orbits because chaos emerges around unstable periodic orbits. We first propose a new set of criteria for determining whether quantum evolution will correspond to the classical trajectory in a localized manner at stable periodic orbits in periodically driven systems. These criteria can be used to calculate the quantum numbers that will lead to quantum-classical correspondence even in a deep quantum regime, and thus to quantify the well-known Bohr correspondence principle. Next, we analytically show a direct connection between entanglement generation and a measure of delocalization of a quantum state in spin systems. More concretely, we describe a method to calculate an upper bound on entanglement generation in any bipartition of spin systems, where the upper bound is a function of trace distance between the evolved state and the most localized classical-like separable states. This method along with our criteria for localized evolution enables us to explain the behaviour of entanglement in both deep quantum and semiclassical regimes for regular as well as chaotic regions. Hence, our analysis resolves the long-standing debates regarding the connection between classical chaos and quantum entanglement in deep quantum and semiclassical regimes.

In addition to the study of entanglement, we perform the first study of nonlocality, and the effect of chaos on its generation in the QKT. Since nonlocality and entanglement are inequivalent quantum resources, the effect of chaos on nonlocality merits an explicit study. Violations of Bell inequalities in the presence of spacelike separation among the subsystems imply nonlocality - meaning nonlocal correlations between subsystems of the total spin system. We show that the QKT evolution can lead to states that violate multiqubit Bell inequalities and hence provides a deterministic method to prepare nonlocal quantum states. Our numerical results suggest a correlation between delocalized evolution of a pure quantum state and generation of nonlocality in the quantum state. We further demonstrate that dynamical tunnelling - a classically forbidden phenomenon - in the QKT

leads to the generation of Greenberger-Horne-Zeilinger (GHZ)-like states for even numbers of qubits. We analytically prove that these states are maximally nonlocal. On the other hand, we numerically show that any reduced state of the QKT obtained by tracing out a subsystem of the total spin system does not violate Bell inequalities. We provide an analytical explanation of the numerical results for $2-$qubit reduced states by formulating and proving two general theorems regarding $2-$qubit Bell inequalities. These theorems imply that any $2-$qubit mixed state having a symmetric extension or symmetric purification cannot violate the Clauser-Horne-Shimony-Holt inequality. This highlights fundamental connections between two important and distinct concepts in quantum information science - Bell inequalities and symmetric extension of quantum states.

Apart from providing deeper insights into the fundamental questions of quantum-classical correspondence and new approaches to analyze quantum chaos, the methods developed in this thesis can be used to design quantum systems that can efficiently generate entanglement and nonlocality. Thus, our results could have interesting applications in quantum computing and quantum information science.

Acknowledgements

The experience of graduate school has not been less than any roller coaster ride, and I have thoroughly enjoyed it for the most part. Apart from an opportunity to pursue my passion for physics, it has allowed me to explore a different culture than my own country, and a great opportunity for introspection due to the solitude that I have experienced as a theoretical physicist. These have immensely helped me in growing as a person and broaden my perspective. This journey would not have been possible without the support of several people to whom I would like to express my gratitude.

First and foremost, I would like to express my deepest gratitude to Shohini Ghose, my PhD advisor, for her never-ending encouragement, persistent guidance, and for sharing my enthusiasm for fundamental physics. Thank you for teaching me the much-needed art of being critical as well as confident about my work simultaneously, along with the quest of finding simple physics in the complicated algebra and numerical results. I am deeply grateful to Robert Mann, my co-advisor, for giving me an opportunity to become a part of his research group in the middle of my PhD. Thank you for introducing me to new areas of physics, for illuminating discussions and for always being very responsive. This thesis would not have been possible without the critical insights and constant support from both of my advisors. I am also thankful to both of my advisors for providing me numerous opportunities for attending conferences and visiting universities worldwide. The interactions with several researchers across the globe have enriched my knowledge and enhanced my confidence. Special thanks to Michele Mosca for supporting my PhD as a co-advisor in the beginning years of my PhD. It has been my pleasure to collaborate with Achim Kempf and Eduardo Martín-Martínez during my PhD. I am indebted to Achim for his guidance and occasional mentorship that has played an instrumental role in my PhD. I would also like to thank Norbert Lütkenhaus for serving on my advisory committee and for the insightful discussion regarding symmetric extensions. Most importantly, I would like to acknowledge IQC for the Mike and Ophelia Lazaridis fellowship that funded the last two years of my PhD.

I would like to thank the rest of my collaborators of a few ongoing projects - Fabio, Sayonee, Namit, and Kunal - for introducing me to new topics and for some insightful discussions. Several other people have been there to discuss and clear my doubts at some point or the other during my PhD - Shima, Suryanarayan, Ravi, Jack, Hemant, Efim, and Shitikanth - thank you, everyone. I would also like to acknowledge John Watrous for his course on the theory of quantum computation. It instilled my interest in theoretical quantum information science to a good extent.

It has been a great pleasure to be a part of the diverse community of the University of Waterloo and IQC. The dissertation boot camp and the grad writing cafe organized by the Writing and Communication Center at UWaterloo has helped me to finish the daunting task of thesis writing without building up a lot of stress. The mindfulness meditation programs and their facilitators at the university were of great help during some stressful times. I am also grateful to Judy McDonnell, Physics graduate program co-ordinator, for taking care of all the administrative things in the PhD program in a timely manner. Moreover, I would like to acknowledge the support from Graduate Studies Office at UWaterloo for partially funding a few of the conferences I attended, as well as JQI and Victor Galitski for partially funding my visit to the many-body quantum chaos conference in Aspen.

My life in Waterloo has been a pleasant one, partly owing to all the friendly and caring people I have interacted with over the course of last five years. I cherish the memories of all the weekends' get-togethers with Nikky, Deepak, Shitikanth and Jalaj in the initial years of my PhD. In the later part, the get-togethers with Archana, Hemant and Dennis have been a source of joy and relaxation at times. The occasional conversations with Sainath, Zeeshan, Vadiraj, Nayeli, Nigar, Laura, Jitendra, Satish, Nikhil, Vinay and Dhinakaran have been delightful. Special thanks to Gannaya uncle, Anil uncle and Anju aunty for always having their doors open for me and making me feel at home whenever I missed my family. I would also like to thank some old friends - Shilpi, Jaya and Anshu - for always being there especially when I needed any emotional support. Last but not the least, I would like to thank Ravi for his valuable suggestions in various spheres of life and his belief in me, my mother for her unconditional love and support even in my unconventional life choices, my sisters for ensuring a better life for me, and my brother for caring like a parent for the most part of my life. Thank you, everyone!

Dedication

To all the physicists whose efforts have contributed to the development of theories that helped mankind to fathom this universe beyond the direct reach of our senses.

Table of Contents

List of Tables

List of Figures

Chapter 1

Introduction

Classical chaos and quantum physics mark two important discoveries in physics in the twentieth century, among major discoveries like special and general relativity. Understanding the intersection of two different theories can sometimes be natural as in the case of special relativity and general relativity. On the other hand, it can be extremely challenging as in the case of quantum theory and general relativity. The intersection of quantum physics and classical physics lie somewhere between these two extremes. Although a lot has been done and understood about this quantum-classical correspondence for classically regular systems, it remains poorly understood for chaotic systems.

In this thesis, we explore the quantum-classical correspondence using approaches inspired by quantum information science. We explore information-theoretic measures such as entanglement and nonlocality in periodically driven spin systems. Specifically, we illustrate our studies in the quantum kicked top - a textbook model of quantum chaos.

1.1 Classical and Quantum Physics

Hamilton's equations of motion are the standard method for studying the classical dynamics of any system. The classical dynamics of a system with n degrees of freedom is described using trajectories in a $2n$-dimensional phase space - a multidimensional space whose axes are generalized coordinates and their corresponding conjugate momenta. Hamiltonian systems can be broadly classified into integrable and non-integrable systems [1]. Systems that have n independent constants of motion are called integrable systems while those with less than n independent constants of motion are non-integrable. The dynamics of integrable

systems is restricted to an $n-$dimensional surface in the $2n-$dimensional phase space. In contrast, non-integrable systems explore more areas of the phase space due to the lack of enough symmetries [1]. Let us consider as an example the harmonic oscillator. Its Hamiltonian is given by $H = \frac{p^2}{2m} + \frac{1}{2}m\omega^2 x^2$. It is a system with one degree of freedom. The phase space of a harmonic oscillator is the $2-$dimensional space whose axes are x and p. The energy of the harmonic oscillator is a constant of motion. Hence, it is an integrable system as the number of independent constants of motion equals the number of degrees of freedom.

One of the most surprising properties often exhibited by non-integrable systems is unpredictability in the evolution due to exponential sensitivity to initial conditions. This property is known as chaos, popularly known as the 'butterfly effect'. The seeds for the discovery of chaos were sown by Henri Poincare in the late nineteenth century when he proved that the $3-$body problem with mutual gravitational attraction can exhibit unstable aperiodic motion [2]. Later in 1945, Mary Cartwright and John Littlewood discovered chaotic behaviour in the solutions of a nonlinear differential equation [3]. However, it was only after the advent of computers and the work of a meteorologist, Edward Lorenz, in 1963 that chaotic phenomena began to be recognized and studied widely. Lorenz was modelling convection in the atmosphere on a computer when he realized that very small differences in the initial conditions led to significant differences in the evolution of the system that can render the evolution unpredictable [4]. It is indeed surprising that even very simple systems like double pendulums and driven simple pendulums can display unpredictable behavior [5, 1].

Chaos is a property of nonlinear systems and it is characterized by positive Lyapunov exponents. To understand the definition of Lyapunov exponents, let us consider the evolution of two initial vectors in the $2n-$dimensional phase space, $\mathbf{X_0}$ and $\mathbf{Y_0} = \mathbf{X_0} + \mathbf{\Delta X_0}$ [1]. $\mathbf{X_0}$ and $\mathbf{Y_0}$ evolve to $\mathbf{X_t}$ and $\mathbf{Y_t}$ respectively in time t. The evolution of the displacement, $\mathbf{\Delta X_t}$ leads to the definition of Lyapunov exponents. Let

$$d_t(\mathbf{X_0}, \mathbf{Y_0}) = |\mathbf{\Delta X_t}| = \sqrt{\mathbf{\Delta X_t} \cdot \mathbf{\Delta X_t}}. \tag{1.1}$$

The classical Lyapunov exponent is given by

$$\lambda(\mathbf{X_0}) = \lim_{t\to\infty} \lim_{d_0\to 0} \frac{1}{t} \ln\left(\frac{d_t(\mathbf{X_0}, \mathbf{Y_0})}{d_0(\mathbf{X_0}, \mathbf{Y_0})}\right). \tag{1.2}$$

A strictly positive $\lambda(\mathbf{X_0})$ signifies that the difference between the evolution of $\mathbf{X_0}$ and any neighboring point grows exponentially. A system is called globally chaotic if λ is positive for all initial states in the phase space.

Another characterization of classical chaos is via the Kolmogorov-Sinai entropy (KS entropy) [1]. It is known to be equivalent to the sum of positive Lyapunov exponents of a system. Thus a strictly positive value of KS entropy signifies chaos in the system [6].

Observations of a few phenomena that could not be explained using classical physics led to the advent of quantum physics in the beginning of the twentieth century [7]. Unlike the evolution of phase space variables in classical physics, the quantum theory of any system describes wave functions evolving according to the linear Schrodinger equation [8]. The variables of classical physics are replaced by observables in quantum physics that are Hermitian operators in the relevant Hilbert space. One of the striking distinctions between classical and quantum physics is Heisenberg's uncertainty principle. According to this principle, the values of conjugate variables of any particle, say position and momentum, cannot be simultaneously determined to arbitrary precision. This prohibits any description of quantum physics in terms of trajectories in the phase space without invoking strong or weak measurements [9, 10, 11]. Moreover, the linearity of the Schrodinger equation prohibits any exponential divergence in the evolution of the wave functions, quite unlike the possibility of exponential divergence of trajectories in the classical physics. Unitarity further constrains the distance between any two initial wave functions to remain constant throughout the evolution ($\langle\psi_0|U_t^\dagger U_t|\psi_1\rangle = \langle\psi_0|\psi_1\rangle$ for all t).

There are striking differences in the formulation and description of classical and quantum physics. Thus devising a correspondence principle that can explain all possible classical behaviors in appropriate limits is very difficult. Though a few candidate approaches have been proposed, all of them are known to break down, particularly for chaotic systems. We review the quantum-classical correspondence in the next section briefly.

1.2 Quantum-Classical Correspondence

Quantum theory successfully explained many phenomena that were incomprehensible using classical physics, such as the stability of atoms, the photoelectric effect and black-body radiation to name a few. Nevertheless, a complete theory should merge with the old theory in appropriate limits wherever the old theory is applicable. This requires the predictions of quantum physics to merge with the predictions of classical physics in the classical limit – including chaotic phenomena.

However, limited success has been achieved in this regard. The correspondence principles formulated so far are known to break down for chaotic systems. For example, the Ehrenfest correspondence principle proposes a correspondence in the quantum evolution of

observables and classical trajectories up to Ehrenfest time scales (t_{Eh}) wherever classical physics holds true [12]. The t_{Eh} was initially assumed to be extremely large in the limit of large quantum numbers. However, it was later on shown to be very small for chaotic systems even in the macroscopic limit of large quantum numbers. $t_{\text{Eh}}^{\text{chaotic}} \approx \frac{1}{\lambda} \ln \frac{A_0}{\hbar}$ where A_0 is characteristic action of the system and λ is the classical Lyapunov exponent defined in (1.2) [13]. For instance, consider the case of Hyperion - a moon of Saturn - which is a weakly chaotic system [14]. t_{Eh} for Hyperion, calculated using $\frac{1}{\lambda} \ln \frac{A_0}{\hbar}$, was shown to be of the order of 20 years which is much smaller than the age of solar systems [13]. This breakdown of correspondence principles for chaotic systems calls for a more rigorous study of quantum-classical correspondence.

Another line of research has focused on finding signatures of classical dynamics, particularly chaos, in the study of quantum physics. Researchers have focused on identifying properties in the quantum realm that can distinguish the underlying regular versus chaotic classical dynamics of the system. Examples include level statistics [15], fidelity decay [16, 17], hypersensitivity to perturbations [18], scarring of eigenfunctions [19], and out-of-time-order correlators (OTOCs) [20]. However, these examples suffer from limitations too, as we shall now discuss.

1.2.1 Signatures of quantum-classical correspondence

Level statistics

The statistics of energy levels of a quantum system has been known to be a predominant signature of chaos in the underlying classical system for decades [15]. Let $P(s)$ denote the nearest neighbor energy level spacing distribution. $P(s)$ is known to exhibit level clustering for regular systems. Thus these systems display Poissonian level statistics, $P(s) \sim \exp(-s)$. On the other hand, $P(s)$ is known to exhibit level repulsion as well as resistance to level crossings for chaotic systems. Thus these systems display Wigner-Dyson level statistics, $P(s) \sim s^{\beta}$ (for $s \to 0$) where β can take values $1, 2$ and 4 depending on the symmetries of the system [15].

Nevertheless, there exist exceptions to this relationship between classical dynamics and quantum level statistics. For example, the kicked rotor is known to exhibit global chaos for strong enough kicking strengths. However, it does not display level repulsion owing to its dynamical localization property in the quantum realm [15]. On the other hand, systems like pseudointegrable polygonal billiards display level repulsion to some extent although they do not display classical chaos [21, 22]. Thus, quantum level statistics cannot be considered a universal indicator of regular versus chaotic dynamics at the classical level.

Fidelity decay

In closed quantum systems that do not interact with an environment or a detector, quantum states evolve unitarily according to the Schrodinger equation. Thus, the overlap of two different initial quantum states remains constant under time evolution. So using this measure, quantum states cannot exhibit exponential divergence in their evolution even for chaotic systems. However, a perturbation in the Hamiltonian instead of the quantum state can lead to exponential sensitivity. Peres used this criterion to propose fidelity decay as a signature for quantum-classical correspondence [16]. The quantum fidelity F is defined to be the overlap of two states evolved from the same initial state: the first state evolves with the Hamiltonian, H_0, and the second evolves with a perturbed Hamiltonian, $H_\epsilon = H_0 + \epsilon V$,

$$F(|\psi(t)\rangle, |\psi_\epsilon(t)\rangle) = |\langle\psi(0)|U^\dagger_{\text{sys}}(t)U^\epsilon_{\text{sys}}(t)|\psi(0)\rangle|. \tag{1.3}$$

Here U_{sys} and U^ϵ_{sys} are the time evolution unitary operators corresponding to the unperturbed and the perturbed Hamiltonian respectively. Based on numerical evidence, Peres initially conjectured that the quantum fidelity will remain close to one for classically regular dynamics, and will decay significantly for classically chaotic dynamics [16]. However, further research provided evidence that classically regular systems and systems with mixed phase space can show a variety of behaviours of the fidelity decay, including faster than exponential decay [23, 24]. Also, the fidelity decay was shown to be dependent on the characteristics of the perturbation rather than the unperturbed Hamiltonian [17]. These results make it challenging to use fidelity decay as a universal indicator of the underlying classical dynamics.

Out-of-Time-Order Correlators (OTOCs)

A positive Lyapunov exponent is a well-defined characterization of classical chaos. Quantum chaos lacks such a characterization. Out-of-Time-Order Correlators (OTOCs) were recently proposed as a promising candidate for quantum Lyapunov exponent analogous to the classical Lyapunov exponent [20]. OTOCs have begun to be widely recognized as the quantum Lyapunov exponent in the literature though their validity remains to be rigorously analyzed and proved. We briefly review OTOCs here.

Let us consider the operator $\hat{C}(t)$ given by

$$\hat{C}(t) = -[\hat{x}(t), \hat{p}(0)]^2. \tag{1.4}$$

The operator $\hat{C}(t)$ is related to a four-point correlator function given the arguments in the commutator in (1.4) are unitary operators at distinct times [25]. Thus $\hat{C}(t)$ is known as

OTOC. Expanding the commutator (1.4) using a test function f gives

$$\begin{aligned}[\hat{x}(t),\hat{p}(0)]f &= -\mathrm{i}\hbar\left(\hat{x}(t)\frac{\partial f}{\partial\hat{x}(0)}-\frac{\partial\hat{x}(t)f}{\partial\hat{x}(0)}\right)\\ &= \mathrm{i}\hbar f\frac{\partial\hat{x}(t)}{\partial\hat{x}(0)}.\end{aligned}$$

This simple calculation of the commutator $[\hat{x}(t),\hat{p}(0)]$ leads to the following result:

$$[\hat{x}(t),\hat{p}(0)] = \mathrm{i}\hbar\frac{\partial\hat{x}(t)}{\partial\hat{x}(0)}. \tag{1.5}$$

Equation (1.5) simplifies (1.4) as follows:

$$\hat{C}(t) = \hbar^2\left(\frac{\partial\hat{x}(t)}{\partial\hat{x}(0)}\right)^2. \tag{1.6}$$

Taking the expectation value of $\hat{C}(t)$ with respect to any quantum state $|\psi\rangle$ yields

$$C(t) = \hbar^2\left\langle\left(\frac{\partial\hat{x}(t)}{\partial\hat{x}(0)}\right)^2\right\rangle. \tag{1.7}$$

Classically, $\left(\frac{\partial\hat{x}(t)}{\partial\hat{x}(0)}\right)\approx\left(\frac{\Delta x(t)}{\Delta x(0)}\right)$. Exploiting the definition of classical Lyapunov exponent λ in (1.2), we get

$$\left(\frac{\Delta x(t)}{\Delta x(0)}\right)^2 \equiv \exp\left(2\lambda t\right) \tag{1.8}$$

in appropriate limits. Drawing analogy from the above equations, the out-of-time-ordered correlator $C(t)$ is conjectured to exhibit exponential growth up to Ehrenfest time scales for classically chaotic systems. The rate of exponential growth captured by the quantum Lyapunov exponent, $\tilde{\lambda}_q$, can be extracted from the following:

$$C(t)\propto\exp\left(2\tilde{\lambda}_q t\right). \tag{1.9}$$

Though $\tilde{\lambda}_q$ seems to be a convincing quantum analog to the classical Lyapunov exponent, it has been shown to be unequal in magnitude to the classical Lyapunov exponent for the case of the classically chaotic kicked rotor [26]. Further, it has also been shown to have positive value for the case of classically non-chaotic billiards [27]. Thus, it remains unclear whether OTOCs can be the quantum analog of classical Lyapunov exponents as claimed in the literature.

We can safely conclude that the quest to find a well-defined characterization or signature of quantum chaos continues to be an open problem. There have been several attempts to identify signatures of quantum chaos in the dynamics of quantum entanglement. We review this aspect in the next section.

1.3 Quantum Information-Theoretic Measures

Quantum properties such as quantum superposition, quantum entanglement, quantum steering and nonlocal correlations have revolutionized our understanding of physical phenomena, especially at the microscopic level. Can these quantum properties be used to gain any insight into the question of quantum-classical correspondence? Specifically, can the study of evolution of these properties for a given Hamiltonian give any insight into the underlying classical dynamics of the corresponding Hamiltonian? These questions have gained a lot of attention in the context of quantum entanglement [28, 29, 30].

Additionally, harnessing these quantum properties could have applications in numerous technologies, such as quantum teleportation, quantum cryptography and quantum communication [31, 32]. Thus preparation of quantum states with useful quantum properties is an important task. Can such quantum states be efficiently prepared using quantum chaotic Hamiltonians?

In the light of these questions, the purpose of this thesis is to study quantum entanglement and nonlocality in the model quantum kicked top (QKT). In the following subsections, we review quantum entanglement, its relationship with classical dynamics, and nonlocality.

1.3.1 Quantum entanglement

"The whole is greater than the sum of its parts."
- Aristotle

Suppose we are given a system of two particles, A and B. According to classical physics, we can gain full knowledge about the joint state of AB by knowing the state of individual particles A and B. Quantum mechanically, this is no longer true in general. Quantum entanglement is a purely quantum property that prohibits us from knowing everything

about the joint state of two particles just from the complete knowledge of individual particles. Mathematically, a quantum state ρ^{AB} shared between parties A and B is said to be entangled if it cannot be written in the following form:

$$\rho^{AB} = \sum_{i=1}^{n} p_i \rho^A \otimes \rho^B \tag{1.10}$$

where p_i's are non-negative real numbers and obey $\sum_{i=1}^{n} p_i = 1$, $\rho^A \in \mathcal{H}^A$ (the Hilbert space corresponding to subsystem A) and $\rho^B \in \mathcal{H}^B$ [33].

When ρ^{AB} is a pure state ($\rho^{AB} \equiv |\psi^{AB}\rangle\langle\psi^{AB}|$), the Schmidt decomposition can be used to determine whether a state is entangled or not [33]. Let $|\psi^{AB}\rangle \in \mathcal{H}^{AB}$ be a pure state. Let $\dim(\mathcal{H}^A) = d_A$ and $\dim(\mathcal{H}^B) = d_B$, so $\dim(\mathcal{H}^{AB}) = d_A d_B$. Then there exists an orthonormal basis $\{|i_A\rangle\} \in \mathcal{H}^A$ and $\{|i_B\rangle\} \in \mathcal{H}^B$, such that

$$|\psi^{AB}\rangle = \sum_{i=1}^{d} \lambda_i |i_A\rangle |i_B\rangle \tag{1.11}$$

where $d = \min(d_A, d_B)$, and λ_i's are non-negative real numbers called Schmidt co-efficients which satisfy $\sum_i \lambda_i^2 = 1$. The number of strictly positive λ_i's in (1.11) for any $|\psi^{AB}\rangle$ is called its Schmidt rank. A pure state $|\psi^{AB}\rangle$ is entangled iff its Schmidt rank is strictly greater than 1.

The resource theories of entanglement need entanglement measures in order to quantify entanglement in any given quantum state. A few well-known entanglement measures are entanglement cost, entanglement of formation and distillable entanglement [31]. In this thesis, we study entanglement in bipartite pure states. A natural measure of entanglement in bipartite pure states is the von Neumann entropy of its reduced states,

$$\text{Entanglement}(|\psi^{AB}\rangle) = S(\rho^A) \equiv S(\rho^B) \tag{1.12}$$

where $S(\rho) = -\operatorname{Tr}(\rho \log_2 \rho) = \sum_l \lambda_l$, λ_l's are the eigenvalues of ρ. ρ^A and ρ^B in (1.12) are obtained by tracing out subsystem B and A respectively from the quantum state $|\psi^{AB}\rangle$. The distillable entanglement and entanglement cost for any $|\psi^{AB}\rangle$ is equal to the von Neumann entropy of its reduced states [34, 31].

We explore the generation of entanglement in quantum states which are evolving according to a given Hamiltonian. We also explore the relationship of entanglement generation to the underlying classical dynamics of the Hamiltonian.

Entanglement as a signature of chaos

The relationship between dynamical entanglement and the underlying classical dynamics of the system was first investigated in [35] a couple of decades ago. This study was motivated by the work of Zurek and Paz about restoring quantum-classical correspondence in chaotic systems using decoherence [36]. In a series of numerical investigations of the N-atom Jaynes-Cummings model coupled to a radiation field [35, 37, 38], the authors concluded two things. First, the rate of entanglement generation (related to the decoherence rate) is much faster for initial quantum states centered in the chaotic region as opposed to initial quantum states centered in the regular region of the classical phase space (with exceptions [37]). Second, the entanglement evolution depicts notable partial recoherences for initial quantum states centered in the regular region. These studies initiated a host of investigations into the relationship between entanglement and chaos in other models, such as, coupled kicked tops [39, 40, 41, 42, 43], coupled standard map [44], coupled Duffing oscillators [45], kicked Harper model [46], Dicke model [47], coupled quartic oscillators [48], and coupled kicked rotors [49]. All these studies in various models led to the generic understanding that the presence of chaos in the classical system leads to enhanced entanglement in the quantum counterpart. In the semiclassical regime and for initial quantum states centered in the chaotic sea, the rate of entanglement generation is high and often increases exponentially fast. The entanglement levels saturate to a value close to the maximum possible value, and exhibit small fluctuations as the system continues to evolve. In [28], the exponential growth of entanglement was analytically shown to be limited by the classical Lyapunov exponent of the underlying classical subsystems in the short time regime in a weakly coupled two-particle system. The saturation level of entanglement generation has been analytically derived using random matrix theory (RMT) for coupled systems [40, 50, 43, 51, 52]. This holds because RMT is well-known to describe the statistical properties of chaotic Hamiltonians given that the random matrix ensemble and the Hamiltonian share the same symmetry class [15].

A few noteworthy points are:

(a) Most of the aforementioned studies investigated the relationship of entanglement to the underlying classical dynamics in coupled systems where the individual systems were taken to be chaotic or regular. The strength of the coupling parameter adds another degree of freedom to the problem under investigation. Finding a general connection between entanglement and chaos becomes more difficult in the presence of added degrees of freedom.

(b) A few of the systems investigated are infinite-dimensional and their numerical studies

lead to truncation errors. These errors may build up in chaotic systems since chaos is sensitive to very small deviations.

(c) Though there is a broad understanding of entanglement behaviour in chaotic systems, there is still a lack of understanding of entanglement dynamics in regular systems. It has been noted that regular systems can exhibit maximal entanglement for specific initial states in some systems. Additionally, the initial rate of entanglement generation in regular systems can be as high as in chaotic systems for specific initial states [37, 53]. So neither the rate nor the magnitude of entanglement generation can be considered as a hallmark or signature of chaos in quantum systems. This leads us to the question of whether there is any universal difference between entanglement generation in regular versus chaotic systems.

The relationship between entanglement and classical dynamics has been studied in a textbook model of quantum chaos, the quantum kicked top (QKT). This model does not suffer from issues (a) and (b) above. It is a finite-dimensional model whose classical limit exhibits different kinds of classical dynamics including chaos (see Sec. 2.2 for details). We can study entanglement in the internal degrees of freedom of the QKT, thus eliminating the need of coupling to another particle to study entanglement (Sec. 2.3). Dynamical entanglement in the QKT and its relationship to regular and chaotic dynamics has been investigated both numerically and analytically in theoretical studies [54, 55, 53, 56, 57, 58, 59] as well as experimentally [29, 30, 60]. In [54, 55], the authors concluded that there is a rapid growth of bipartite entanglement in the chaotic region compared to the regular region in the semiclassical regime on the basis of numerical studies. On the other hand, they did not observe a significant difference in the growth rate of entanglement in the deep quantum regime in regular versus chaotic regions, and they attributed it to the small size of the Hilbert space in the deep quantum regime. They also observed collapses and revivals in the entanglement evolution for regular regions but not for chaotic regions. The numerical observations in the deep quantum regime were verified experimentally for the first time in [29] in a QKT with $j = 3$ ($\equiv$ 6-qubit QKT). It was also shown that the time-averaged entanglement (for a finite number of time periods) in regular regions is smaller than in chaotic regions even in the deep quantum regime.

This surprising result in the deep quantum regime led to a series of further investigations to study whether high entanglement was a hallmark of chaos in the QKT even in the deep quantum regime [53, 61, 62, 56, 57, 58, 59]. In [53], Lombardi *et. al* concluded that "the entanglement of the quantum top depends on the specific details of the dynamics of the classical top rather than depending universally on the global properties of the classical regime". In a comment on this paper, Madhok [61] claimed that there

exists is a correlation between dynamically generated time-averaged entanglement with the classical phase space structures though in a coarse grained manner. This claim was based on some numerical analysis and arguments using the RMT. In a subsequent reply [62], Lombardi *et. al* mentioned that though the arguments presented in [61] seem logical, it remains to be shown that they hold generically. On the basis of additional numerics, the authors remained firm on their initial conclusions in [53]. These works were followed by another experimental study of entanglement in a QKT with $j = 3/2$ ($\equiv$ 3-qubit QKT) [30]. From the experimental results, the authors claimed that the initial states in regular regions lead to low time-averaged entanglement, and the initial states in chaotic regions lead to high time-averaged entanglement even in a very deep quantum regime [30]. Adding to the existing debates, Ruebeck *et. al* studied infinite time-averaged entanglement (which they refer as S_Q) in [56] for a QKT with $j = 1$ ($\equiv$ 2-qubit QKT). This paper concluded that classical regular dynamics corresponds to either high or low value of S_Q, and classical chaotic dynamics corresponds to intermediate values of S_Q. This literature survey makes it clear that the relationship between entanglement generation and classical dynamics of the underlying system is very unclear even in a specific model, the QKT. We resolve these existing debates in Chapter 4 of this thesis.

1.3.2 Nonlocality

The study of the relationship between chaos and entanglement naturally leads us to the question of the relationship between chaos and other quantum properties such as nonlocal correlations. Surprisingly, the relationship between the classical dynamics and nonlocal correlations has not been investigated in the literature so far except in [63].

In order to understand nonlocality, let us suppose Alice and Bob share a $2-$qubit quantum state $|\psi^{AB}\rangle = \frac{1}{\sqrt{2}}\big(|00\rangle + |11\rangle\big)$. They perform a measurement on their respective qubits. The measurement results are found to be correlated even with a spacelike separation between them. The correlations shared between Alice and Bob in such a scenario cannot be explained using any local hidden variable model [32]. Thus, quantum states with such correlations either violate the assumptions of locality or realism. In this thesis, we refer to violations of Bell inequalities as nonlocality for convenience, (although this label includes violations of either assumption of locality or realism [64, 65, 66]). When Einstein and his colleagues, Podolsky and Rosen, first described these correlations in a thought experiment in 1935, they termed it as 'spooky action at a distance' [66]. It was later realized that though these correlations are spooky in nature but there is no 'action at a distance'. In 1964, John Bell proposed a simple test using an inequality to test the existence of nonlocal correlations [67]. The quantum states that violate this inequality

in the presence of spacelike separation between the particles exhibit nonlocal correlations. The existence of nonlocal correlations has been proved experimentally [68] though it is still difficult to fathom the concept of nonlocality since it is highly counterintuitive. Nonlocality is a useful resource in applications such as quantum key distribution and quantum communication protocols [32]. Further, experimental measurement of nonlocality requires only local measurements on the quantum state as opposed to full state tomography for measuring entanglement. Thus, theoretical results on nonlocality are more easily experimentally verifiable once the optimal measurement operators are known. We explore the existence of nonlocal correlations in the quantum kicked top in chapter 5 of this thesis.

1.4 Overview

This thesis first investigates the much studied relationship between chaos and entanglement using quantum-classical correspondence, and then undertakes a new study investigating the relationship between chaos and nonlocality. We illustrate our studies in a periodically driven spin system, the quantum kicked top (QKT), which is a textbook model of quantum chaos.

In chapter 2, we briefly describe the model QKT. We derive its classical equations of motion and then study a few fixed points and periodic orbits using these equations of motion. We analyze their stability and bifurcations. We review the derivation of the unitary operator for one time period of the QKT. We further review how a system whose Hamiltonian commutes with the squared angular momentum operator can be considered as a symmetric multi-qubit system. Thus, the QKT has a multi-qubit representation, which paves the path to the study of quantum correlations among its qubits. Additionally, we review spin coherent states which are the most classical-like quantum states, and the Husimi quasi-probability distribution function used for the study of quantum dynamics in phase space.

Chapter 3 deals with the study of quantum-classical correspondence in periodically driven systems. We propose a set of criteria for localized evolution of initial spin coherent states centered at stable periodic orbits in such systems. Further, we use these criteria to identify quantum signatures of classical bifurcations even in a deep quantum regime. We illustrate these results at the fixed points and periodic orbits in the QKT described in chapter 2.

Chapter 4 presents a systematic analysis of the debates in the literature concerning the relationship between entanglement and chaos. We begin by presenting a framework to

obtain a tight upper bound on entanglement generation in spin systems. This framework explains the mechanism of entanglement generation in these systems. We demonstrate that the upper bound gives a good estimate of entanglement in the QKT for regular as well as chaotic initial states. Using this framework and the criteria for quantum-classical correspondence at stable periodic orbits proposed in chapter 3, we resolve the previous conflicting results in the literature.

In chapter 5, we undertake a study of nonlocality in the QKT. We first review the generalizations of Bell inequality, Clauser-Horne-Shimony-Holt (CHSH) inequality and Svetlichny's inequality for $2-$qubit and $N-$qubit states respectively. Their violations imply the presence of nonlocal correlations in the respective quantum states. While the $2-$qubit and $3-$qubit subsystems of the QKT do not violate Bell-type inequalities, the pure state evolving according to the QKT Hamiltonian often does violate Bell-type inequalities. We analytically prove that the $2-$qubit subsystems of the QKT cannot violate Bell-type inequalities. We further show that dynamical tunnelling in the QKT leads to generation of GHZ-like states for even number of qubits. These GHZ-like states exhibit maximal violation of Svetlichny's inequality analogous to the GHZ states. Our numerical studies provide preliminary evidence suggesting that a delocalized evolution in the phase space leads to generation of multipartite nonlocality in the multi-qubit pure state. Since classical chaos leads to a delocalized quantum evolution within a very short time, chaos may lead to generation of multipartite nonlocality in the multi-qubit pure states in general.

In chapter 6, we summarize the results in this thesis and provide an outlook for future work.

Chapter 2

The Model: Quantum Kicked Top

This chapter is partially based on Kumari and Ghose [69].

The quantum kicked top (QKT) model was first introduced by Haake, Kus and Scharf in 1987 [70]. It is a paradigmatic model for the study of quantum chaos. It is a finite-dimensional model. Thus, there are no truncation errors in the quantum mechanical study of this system. The QKT has been widely studied in the context of quantum chaos and quantum information [71, 72, 18, 39, 73, 54, 41, 74, 55, 43, 53, 75, 76, 77, 57, 58, 59]. It was first experimentally realized in a system of Caesium atoms [29] and then subsequently in other systems such as superconducting circuits [30], NMR [60] and Bose-Einstein condensate [78].

The QKT is a time-dependent periodic system governed by the Hamiltonian [70]

$$H = \hbar\frac{\kappa}{2j}J_z^2\sum_{n=-\infty}^{\infty}\delta(t-n\tau) + \hbar\frac{p}{\tau}J_y \tag{2.1}$$

where J_x, J_y and J_z are total angular momentum operators satisfying $[J_i, J_j] = \mathrm{i}\hbar\epsilon_{ijk}J_k$, κ and p are parameters.

A brief outline of the chapter is as follows. In Sec. 2.1, we first calculate the unitary operator for one time period for the QKT in order to study its quantum dynamics. In Sec. 2.2.1, we find the classical equations of motion for the kicked top using Hamilton's equations of motion. In Sec. 2.2.2, we study a select few periodic orbits of the classical kicked top and their bifurcations. In Sec. 2.3, we illustrate how the QKT can be considered as a multi-qubit system. In Sec. 2.4, we review the spin coherent states which are taken as initial quantum states to study the quantum dynamics of the QKT. In Sec. 2.5, we review

the Husimi quasi-probability distribution function and its use in visualizing the quantum dynamics of the QKT in phase space.

2.1 Quantum Dynamics

The square of the angular momentum operator commutes with the Hamiltonian of the QKT ($[H, J^2] = 0$). Thus, the eigenvalues of J^2, $j(j+1)\hbar^2$ (and hence j) are constants of motion of the QKT. The Hilbert space spanned by the QKT is $(2j+1)$-dimensional.

2.1.1 Floquet operator

Periodically driven systems are in general referred to as Floquet systems. We study the stroboscopic time evolution of the QKT, that is, evolution from one kick to another kick. Kicks are provided by the $\delta(t - n\tau)$ term in the Hamiltonian (2.1). The δ function can be approximated by a pulse (a top-hat function) of width and height equal to $\Delta\tau$ and $1/\Delta\tau$ respectively in the limit $\Delta\tau \to 0$. Thus, the Hamiltonian (2.1) of the kicked top can be written as

$$H = \begin{array}{ll} \hbar\frac{p}{\tau}J_y, & n\tau < t < (n+1)\tau - \Delta\tau \\ \hbar\frac{p}{\tau}J_y + \hbar\frac{\kappa}{2j\Delta\tau}J_z^2, & (n+1)\tau - \Delta\tau < t < (n+1)\tau \end{array} \tag{2.2}$$

in the limit $\Delta\tau \to 0$. The Floquet time evolution operator for one time period, τ, can be calculated as follows:

$$\begin{aligned} U &= \lim_{\Delta\tau\to 0} U(\tau, \tau-\Delta\tau)U(\tau-\Delta\tau, 0) \\ &= \lim_{\Delta\tau\to 0} \exp\left(-\frac{\mathrm{i}}{\hbar}\int_{\tau-\Delta\tau}^{\tau}\left(\hbar\frac{p}{\tau}J_y + \hbar\frac{\kappa}{2j\Delta\tau}J_z^2\right)dt\right)\exp\left(-\frac{\mathrm{i}}{\hbar}\int_0^{\tau-\Delta\tau}\left(\hbar\frac{p}{\tau}J_y\right)dt\right) \\ &= \lim_{\Delta\tau\to 0} \exp\left(-\mathrm{i}\left(\frac{p}{\tau}J_y\Delta\tau + \frac{\kappa}{2j}J_z^2\right)\right)\exp\left(-\mathrm{i}\frac{p}{\tau}J_y\left(\tau-\Delta\tau\right)\right) \\ &= \exp\left(-\mathrm{i}\frac{\kappa}{2j}J_z^2\right)\exp\left(-\mathrm{i}pJ_y\right) \end{aligned} \tag{2.3}$$

Given any initial quantum state $|\psi(0)\rangle$, the subsequent states $|\psi(n)\rangle$ after n kicks are obtained via applying the Floquet operator, U, n times on $|\psi(0)\rangle$ as in $|\psi(n)\rangle = U^n|\psi(0)\rangle$.

2.2 Classical Dynamics of the Kicked Top

The quantum dynamics of a system can approach classical behaviour in the limit of $\frac{A_0}{\hbar} \to \infty$ where A_0 is characteristic action of the system. For the kicked top, $A_0 \sim j\hbar$ where j is the magnitude of the angular momentum which is a conserved quantity for this system. Hence, a classical analog of the kicked top is obtained in the limit $j \to \infty$ [79, 70]. The classical equations of motion for the kicked top can be obtained by writing the Heisenberg equations of motion for the angular momentum operators, J_x, J_y and J_z, and then taking the limit $j \to \infty$ [70, 15]. Here, we derive the same result using the classical Hamilton equations of motion.

2.2.1 Classical equation of motion

We know that the classical angular momentum vector, $\vec{J}$, is the cross product of position and momentum vectors, that is,

$$\vec{J} = \vec{r} \times \vec{p}, \tag{2.4}$$

with individual components being

$$\begin{aligned} J_x &= yp_z - zp_y, \\ J_y &= zp_x - xp_z, \\ J_z &= xp_y - yp_x. \end{aligned} \tag{2.5}$$

Substituting (2.5) in the Hamiltonian (2.1)

$$H = \frac{\kappa}{2j}(xp_y - yp_x)^2 \sum_{n=-\infty}^{\infty} \delta(t - n\tau) + \frac{p}{\tau}(zp_x - xp_z). \tag{2.6}$$

Using Hamilton's equations of motion, $\dot{q}_i = \frac{\partial H}{\partial p_i}$ and $\dot{p}_i = -\frac{\partial H}{\partial q_i}$, we obtain

$$\dot{x} = -\frac{\kappa}{j} y J_z \sum_{n=-\infty}^{\infty} \delta(t - n\tau) + \frac{p}{\tau} z, \tag{2.7a}$$

$$\dot{p}_x = -\frac{\kappa}{j} p_y J_z \sum_{n=-\infty}^{\infty} \delta(t - n\tau) + \frac{p}{\tau} p_z, \tag{2.7b}$$

$$\dot{y} = \frac{\kappa}{j} x J_z \sum_{n=-\infty}^{\infty} \delta(t - n\tau), \tag{2.7c}$$

$$\dot{p}_y = \frac{\kappa}{j} p_x J_z \sum_{n=-\infty}^{\infty} \delta(t - n\tau), \tag{2.7d}$$

$$\dot{z} = -\frac{p}{\tau} x, \tag{2.7e}$$

$$\dot{p}_z = -\frac{p}{\tau} p_x. \tag{2.7f}$$

Thus, the classical equation of motion for the components of the angular momentum vector will be

$$\begin{aligned} \dot{J}_x &= \dot{y} p_z + y \dot{p}_y - \dot{z} p_y - z \dot{p}_y \\ &= -\frac{\kappa}{j} J_y J_z \sum_{n=-\infty}^{\infty} \delta(t - n\tau) + \frac{p}{\tau} J_z, \end{aligned} \tag{2.8a}$$

$$\begin{aligned} \dot{J}_y &= \dot{z} p_x + z \dot{p}_x - \dot{x} p_z - x \dot{p}_z \\ &= \frac{\kappa}{j} J_x J_z \sum_{n=-\infty}^{\infty} \delta(t - n\tau), \end{aligned} \tag{2.8b}$$

$$\begin{aligned} \dot{J}_x &= \dot{x} p_y + x \dot{p}_y - \dot{y} p_x - y \dot{p}_x \\ &= -\frac{p}{\tau} J_x. \end{aligned} \tag{2.8c}$$

Substituting $X = J_x/j$, $Y = J_y/j$ and $Z = J_z/j$ in (2.8a)-(2.8c), we get

$$\dot{X} = -\kappa Y Z \sum_{n=-\infty}^{\infty} \delta(t - n\tau) + \frac{p}{\tau} Z, \tag{2.9a}$$

$$\dot{Y} = \kappa X Z \sum_{n=-\infty}^{\infty} \delta(t - n\tau), \tag{2.9b}$$

$$\dot{Z} = -\frac{p}{\tau} X. \tag{2.9c}$$

We obtain the stroboscopic classical equation of motion for the kicked top by integrating (2.9a)-(2.9c) for one time period, τ, in the interval $[\epsilon, \tau + \epsilon]$ with the initial condition (X_n, Y_n, Z_n). This is done by integrating the equations first in the time interval $\lim_{\epsilon \to 0}[\epsilon, \tau - \epsilon]$, followed by integrating in the time interval $\lim_{\epsilon \to 0}[\tau - \epsilon, \tau + \epsilon]$. The equations (2.9a)-(2.9c) in the time interval $\lim_{\epsilon \to 0}[\epsilon, \tau - \epsilon]$ take the form

$$\dot{X} = \frac{p}{\tau} Z, \tag{2.10a}$$

$$\dot{Y} = 0, \tag{2.10b}$$

$$\dot{Z} = -\frac{p}{\tau} X. \tag{2.10c}$$

Let $[X(\tau - \epsilon), Y(\tau - \epsilon), Z(\tau - \epsilon)] = [\tilde{X}_n, \tilde{Y}_n, \tilde{Z}_n]$. Integration of (2.10a)-(2.10c) in the time interval $\lim_{\epsilon \to 0}[\epsilon, \tau - \epsilon]$ yields

$$\tilde{X}_n = X_n \cos p + Z_n \sin p, \tag{2.11a}$$

$$\tilde{Y}_n = Y_n, \tag{2.11b}$$

$$\tilde{Z}_n = Z_n \cos p - X_n \sin p. \tag{2.11c}$$

The equations (2.9a)-(2.9c) in the time interval $\lim_{\epsilon \to 0}[\tau - \epsilon, \tau + \epsilon]$ take the form

$$\dot{X} = -\kappa Y Z \delta(t - \tau), \tag{2.12a}$$

$$\dot{Y} = \kappa X Z \delta(t - \tau), \tag{2.12b}$$

$$\dot{Z} = 0. \tag{2.12c}$$

The solution to the equations (2.12a)-(2.12c) in the time interval $\lim_{\epsilon\to 0}[\tau-\epsilon,\tau+\epsilon]$ is given by

$$X(t) = \tilde{X}_n \cos\Big(\kappa\tilde{Z}_n f_H(t-\tau)\Big) - \tilde{Y}_n \sin\Big(\kappa\tilde{Z}_n f_H(t-\tau)\Big), \tag{2.13a}$$

$$Y(t) = \tilde{Y}_n \cos\Big(\kappa\tilde{Z}_n f_H(t-\tau)\Big) + \tilde{X}_n \sin\Big(\kappa\tilde{Z}_n f_H(t-\tau)\Big), \tag{2.13b}$$

$$Z(t) = \tilde{Z}_n \tag{2.13c}$$

where $f_H(t-\tau)$ is the heaviside function whose value is 0 for $t<\tau$, and 1 for $t\geq\tau$. This yields

$$X_{n+1} = \tilde{X}_n \cos\Big(\kappa\tilde{Z}_n\Big) - \tilde{Y}_n \sin\Big(\kappa\tilde{Z}_n\Big), \tag{2.14a}$$

$$Y_{n+1} = \tilde{Y}_n \cos\Big(\kappa\tilde{Z}_n\Big) + \tilde{X}_n \sin\Big(\kappa\tilde{Z}_n\Big), \tag{2.14b}$$

$$Z_{n+1} = \tilde{Z}_n \tag{2.14c}$$

where $[X_{n+1},Y_{n+1},Z_{n+1}] = \lim_{\epsilon\to 0}[X(\tau+\epsilon),Y(\tau+\epsilon),Z(\tau+\epsilon)]$. Equations (2.11a)-(2.11c) together with (2.14a)-(2.14c) constitute the stroboscopic classical equations of motion for the kicked top. For $p=\pi/2$, these equations reduce to

$$X_{n+1} = Z_n \cos(\kappa X_n) + Y_n \sin(\kappa X_n), \tag{2.15a}$$

$$Y_{n+1} = Y_n \cos(\kappa X_n) - Z_n \sin(\kappa X_n), \tag{2.15b}$$

$$Z_{n+1} = -X_n. \tag{2.15c}$$

We refer to the (2.15a)-(2.15c) as the F-map such that

$$[X_{n+1},Y_{n+1},Z_{n+1}] = F[X_n,Y_n,Z_n].$$

Following standard practise in the literature, we fix $p=\pi/2$ henceforth in this thesis unless otherwise mentioned.

Since j is a constant of motion of the QKT, the magnitude of the angular momentum vector does not change upon evolution with the kicked top Hamiltonian. As evident from the classical equation of motion for the kicked top, each time period consists of a linear rotation of the angular momentum vector by angle p about the y axis followed by a non-linear rotation about the z axis. The amount of this nonlinear rotation during the kick is proportional to the z-component of the angular momentum vector. This nonlinearity is essential for the kicked top to exhibit chaotic behavior.

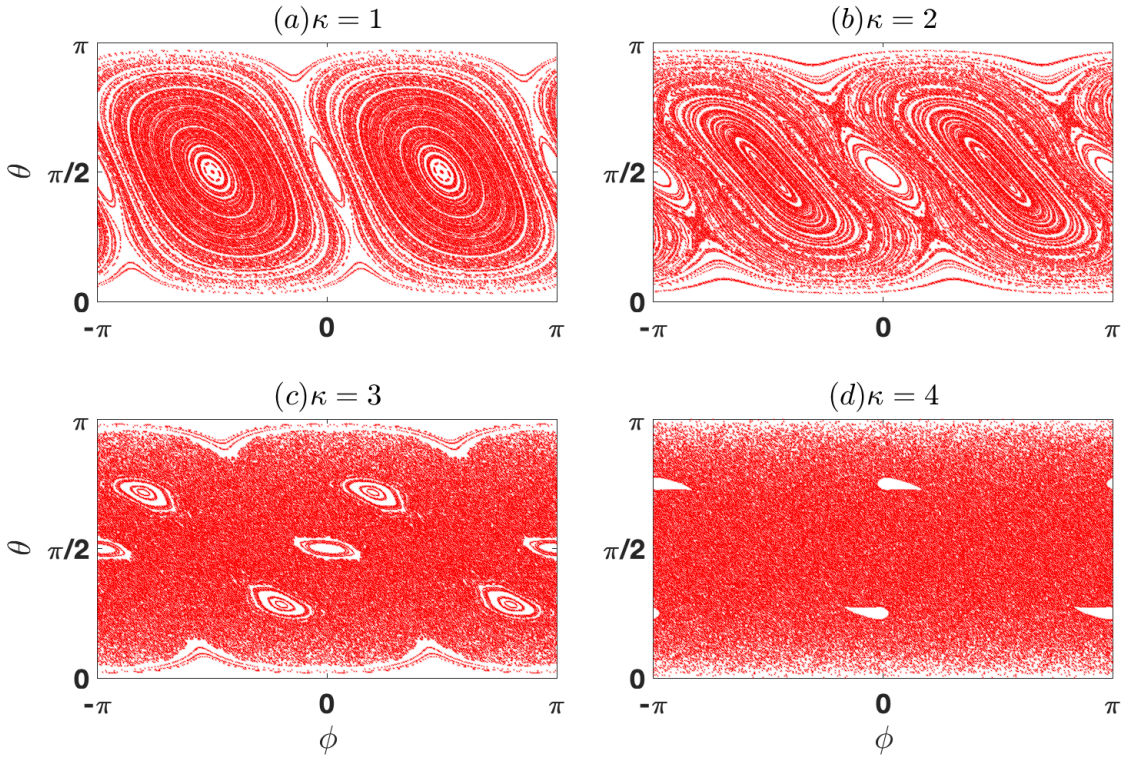

Figure 2.1: Classical stroboscopic phase space of the kicked top for four different values of the parameter κ, with $\tau = 1.0$, $p = \frac{\pi}{2}$. θ and ϕ are plotted after each kick for 1064 initial conditions, each initial condition being evolved for 150 kicks.

The kicked top exhibits regular, chaotic, as well as mixed phase space behaviour depending on the value of the parameter, κ. For $\kappa = 0$, the kicked top is an integrable system as the kicking term in the Hamiltonian vanishes. The classical phase space is dominated by regular islands for small values of κ and by a chaotic sea for larger values of κ (approximately beyond $\kappa = 4.4$). Tuning the value of the parameter κ leads to chaos in the kicked top, and thus κ is known as the chaoticity parameter. The classical stroboscopic map or kick-to-kick evolution (in polar co-ordinates) for a range of initial conditions with four different values of κ is shown in Fig. 2.1.

2.2.2 Fixed points, periodic orbits and classical bifurcations

In this subsection, we analyze some classical fixed points, period-2 and period-4 orbits together with their stability as the parameter κ is varied. As mentioned earlier, the classical map for one time period is denoted by F. Solutions of the equation, $F^n(X,Y,Z) = (X,Y,Z)$, leads to fixed points (corresponding to $n=1$) and period$-n$ orbits of the kicked top. Table 2.1 lists some of these fixed points and periodic orbits of the kicked top. Any classical state (X,Y,Z) satisfies the normalization condition $X^2+Y^2+Z^2=1$. The variable x_0 in FP_1, FP_2 and $P2_A$ in Table 2.1 is obtained from the normalization condition,

$$2x_0^2 + \frac{[x_0 \sin(\kappa x_0)]^2}{[1-\cos(\kappa x_0)]^2} = 1. \tag{2.16}$$

Next, we study the stability of the fixed points and periodic orbits listed in Table 2.1. To study the stability of a period-n orbit, we calculate the eigenvalues, λ_i, of the Jacobian of the classical map F^n at the period-n point [80]. If $|\lambda_i| \leq 1$ for all possible values of i, then the period-n orbit is stable, otherwise it is unstable.

FP_1 and FP_2 are fixed points for all values of κ. The eigenvalues of the Jacobian at FP_1 are $\left\{1, \frac{\kappa+\sqrt{\kappa^2-4}}{2}, \frac{\kappa-\sqrt{\kappa^2-4}}{2}\right\}$. Clearly, for $\kappa > 2$, the eigenvalue, $\frac{\kappa+\sqrt{\kappa^2-4}}{2} > 1$. Thus, this fixed point loses stability at $\kappa = 2$, which implies that $\kappa = 2$ is a bifurcation point.

At $\kappa = 2$, FP_1 gives rise to two stable fixed points: FP_3 and FP_4. FP_2 bifurcate to a period-2 orbit, $P2_A$. FP_3, FP_4 and $P2_A$ lose stability at $\kappa = \sqrt{2}\pi$ (Fig. 2.2) and give rise to four stable period-2 orbits: $P2_B, P2_C, P2_D$ and $P2_E$. These four period-2 orbits lose stability at $\kappa \approx 4.8725$ (Fig. 2.2). There exists a period-4 orbit, $P4$, at all values of κ. It loses its stability at $\kappa = \pi$ (Fig. 2.2). Figure 2.3 shows the bifurcation diagram for the mentioned periodic orbits, explicitly showing the bifurcation points $\kappa = 2, \pi, \sqrt{2}\pi, 4.8725$.

2.3 QKT as an N=2j Multiqubit System

Any system whose Hamiltonian commutes with the square of the angular momentum operator as in

$$[H, J^2] = 0 \tag{2.17}$$

preserves the angular momentum of a quantum state upon evolution. The angular momentum can be either of the following: spin angular momentum, orbital angular momentum, or

$$
\begin{array}{lcl}
FP_1 & = & (0,1,0) \\
FP_2 & = & (0,-1,0) \\
FP_3 & = & \left(x_0, \dfrac{x_0 \sin(\kappa x_0)}{(1-\cos(\kappa x_0))}, -x_0\right) \\
FP_4 & = & \left(-x_0, \dfrac{x_0 \sin(\kappa x_0)}{(1-\cos(\kappa x_0))}, x_0\right) \\
P2_A & = & \left(x_0, -\dfrac{x_0 \sin(\kappa x_0)}{(1-\cos(\kappa x_0))}, x_0\right) \leftrightarrow \left(-x_0, -\dfrac{x_0 \sin(\kappa x_0)}{(1-\cos(\kappa x_0))}, -x_0\right) \\
P4 & = & (1,0,0) \to (0,0,-1) \to (-1,0,0) \to (0,0,1) \to (1,0,0) \\
P2_B & = & \left(\dfrac{\pi}{\kappa}, \sqrt{1-2\left(\dfrac{\pi}{\kappa}\right)^2}, \dfrac{\pi}{\kappa}\right) \leftrightarrow \left(-\dfrac{\pi}{\kappa}, -\sqrt{1-2\left(\dfrac{\pi}{\kappa}\right)^2}, -\dfrac{\pi}{\kappa}\right) \\
P2_C & = & \left(-\dfrac{\pi}{\kappa}, \sqrt{1-2\left(\dfrac{\pi}{\kappa}\right)^2}, \dfrac{\pi}{\kappa}\right) \leftrightarrow \left(-\dfrac{\pi}{\kappa}, -\sqrt{1-2\left(\dfrac{\pi}{\kappa}\right)^2}, \dfrac{\pi}{\kappa}\right) \\
P2_D & = & \left(\dfrac{\pi}{\kappa}, \sqrt{1-2\left(\dfrac{\pi}{\kappa}\right)^2}, -\dfrac{\pi}{\kappa}\right) \leftrightarrow \left(\dfrac{\pi}{\kappa}, -\sqrt{1-2\left(\dfrac{\pi}{\kappa}\right)^2}, -\dfrac{\pi}{\kappa}\right) \\
P2_E & = & \left(\dfrac{\pi}{\kappa}, -\sqrt{1-2\left(\dfrac{\pi}{\kappa}\right)^2}, \dfrac{\pi}{\kappa}\right) \leftrightarrow \left(-\dfrac{\pi}{\kappa}, \sqrt{1-2\left(\dfrac{\pi}{\kappa}\right)^2}, -\dfrac{\pi}{\kappa}\right)
\end{array}
$$

Table 2.1: Fixed points and periodic orbits of the kicked top [in the form (X, Y, Z)].

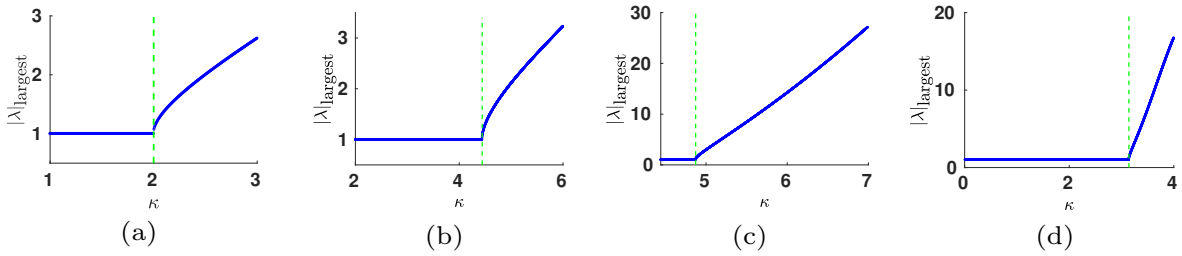

Figure 2.2: (a) Largest eigenvalue of the Jacobian matrix of F at FP_1 as a function of κ showing loss of stability of FP_1 at $\kappa = 2$. (b) Largest eigenvalue of the Jacobian matrix of F at FP_3 as a function of κ showing loss of stability of FP_3 at $\kappa = \sqrt{2}\pi$. (c) Largest eigenvalue of the Jacobian matrix of F^2 at $P2_B$ as a function of κ showing loss of stability of $P2_B$ at $\kappa \approx 4.8725$. (d) Largest eigenvalue of the Jacobian matrix of F^4 at $P4$ as a function of κ showing loss of stability of $P4$ at $\kappa = \pi$. Vertical dashed lines in the four plots represent the bifurcation parameter value at which loss of stability occurs.

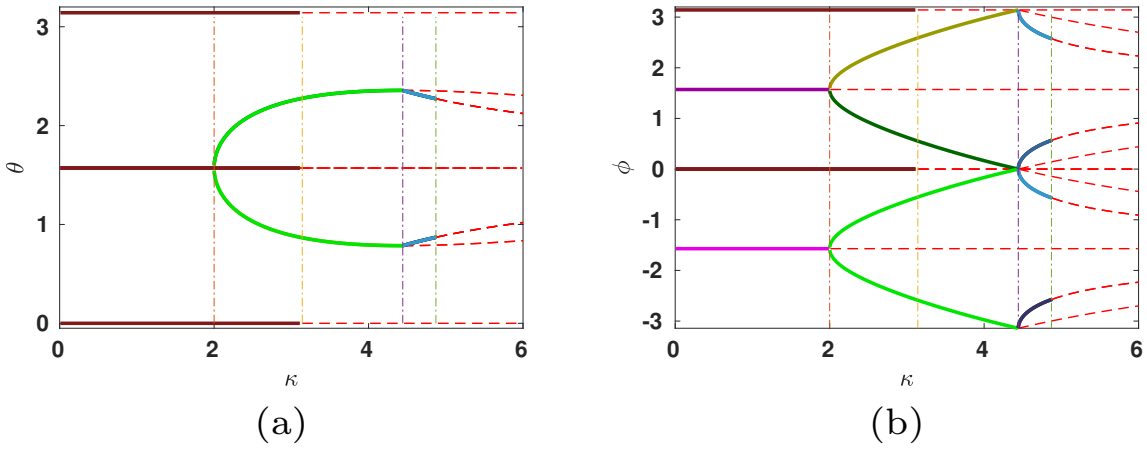

Figure 2.3: Classical bifurcation diagram (a) θ vs κ, (b) ϕ vs κ. All solid lines represent stable fixed points and periodic orbits. Dashed lines represent unstable fixed points and periodic orbits. Dashed dotted vertical lines represent bifurcation parameter values. The same color in different solid lines indicate that they are different points of the same periodic orbit.

total angular momentum. Further, any quantum state with spin j can be considered as an $N = 2j$ qubit state lying in the symmetric subspace of $2j$ qubits. This can be understood in the following way. The Hilbert space of $2j$ qubits is 2^{2j}-dimensional. However, the dimension of the symmetric subspace of these $2j$ qubits (symmetric under pair exchange) is only $2j + 1$-dimensional [81, 82]. The value of the collective spin of any quantum state in this symmetric subspace of the $2j$ qubits is j. This $(2j+1)$-dimensional symmetric subspace of j qubits is spanned by the eigenstates of J^2 and J_z, $|j, m\rangle$, where $m = \{-j, -j-1, ...j\}$, called the Dicke basis. The quantum states in this subspace evolve only in this subspace under the Hamiltonians which preserve the collective spin of the state. Thus, systems whose Hamiltonian commutes with the square of the angular momentum operator can be considered as an $N = 2j$ multiqubit system. j is the total angular momentum of $N = 2j$ spin$-1/2$ qubits in such systems.

Since (2.17) holds for the QKT Hamiltonian, the QKT can be considered as an $N = 2j$ multiqubit system [54]. The spin-j operators in terms of Pauli matrices of individual qubits are given by

$$J_\alpha = \frac{1}{2}\sum_{i=1}^{2j}\sigma_{i\alpha}, \qquad \alpha \in \{x, y, z\}, \tag{2.18}$$

where $\sigma_{i\alpha}$ implies σ_α operation on i^{th} qubit and identity operation on rest of the qubits. Using (2.18) and (2.1), the $2j-$qubit Hamiltonian of the QKT is given by

$$H = \hbar\frac{\kappa}{8j}\left(2j + \sum_{\substack{i,k=1\\ i\neq k}}^{2j}\sigma_{iz}\otimes\sigma_{kz}\right)\sum_{n=-\infty}^{\infty}\delta(t - n\tau) + \hbar\frac{p}{2\tau}\sum_{i=1}^{2j}\sigma_{iy}. \tag{2.19}$$

For instance, the Hamiltonian of the $3-$qubit QKT is given by

$$\begin{aligned} H &= \hbar\frac{\kappa}{12}\left(3 + 2\left(\sigma_z\otimes\sigma_z\otimes 1 + \sigma_z\otimes 1\otimes\sigma_z + 1\otimes\sigma_z\otimes\sigma_z\right)\right)\sum_n\delta(t - n\tau) \\ &\quad + \hbar\frac{p}{2\tau}\left(\sigma_y\otimes 1\otimes 1 + 1\otimes\sigma_y\otimes 1 + 1\otimes 1\otimes\sigma_y\right) \end{aligned} \tag{2.20}$$

2.4 Initial State: Spin Coherent State (SCS)

Coherent states are minimum-uncertainty states as they saturate the Heisenberg's uncertainty relation, $\Delta x\Delta p \geq \hbar/2$ [83]. For spin systems, the minimum-uncertainty states

correspond to the so-called spin coherent states (SCSs) [84, 85], which satisfy the analogous relation

$$\Delta J_i \Delta J_k = \frac{\hbar}{2}|\Delta J_l| \tag{2.21}$$

where i, k and l are permutations of x, y and z, and $\Delta J_l = \sqrt{\langle J_l^2\rangle - \langle J_l\rangle^2}$. In addition, the uncertainties in the operators have a symmetric distribution. Asymmetry in the uncertainties of the operators lead to spin squeezed states. These spin squeezed states may be highly quantum mechanical in nature as they can display entanglement in the corresponding multi-qubit representation unlike the spin coherent states [86].

Just like coherent states can be prepared by applying a displacement operator to the vacuum states, SCSs can be prepared by applying a rotation operator to the $|j, j\rangle$ state. Given any point (θ, ϕ) in the classical phase space, we can construct SCS$|j; \theta, \phi\rangle$ by applying the rotation operator $R(\theta, \phi) = \exp\left[i\theta(J_x \sin\phi - J_y \cos\phi)\right]$ on the state $|j, j\rangle$, that is,

$$|j; \theta, \phi\rangle = R(\theta, \phi)|j, j\rangle \equiv \exp\left[i\theta(J_x \sin\phi - J_y \cos\phi)\right]|j, j\rangle. \tag{2.22}$$

This yields a minimum uncertainty state centered on the point (θ, ϕ). That is, the expectation value of the angular momentum of this state is $(j \sin\theta\cos\phi, j \sin\theta \sin\phi, j\cos\theta)$. The normalized variance of this state is $(\langle \mathbf{J}^2\rangle - \langle \mathbf{J}\rangle^2)/(j(j+1)) = 1/(j+1)$ which is also the minimum attainable value by a quantum state of angular momentum j [79]. Thus, for larger j values, the SCS becomes highly localized at the point (θ, ϕ) in the phase space. In the classical limit of the system $j \to \infty$ (as explained in Sec. 2.2), the normalized variance, and hence the uncertainty of the SCS tends to zero. Thus, an SCS approximates a classical angular momentum state in the classical limit. In this sense, the SCSs are classical-like quantum states.

As explained in Sec. 2.3, a quantum state with spin angular momentum j, and corresponding SCS$|j; \theta, \phi\rangle$, can be regarded as a $2j-$qubit system. The $2j-$qubit representation of SCS$|j; \theta, \phi\rangle$ is given as

$$\text{SCS}|j; \theta, \phi\rangle = |\theta, \phi\rangle^{\otimes 2j} \tag{2.23}$$

where

$$|\theta, \phi\rangle = \cos\left(\frac{\theta}{2}\right)|0\rangle + \exp\left(\mathrm{i}\phi\right)\sin\left(\frac{\theta}{2}\right)|1\rangle \tag{2.24}$$

is the representation of a qubit on the Bloch sphere.

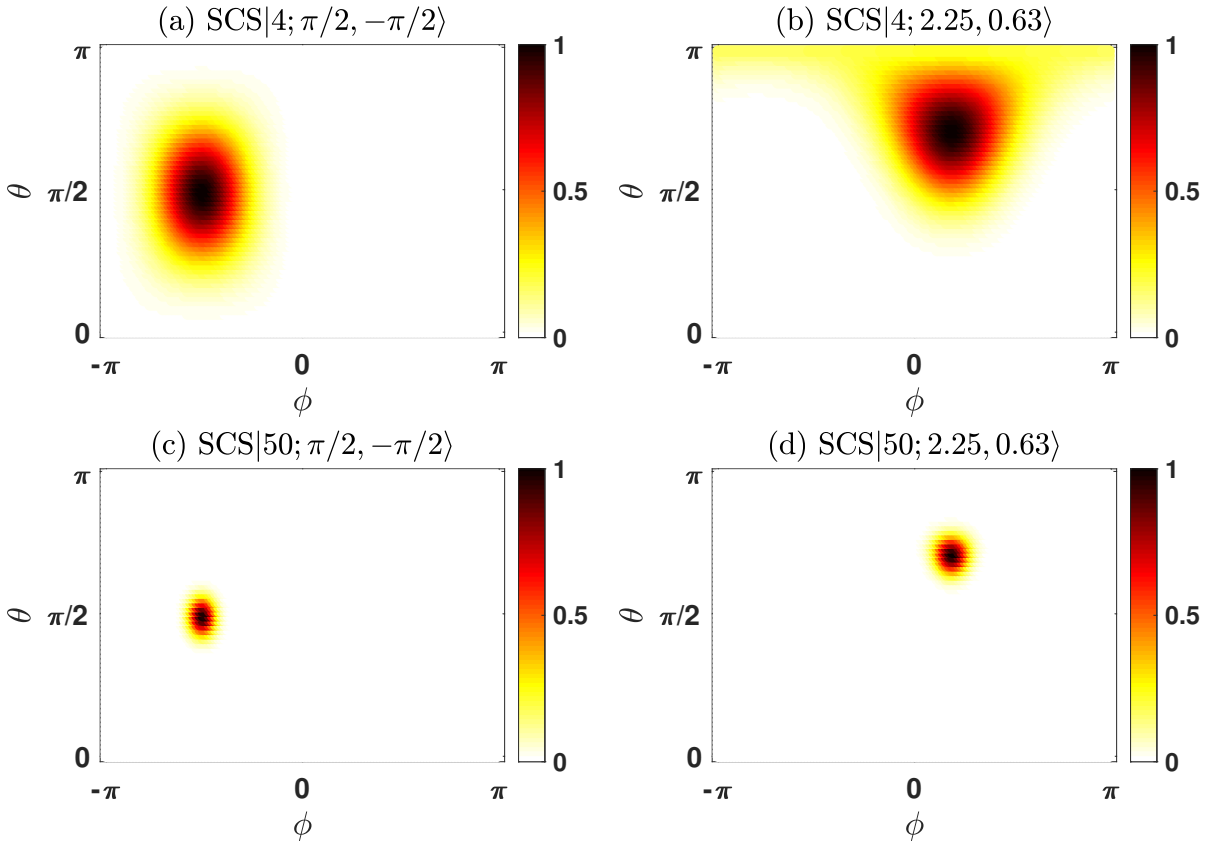

Figure 2.4: Plot of Husimi phase space distribution (without the factor $\frac{2j+1}{4\pi}$ in (2.25)) of the SCS$|j;\theta,\phi\rangle$ corresponding to $(\theta,\phi) = (\frac{\pi}{2}, -\frac{\pi}{2})$ and $(2.25, 0.63)$ for two different j values, 4 and 50.

2.5 Husimi Phase Space Distribution

Classical dynamics is usually studied using trajectories in phase space, which is a $2n-$ dimensional space for a system with n degrees of freedom. In order to study quantum-classical correspondence for any classical trajectory, it is desirable to faithfully represent quantum states as functions over phase space. Two of the widely used phase space distribution functions for quantum mechanics are: (a) the Wigner distribution function, and (b) the Husimi distribution function [87, 88, 8]. The desirable properties of a quantum phase space distribution include the following: (i) it should be nonnegative, (ii) the reduced marginal distributions for position and momentum should coincide with the usual position and momentum probability distribution respectively. Neither the Husimi nor the Wigner distribution functions satisfy both these properties. While the Wigner distribution function can take negative values, the Husimi distribution function does not yield correct reduced marginal distributions.

In the study of quantum-classical correspondence of the kicked top (in the next chapter), our aim is to find footprints of classical dynamics in the quantum evolution. Since we are interested in the overall probability distribution in the phase space rather than the reduced marginal distribution, we choose the Husimi distribution function over the Wigner distribution function for this study. Moreover, the study of the Husimi distribution function for large j values is computationally efficient as compared to the Wigner distribution function. Hence the Husimi distribution facilitates the numerical study of QKT in the semiclassical limit.

Given any angular momentum quantum state ρ, the Husimi distribution is given by

$$Q(\theta, \phi) = \frac{2j+1}{4\pi} \langle \theta, \phi | \rho | \theta, \phi \rangle, \tag{2.25}$$

which is equal to $\frac{2j+1}{4\pi} |\langle \theta, \phi | \psi \rangle|^2$ for pure states. In Fig. 2.4, we illustrate the Husimi phase space distribution of a few SCSs that was described in the previous section.

2.6 Summary

In this chapter, we studied various aspects of the model kicked top. First, we studied the classical dynamics of the kicked top. We derived the classical equation of motion for one time period for the kicked top using the Hamilton's equation of motion. We analyzed a few fixed points and periodic orbits of the classical kicked top together with their stability. We identified the bifurcation parameters for the classical bifurcations of these periodic orbits.

Furthermore, we reviewed a few things required for the quantum mechanical study of the kicked top. We derived the Floquet operator - the unitary operator for one time period - for the kicked top to study its quantum dynamics. We described how the quantum kicked top can be understood as a multiqubit system. Hence, one can study quantum correlations among the qubits in the system. We reviewed the spin coherent states which are the most classical-like quantum states, and thus will be used as initial quantum states in further chapters. We also reviewed Husimi distribution function which we use to study quantum dynamics of the kicked top in the phase space in the next chapter.

Chapter 3

Quantum-Classical Correspondence in Periodically Driven Systems

This chapter is based on Kumari and Ghose [69].

Quantum-classical correspondence and quantum-to-classical transition, especially for chaotic systems, remains a partially understood subject even after a century of analysing quantum mechanics. According to the correspondence principle, the predictions of quantum physics should agree with the predictions of classical physics in appropriate limits wherever classical physics is applicable. There are multiple ways in which the correspondence principle has been formulated. These include Bohr correspondence principle [89], Ehrenfest's theorem [90], and Liouville correspondence [91, 92], with each having its own subtleties [93, 94, 95]. According to Bohr, quantum-classical correspondence is attained in the limit of large quantum numbers (or when $\hbar \to 0$ relative to the phase space of the dynamics). According to Ehrenfest's theorem, the evolution of expectation values of observables in a quantum system should coincide with the corresponding classical evolution until a time known as Ehrenfest's time ($t_{\rm EH}$) that depends on the system dynamics. While $t_{\rm EH}$ is large for regular systems in the semiclassical regime, it can be very small for chaotic systems even in the semiclassical limit as described in Sec. 1.2 [96, 36, 97]. Thus, quantum-classical correspondence breaks down for chaotic systems much earlier than for regular systems. A few ways have been proposed to reconcile the breakdown of the correspondence principle in chaotic systems. These include, for example, the effect of decoherence [36], and the application of continuous but sufficiently weak measurements [9].

Quantum-classical correspondence for systems with mixed phase space are notoriously more difficult to study than completely regular and completely chaotic systems. Fully

regular systems can be understood via the Hamilton-Jacobi formulation [98] and fully chaotic systems are well described by random matrix theory [15]. On the other hand, systems with a mixed phase space do not have a universal tool for their study. In this chapter, we explore the quantum-classical correspondence in periodically driven systems (which are commonly known as Floquet systems) focusing specifically on systems with a mixed phase space. The correspondence principles stated above are said to hold in the semiclassical regime. The semiclassical versus deep quantum regime is generally quantified using the magnitude of quantum numbers or the effective Planck's constant ($\hbar_{\text{eff}} = \frac{\hbar}{A_0}$ where A_0 is the characteristic action of the system). However, the transition between these two regimes does not happen at a well defined sharp value but smoothly as one changes the magnitude of quantum numbers. This leads us to the following questions:

- What is the magnitude of the quantum numbers at which the correspondence will be first observed?
- How does the correspondence depend on the structure of the classical phase space, for example, the existence of fixed points and periodic orbits? This question is more relevant to regular systems and systems with a mixed phase space where any initial state evolves only within a subset of the phase space unlike fully chaotic systems.

In order to develop an understanding for these open problems, we explore the following question: when does the quantum dynamics corresponding to an initial coherent state in the regular region follow the classical evolution to the same initial state? We address this question in the vicinity of classical fixed points and periodic orbits of Floquet systems. Our proposed conjecture for the same helps us in quantifying the magnitude of quantum numbers for which quantum-classical correspondence will be first observed - which we refer to as 'quantification of Bohr correspondence principle'. We illustrate our method of quantification in the model quantum kicked top (QKT) studied in chapter 2.

This chapter is organized as follows. In Sec. 3.1, we describe our criteria for the quantification of Bohr correspondence principle in Floquet systems. In Sec. 3.2, we apply our criteria to the QKT. We show that when the criteria are satisfied, quantum-classical correspondence is evident even in a deep quantum regime. In Sec. 3.3, we use our criteria to identify new quantum signatures of classical bifurcations in the kicked top dynamics, in a deep quantum regime as well as in the semiclassical regime. In Sec. 3.4, we summarize the results presented in this chapter.

3.1 Proposed Quantification of Bohr Correspondence Principle

According to the famous Bohr correspondence principle, quantum-classical correspondence is attained in the limit of large quantum numbers. One of the ways to observe the quantum-classical correspondence is by tracking the similarity between the quantum and classical dynamics in the phase space (when the initial quantum state corresponds to a minimum-uncertainty coherent state centered at the classical initial state). Our goal is to quantify how large the quantum numbers needs to be to observe similarity in the classical and quantum dynamics. We conjecture a set of criteria for observing quantum-classical correspondence near classical periodic orbits in periodically driven systems. We propose that the quantum dynamics in the vicinity of any stable classical period-n orbit for such systems will be similar to the classical dynamics when:

1. the coherent states centered on all the n points in the period-n orbit are (almost) orthogonal to each other .

2. the coherent states centered on multiple periodic orbits that are related by the symmetries of the system are (almost) orthogonal to each other.

The existence of symmetries in the system may lead to quantum mechanical phenomena between the periodic orbits related by these symmetries, such as dynamical tunneling [99, 100]. If so, then the conditions described above will not be sufficient to ensure correspondence in a deeply quantum regime.

The two proposed criteria above can be understood in the following way. The classical states are distinguishable points in phase space. The classical dynamics evolves in a localized manner among these classical states in the phase space given the initial classical state is a point in the classical phase space. At the quantum level, distinguishability between quantum states is associated with their mutual orthogonality. Let us consider a periodically driven system with at least one stable period-n orbit in the classical phase space. Consider the quantum dynamics of the same system with the initial state being a coherent state localized at one of the points in a stable period-n orbit. We would expect the quantum dynamics to be similar to the classical dynamics if the quantum state evolves in a localized manner similar to the classical evolution. Coherent states are states with minimum uncertainty. Thus, there would be a localized evolution if at any time in the evolution, the quantum state has high overlap with a coherent state centered at one of the classical points of the period-n orbit and negligible overlap with coherent states centered

on the rest of the points of the period-n orbit. This can be assured if the set of coherent states centered at the points of a period-n orbit form an (almost) orthogonal set. However, if this is a nonorthogonal set, then high survival probability at any classical point may still allow a significant amount of survival probability at other classical points in the period-n orbit as well, and thus may generally cause a departure from classical dynamics.

For spin systems, the coherent states in the criteria would correspond to SCSs (Sec. 2.4). The overlap between any two SCSs, say SCS$|j;\theta,\phi\rangle$ and SCS$|j;\theta_0,\phi_0\rangle$, is given by

$$|\langle j;\theta,\phi|j;\theta_0,\phi_0\rangle| = \left(\cos\left[\frac{\chi(\theta\phi,\theta_0\phi_0)}{2}\right]\right)^{2j}, \tag{3.1}$$

where $\chi(\theta\phi,\theta_0\phi_0)$ is the angle between the direction vectors, (θ,ϕ) and (θ_0,ϕ_0) on the unit sphere, $\mathbb{S}^2$ [53]. Thus, (3.1) is a handy tool to calculate the orthogonality of the SCSs for our quantification criteria. It is interesting to note that given any SCS, $|j;\theta,\phi\rangle$, there is only one SCS which has zero overlap with it irrespective of the value of j. This SCS corresponds to the antipodal point of (θ,ϕ), that is $(\pi-\theta,\pi+\phi)$. So we can never have exact orthogonality for periodic orbits of periodicity greater than 2 as required by the proposed criteria. However, given any set of n direction vectors, $\{(\theta_k,\phi_k)\}_{k=1}^n$, and an $\epsilon>0$, one can always find a value of j, say j_ϵ, such that for $j\geq j_\epsilon$, $|\langle j;\theta_k,\phi_k|j;\theta_l,\phi_l\rangle|\leq\epsilon$ $(\forall k,l\in\{1,2...,n\})$. The time for which a correspondence will be observed between the classical and quantum dynamics depends on the value of ϵ. The smaller the value of ϵ, the larger the time for which correspondence will be observed. The exact dependence of this time on the value of ϵ has not been pursued in this thesis and has been left for future investigation. We illustrate our conjecture in the kicked top in the next section.

3.2 Illustration of Proposed Criteria in the QKT

As the kicked top is a periodically driven system, our proposed criteria applies to the fixed points and periodic orbits in this system. In Sec. 2.2.2, we showed the existence of a few fixed points and periodic orbits in this system. We also analyzed their stability and bifurcations as the chaoticity parameter, κ, is increased (keeping the parameter $p=\pi/2$ fixed). In this section, we illustrate our quantification criteria in the kicked top for stable periodic orbits in different regimes of κ. We employ the Husimi phase space distribution (Sec. 2.5) to study the quantum-classical correspondence here. For unitary evolution of pure states, it is given by $Q(\theta,\phi)=\frac{2j+1}{4\pi}|\langle\theta,\phi|\psi\rangle|^2$. We plot the Husimi distribution function without the constant $\frac{2j+1}{4\pi}$, that is, $|\langle\theta,\phi|\psi\rangle|^2$ in this section. We have shown

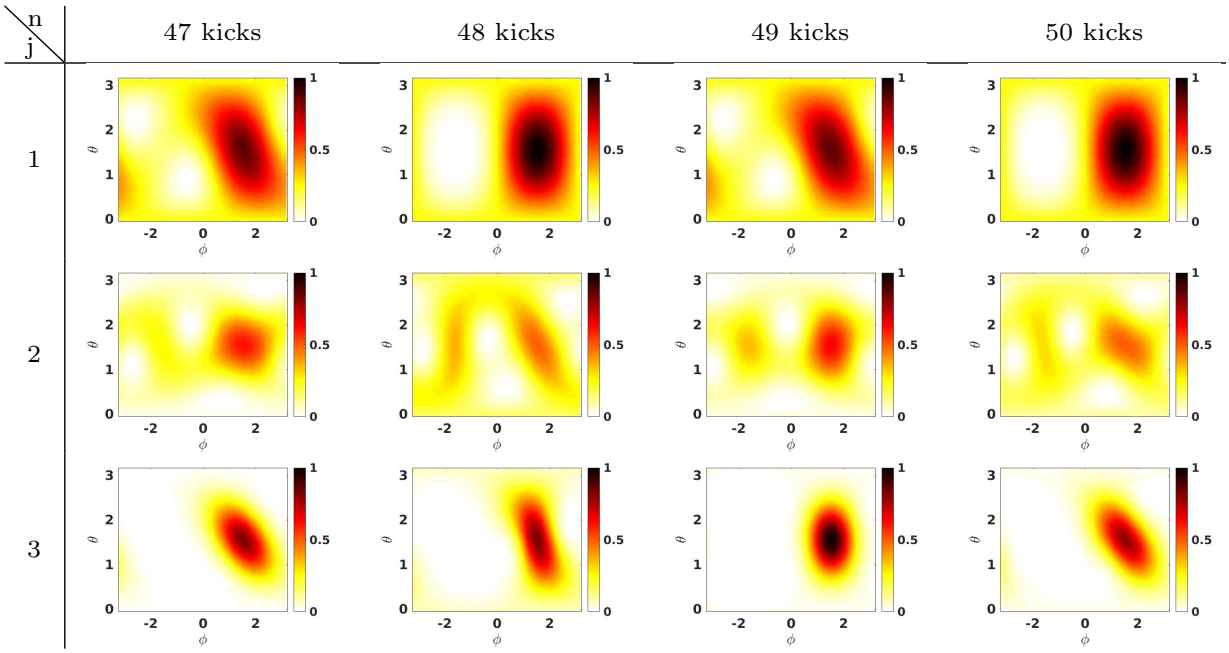

Figure 3.1: Evolution of the Husimi phase space distribution of an SCS centered on FP_1 $[(\theta, \phi) = (\frac{\pi}{2}, \frac{\pi}{2})]$ for three different j values with $\kappa = 1.5$. Like the classical dynamics, the quantum dynamics remains localized at FP_1, even in a deeply quantum regime, except for $j = 2$ when dynamical tunneling to FP_2 occurs.

quantum-classical correspondence or its breakdown via a pictorial representation of the evolving quantum state using the Husimi phase space. It can be rigorously studied by analyzing the maximum overlap of the evolving state with respect to the set of SCSs,

$$O_{\text{SCS}}(|\psi(t)\rangle) = \max_{\text{SCS}} |\langle \text{SCS}|\psi(t)\rangle|. \tag{3.2}$$

Given any $|\psi(t)\rangle = U(t)|\psi(0)\rangle$, if $O_{\text{SCS}}(|\psi(t)\rangle)$ remains close to 1, then $|\psi(0)\rangle$ evolves in a localized manner in the Husimi phase space. On the other hand, if $O_{\text{SCS}}(|\psi(t)\rangle)$ remains close to 0, then $|\psi(0)\rangle$ delocalizes or spreads in the Husimi phase space upon evolution. Localized and delocalized evolution can also be defined in terms of trace distance which is another distance based measure between quantum states discussed in Chapter 4.

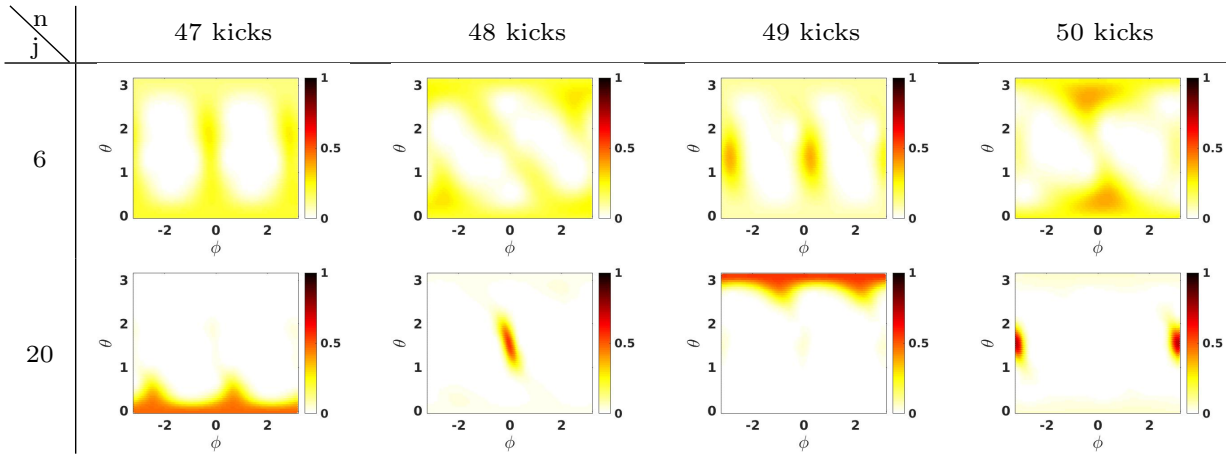

Figure 3.2: Evolution of the Husimi phase space distribution of an SCS centered on a point in $P4$ ($(\theta, \phi) = \left(\frac{\pi}{2}, 0\right)$) for 2 different j values with $\kappa = 1.5$. For $j = 6$ (first row), the quantum dynamics does not correspond to the classical dynamics, but for $j = 20$, there is clear correspondence.

3.2.1 $\kappa < 2$

For $\kappa < 2$, there exists two stable fixed points, FP_1 and FP_2, and a stable period-4 orbit, $P4$ (Table 2.1). Let us first analyze the criteria for the fixed points. In (θ, ϕ) notation, $FP_1 = \left(\frac{\pi}{2}, \frac{\pi}{2}\right)$, and $FP_2 = \left(\frac{\pi}{2}, -\frac{\pi}{2}\right)$. The SCSs centered on FP_1 and FP_2 are orthogonal to each other for all j values. Thus, we observe correspondence between the classical and quantum dynamics at these fixed points, FP_1 and FP_2, for almost all j values, including a low quantum number, $j = 1$, as illustrated in Fig. 3.1. However, in this deep quantum regime, there is the possibility of dynamical tunneling since FP_1 and FP_2 are related by a symmetry of the square of the kicked top map for $p = \frac{\pi}{2}$, that is rotation by angle π around the x-axis [70, 71]. This dynamical tunneling between the two fixed points, can be observed for some small values of j (for example $j = 2$ in Fig. 3.1) but as the value of j is increased further, the correspondence is recovered.

In contrast, the SCSs centered on the four points in the $P4$ orbit are not orthogonal to each other for very small j values. In (θ, ϕ) notation, the $P4$ orbit is $\left(\frac{\pi}{2}, 0\right) \to (\pi, 0) \to \left(\frac{\pi}{2}, \pi\right) \to (0, 0)$. From (3.1), the overlap between the spin coherent states at any two consecutive points in this period-4 orbit is given by $\left(\frac{1}{\sqrt{2}}\right)^{2j}$, which is of the order 10^{-7} for $j = 20$, and ≈ 0.156 for $j = 6$. Thus, for j values $\lesssim 20$, we do not see quantum-classical correspondence if we start at any one of the period-4 points, but we do see correspondence

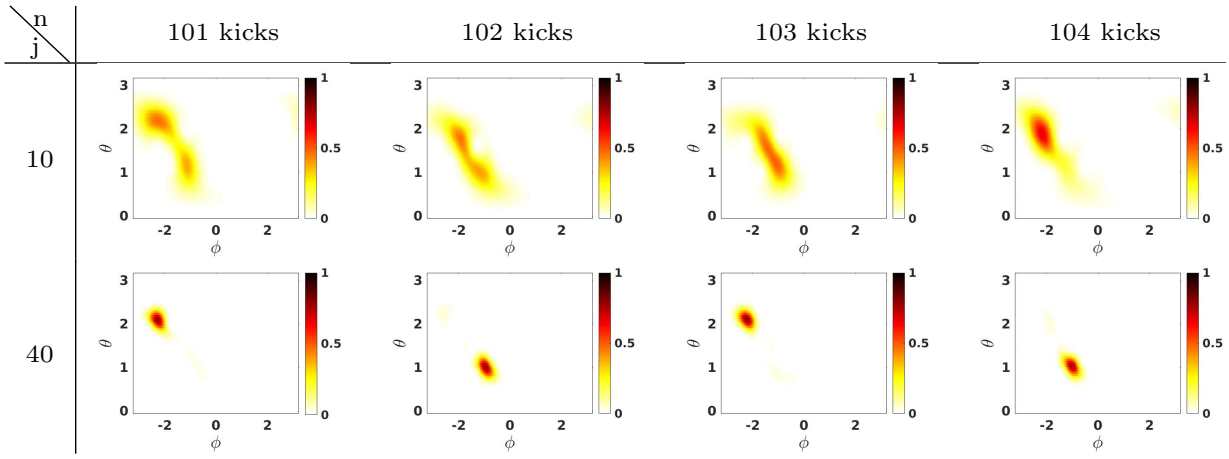

Figure 3.3: Evolution of the Husimi phase space distribution of an SCS centered on a point in $P2_A$ for two different j values with $\kappa = 2.5$. For $j = 10$ (top row), the quantum-classical correspondence is weak compared to $j = 40$.

for large enough j values $\gtrsim 20$ up to relevant time scales, as illustrated in Fig. 3.2.

3.2.2 $2 < \kappa < \pi$

In the range, $2 < \kappa < \pi$, we have two more fixed points, FP_3 and FP_4, and a period-2 orbit, $P2_A$, in addition to the ones present for $\kappa < 2$, as explained in Sec. 2.2.2. FP_1 and FP_2 are unstable in this range while all others are stable. FP_3, FP_4 and $P2_A$ are functions of κ (Table 2.1). For $\kappa = 2.5$, the overlap between the SCSs centered on the two points in $P2_A$ is on the order of 10^{-4} for $j = 10$, and on the order of 10^{-14} for $j = 40$. Correspondingly, we see in Fig. 3.3 that for $j = 40$, the quantum dynamics follows the classical dynamics more closely, compared to $j = 10$.

3.3 Applications of Criteria: Quantum Signatures of Classical Bifurcations

Given our new criteria for quantum-classical correspondence, we would ideally like to use it to identify classical bifurcation behavior (as shown in Fig. 2.3) in the quantum dynamics.

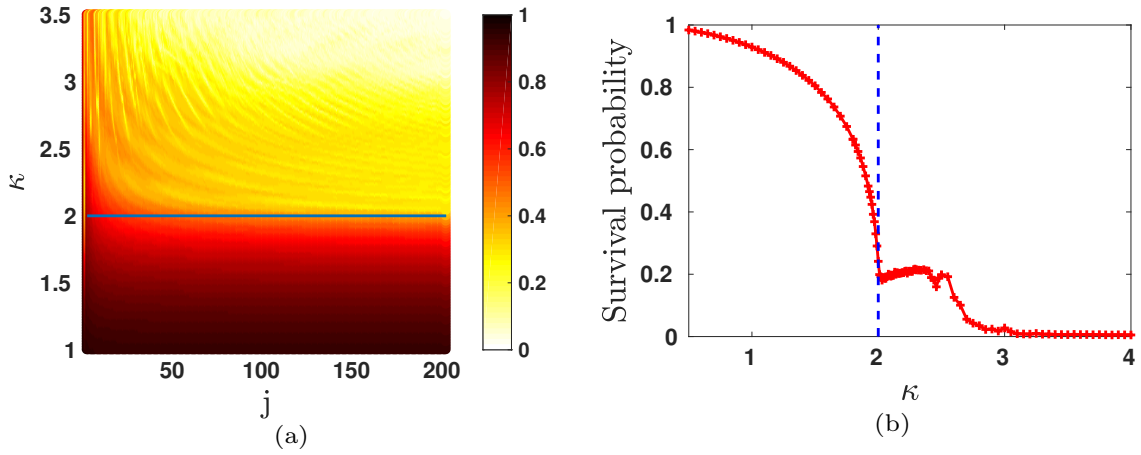

Figure 3.4: (a) Survival probability of an SCS initially centered on FP_1 (in Table 2.1), averaged over 50 kicks as a function of j and κ. The horizontal line depicts the classical bifurcation. Darker color represents higher survival probability in this plot. (b) Survival probability of an SCS initially centered on FP_1, averaged over 200 kicks for $j = 2000$ as a function of κ. The vertical dashed line represents the point of classical bifurcation.

To do so, we first define a measure of quantum dynamics that we can use to explore bifurcations.

The survival probability of a quantum state, $|\psi(0)\rangle$, at time t, evolving according to a unitary operator, $U(t)$ is given by $|\langle\psi(0)|\psi(t)\rangle|^2$, where $|\psi(t)\rangle = U(t)|\psi(0)\rangle$. We analyze here the time-averaged survival probability of quantum states of the kicked top centered on any point of a classical period-n orbit, where $n \geq 1$.

1. Given a classical fixed point, we compute the quantity,

$$S(L) = \frac{1}{L}\sum_{l=1}^{L} |\langle\psi(0)|\psi(l)\rangle|^2, \tag{3.3}$$

   for some L, where $|\psi(l)\rangle = U^l|\psi(0)\rangle$, and $|\psi(0)\rangle$ is the SCS centered on the classical fixed point. Here, U is the unitary operator for one time period of the Floquet system.

2. Given any classical period-n orbit, if F denotes the classical map, then each of the n points of the period-n orbit will be a fixed point of the map, F^n. Thus, we study the

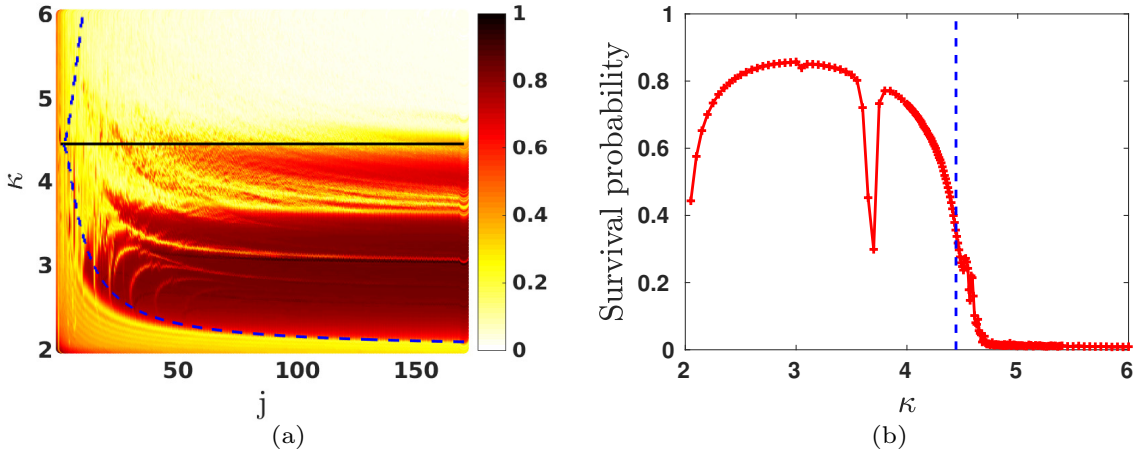

Figure 3.5: (a) Survival probability of SCS initially centered on $P2_A$ (in Table 2.1), averaged over 50 kicks as a function of j and κ. The horizontal line depicts the classical bifurcation, and the dashed curve represents the j value for a given κ at which the overlap between the two SCSs corresponding to $P2_A$ is $\leq 10^{-10}$. Darker color represents higher survival probability in this plot. (b) Survival probability of SCS initially centered on $P2_A$ averaged over 100 kicks for $j = 1000$ as a function of κ. The vertical dashed line represents the point of classical bifurcation.

survival probability of an SCS centered on any point of a classical period-n orbit using the unitary operator, U^n, instead of U. For a classical period-n orbit, we compute the quantity

$$S(L) = \frac{1}{L}\sum_{l=1}^{L} |\langle\psi(0)|\psi(nl)\rangle|^2, \tag{3.4}$$

for some L, where $|\psi(nl)\rangle = U^{nl}|\psi(0)\rangle$, and $|\psi(0)\rangle$ is the SCS centered at any point of the classical period-n orbit.

We have plotted the survival probabilities corresponding to FP_1, $P2_A$ and $P4$ of Table 2.1 in Figs. 3.4, 3.5 and 3.6 respectively. Each figure consists of two plots, one illustrating signatures of bifurcation in the deep quantum regime, and the other in the semiclassical regime. The classical bifurcation of FP_1, $P2_A$ and $P4$ was studied in Sec. 2.2.2. It was shown that FP_1 becomes unstable and bifurcates at $\kappa = 2$, $P2_A$ becomes unstable and bifurcates at $\kappa = \sqrt{2}\pi$, and $P4$ becomes unstable at $\kappa = \pi$.

(a) Analysis of FP_1 (Fig. 3.4): We see clear signatures of classical bifurcation of FP_1 at $\kappa = 2$ in the survival probability plots in Fig. 3.4 in a deep quantum regime as well as the semiclassical regime. The quantum state remains localized at the fixed point prior to bifurcation (because the fixed point is stable prior to bifurcation) and gets delocalized after bifurcation.

(b) Analysis of $P2_A$ (Fig. 3.5): In Fig. 3.5 (a), the classical bifurcation point (solid horizontal line) is easy to identify in the survival probability plot. Above this line, the survival probability is small, indicating that bifurcation has occurred. Below the horizontal line, however, there is some structure in the behavior of the survival probability. This can be understood in the following way. The two points associated with the period-2 orbit, $P2_A$ (Table 2.1), are κ-dependent. Thus, the j value at which the two SCSs centered at these two points are orthogonal to each other is also κ-dependent. The dashed curve in Fig. 3.5(a) represents the j value at which the overlap between the two aforementioned SCSs is less than 10^{-10} for the corresponding κ values. Below this curve, we see small survival probability. This is because of mixing of the quantum dynamics between the two SCSs because they are not orthogonal to each other. Hence for j values below the dashed curve the quantum dynamics does not mimic the corresponding classical dynamics in the period-2 orbit. Above the dashed curve, the quantum and classical dynamics should track, so there should be high survival probability (darker regions in the plot) below the classical bifurcation (solid line), and low survival probability above the bifurcation line. However there are also some lighter regions of low probability below the bifurcation line. One of the reasons for this is the quantum phenomenon of dynamical tunneling. Both the points of $P2_A$ are fixed points for the square of the classical map of the kicked top, thus allowing for dynamical tunneling between the two in addition to the period-2 motion between the two points.

In Fig. 3.5(b), for $j = 1000$ (semiclassical regime), the bifurcation at $\kappa = \sqrt{2}\pi$ is clearly visible. The initial dip in the curve close to $\kappa = 2$ is because of non-zero overlap between the two aforementioned SCSs for κ very close to 2. We also see a surprising dip in the survival probability around $\kappa = 3.7$ though the $P2_A$ orbit is still stable. Further investigation of the classical phase space of the kicked top near this value of κ reveals that a period-6 orbit arises near this period-2 orbit around $\kappa = 3.62$. This period-6 orbit breaks off to the chaotic sea near $\kappa = 3.68$, which results in the period-2 island in the phase space becoming smaller around $\kappa = 3.68$. Thus, the wave packet centered at the period-2 orbit delocalizes to some extent in the phase space around $\kappa = 3.68$. The size of the period-2 island increases again beyond $\kappa = 3.72$ which results in a higher survival probability beyond $\kappa = 3.72$ until bifurcation occurs. Dynamical tunnelling also occurs around $\kappa = 3.7$ to some extent, though the sum of the survival probability at the two

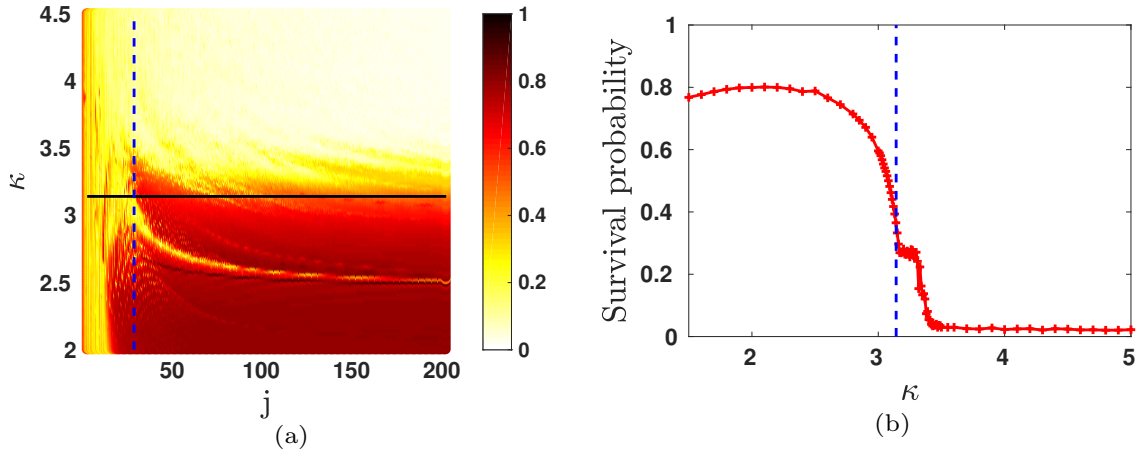

Figure 3.6: (a) Survival probability (3.4) of SCS initially centered on $P4$ (in Table 2.1), averaged over 50 kicks as a function of j and κ. The horizontal line depicts the classical bifurcation, and the vertical dashed line represents the j value at which the overlap between any two of the four SCSs corresponding to $P4$ is $\leq 10^{-8}$. Darker color represents higher survival probability in this plot. (b) Survival probability (3.4) of SCS initially centered on $P4$ averaged over 50 kicks for $j = 1000$ as a function of κ. The vertical dashed line represents the point of classical bifurcation.

points of the periodic orbit is not very close to 1 because of delocalization. These two points explain the dip at $\kappa = 3.7$ in Fig. 3.5(b). As κ increases, we clearly observe very small survival probability after the classical bifurcation point in the deep quantum regime as well as the semiclassical regime.

(c) Analysis of $P4$ (Fig. 3.6): The overlap between each pair of the four points associated with the period-4 orbit, $P4$ (Table 2.1), is less than 10^{-8} for $j \geq 27$. As explained for $P2_A$, mixing of dynamics can happen in $P4$ for small j values. For larger j compared to the critical value of j, we observe a clear signature of bifurcation in the survival probability plots.

We also note some general observations about the signatures of classical bifurcations in the quantum dynamics. The quantum dynamics changes smoothly with the classical bifurcations, unlike the classical dynamics that shows a sudden change. When any local bifurcation occurs that gives rise to new fixed points or periodic orbits, these new orbits are usually close to each other in the classical phase space, due to which the corresponding coherent states are not orthogonal to each other. As the bifurcation parameter (external

control parameter) is varied, these new orbits get further apart which decreases the overlap between the corresponding coherent states. Eventually, they may become orthogonal at which point the correspondence between classical and quantum dynamics near these orbits is restored (as long as other bifurcations do not occur prior to it). Alternatively, one could have increased the quantum number keeping the value of the external control parameter fixed. This explains why the quantum dynamics is affected smoothly by a classical bifurcation which gives rise to new fixed points or periodic orbits.

3.4 Summary

Quantum-classical correspondence for chaotic systems and for systems with a mixed phase space has remained a long-standing open question. Periodic orbits, and their stability and bifurcations play an important role in the transition from regular to chaotic behavior. Thus, gaining insight into quantum-classical correspondence in the vicinity of periodic orbits, and understanding the role of stability of periodic orbits and bifurcations on the quantum-classical correspondence is of vital importance. We have proposed criteria under which coherent states, which are the most classical states in quantum, evolve in close conjunction with classical dynamics for Floquet systems. These criteria can be used to find the magnitude of quantum numbers for which we observe a localized evolution of initial coherent states (spin coherent states in the case of spin systems) near stable periodic orbits in Floquet systems. Thus, our criteria helps us to quantify Bohr correspondence principle. Further, we illustrate these criteria in the model quantum kicked top. We note that in some situations quantum and classical dynamics may correspond even if our conditions are not met, but in general this will not be the case. Our studies of the kicked top seemed to indicate that such exceptions are not common. Additionally, our analysis shows that the survival probability of quantum states centered on the periodic orbits exhibits signatures of classical bifurcations, given the aforementioned criteria are satisfied. In the next chapter, we provide another application of our criteria. Whether high entanglement is a signature of chaos, specifically in a deep quantum regime, has been debated for a couple of decades. We use the criteria to explain when a system generates high versus low entanglement, and thus resolve the debates in the literature.

Chapter 4

Untangling Entanglement and Chaos using Fannes-Audenaert Inequality

This chapter is based on Kumari and Ghose [101].

Classical chaos is a well-defined property of nonlinear deterministic dynamical systems and is characterized by exponential instability due to sensitivity to initial conditions. On the other hand, entanglement is a purely quantum property. The relationship between the two has intrigued physicists for a couple of decades. We have explored the state of the art of this inquiry in the literature in Sec. 1.3.

Whether high entanglement can be considered as a hallmark of chaos has remained unclear even in a specific model such as the quantum kicked top [55, 29, 53, 61, 62, 30, 56]. In this chapter, we explain the puzzling connection between chaos and entanglement generation in spin systems. We provide a relationship between entanglement and trace distance with respect to spin coherent states. We untangle the much debated relationship between chaos and entanglement by making use of an intuitive picture provided by trace distance. We first provide a framework to determine an upper bound on the entanglement dynamics in any spin system with a constant angular momentum value j (symmetric multiqubit systems). Our framework helps to identify when the bound will remain low and limit the entanglement generated. We show that this is the case when the quantum states remain close to minimum-uncertainty classical-like spin-coherent states (SCSs). The bound grows as the distance between the quantum and classical states increases. Thus entanglement is associated with nonclassical dynamics and the breakdown of quantum-classical correspondence. This applies to both regular and chaotic systems.

We illustrate our framework and upper bound in the model quantum kicked top (QKT) system. We show that our bound provides a very good estimate of the entanglement generated in both regular and chaotic regions. We also analyze regular versus chaotic dynamics in the deep quantum and semiclassical regime, and show that entanglement remains low in regular regions only in a semiclassical regime. Our analysis resolves previous debates about the relationship between entanglement and chaos especially in a deep quantum regime corresponding to low quantum numbers. Furthermore, our framework can be used to obtain a computationally efficient loose bound on entanglement.

This chapter is organized as follows. In Sec. 4.1, we describe the Fannes-Audenaert inequality for the von Neumann entropy. We further introduce a framework to find an upper bound on entanglement in bipartite pure states using this inequality. The framework involves an arbitrary choice of pure state. In Sec. 4.2, we propose two choices of the pure state in the framework for spin systems. In Sec. 4.3, we illustrate that the upper bound obtained from the proposed framework, with our choice of pure states, provides a very good estimate of the entanglement in the model QKT. We also describe how this framework helps in reconciling the debates in the literature about the relationship between classical chaos and quantum entanglement. In Sec. 4.4, we summarize the results and some important characteristics of our proposed framework.

4.1 Finding an Upper Bound on Entanglement in Bipartite Systems

In this section, we provide a framework for obtaining an upper bound on entanglement in any pure bipartite state. Entanglement in any bipartite pure state can be exactly calculated using the von Neumann entropy, and this framework does not aim to provide an easier method to calculate entanglement. Rather, this framework helps us understand the mechanism of generation of entanglement in such systems and its relationship to the underlying classical dynamics of the system.

In 1973, M. Fannes proved an inequality for von Neumann entropy [102] in order to show that this entropy function is continuous. Consider two quantum states, ρ and σ, which belong to a Hilbert space of dimension $d < \infty$. Let $D(\rho, \sigma)$ be the trace distance

between ρ and σ,

$$\begin{aligned} D(\rho,\sigma) &= \frac{1}{2}||\rho-\sigma||_1 \\ &= \frac{1}{2}\sum_{i=1}^{d}|\lambda_i|, \end{aligned} \tag{4.1}$$

where λ_i's are the eigenvalues of $(\rho-\sigma)$. According to the Fannes' inequality, given that $D(\rho,\sigma) \leq 1/e$, then [33]

$$|S(\rho)-S(\sigma)| \leq D(\rho,\sigma)\log_2 d + \eta(D(\rho,\sigma)), \tag{4.2}$$

where $\eta(x) \equiv -x\log x$.

In 2007, KM Audenaert presented a generalized version of the Fannes' inequality, which is valid for the entire range of trace distance, $D(\rho,\sigma) \in [0,1]$, rather than being restricted to the range $[0,1/e]$ [103]. This generalized version is known as Fannes-Audenaert inequality for von Neumann entropy, and is given by

$$|S(\rho)-S(\sigma)| \leq D(\rho,\sigma)\log_2(d-1) + h(D(\rho,\sigma)), \tag{4.3}$$

where $h(x)$ is the binary entropy function,

$$h(x) = -x\log_2(x) - (1-x)\log_2(1-x). \tag{4.4}$$

Using the Fannes-Audenaert inequality, we provide a framework to find an upper bound on entanglement in any bipartite pure state. Given any bipartite pure quantum state $|\psi^{RS}\rangle$ belonging to a Hilbert space of dimension d^Rd^S, the entanglement in $|\psi^{RS}\rangle$ is given by the von Neumann entropy of the reduced state of either subsystem, that is, $S(\rho^R)$ or $S(\rho^S)$. We consider

$$E(|\psi^{RS}\rangle) = S(\rho^R). \tag{4.5}$$

Further, consider any pure state, $|\phi\rangle$, which belong to the Hilbert space of the subsystem R. The von Neumann entropy of any pure state is zero. Hence $S(|\phi\rangle\langle\phi|) = 0$. Using this in the Fannes-Audenaert inequality, we get

$$S(\rho^R) \leq D(\rho^R, |\phi\rangle\langle\phi|)\log_2(d^R-1) + h(D(\rho^R, |\phi\rangle\langle\phi|)). \tag{4.6}$$

Thus, we get an upper bound on the entanglement in the bipartite pure state $|\psi^{RS}\rangle$ described by the inequality

$$E(|\psi^{RS}\rangle) \leq D(\rho^R, |\phi\rangle\langle\phi|)\log_2(d^R-1) + h(D(\rho^R, |\phi\rangle\langle\phi|)), \tag{4.7}$$

where $|\phi\rangle$ is any pure state in the Hilbert space of the subsystem R. A good choice of the state $|\phi\rangle$ in (4.7) will lead to a tight upper bound for $E(|\psi^{RS}\rangle)$. The inequality would follow along similar lines with the choice of subsystem S instead of subsystem R in this framework. In this chapter, for convenience, we choose the subsystem with smaller dimension for obtaining the upper bound on entanglement.

4.2 Approximation of Entanglement in Spin Systems using the Upper Bound

In this section, we use the framework provided in the previous section to obtain a good estimate of entanglement in spin systems. We propose two physically relevant choices for the state $|\phi\rangle$ in (4.7), which gives us a tight upper bound as we will show in the QKT model.

Let us consider the systems whose Hamiltonians commute with the square of the total angular momentum operator J^2, that is,

$$[H, J^2] = 0.$$

As we discussed in Chapter 2, the angular momentum value j of a quantum state remains invariant under evolution with such Hamiltonians. Examples include Lipkin-Meshkov-Glick (LMG) model Hamiltonians [104, 105] and the QKT [70]. Such systems can be considered as $N = 2j$ multi-qubit systems evolving under its symmetric subspace as explained in Sec. 2.3. One can study entanglement in such systems in any bipartition of the N qubits, say $m{:}(N-m)$ bipartition where $m \in \{1, ..N-1\}$.

Our goal is to study the relationship between generation of entanglement in spin system and its corresponding classical dynamics. Specifically, given the initial quantum state is chosen to be any spin coherent state (SCS) described in Sec. 2.4, we study the entanglement between qubits in the evolving state and its relationship with the regular versus chaotic nature of the corresponding classical dynamics. As explained in 2.4, the SCS$|j, \theta, \phi\rangle$ is a product state of $2j$ spin-1/2 qubits (2.23) where the state of each qubit is $|\theta, \phi\rangle$ (2.24).

Consider an initial SCS that has evolved with the system Hamiltonian to the state $|\psi(t)\rangle$ after a time t. We propose two choices of state $|\phi\rangle$ in (4.7) to find an upper bound on entanglement in an $m{:}(N-m)$ bipartition of $|\psi(t)\rangle$.

1. Let
$$(\langle J_x\rangle, \langle J_y\rangle, \langle J_z\rangle) = (j\sin\Theta_{\text{ev}}\cos\Phi_{\text{ev}}, j\sin\Theta_{\text{ev}}\sin\Phi_{\text{ev}}, j\cos\Theta_{\text{ev}}),$$

where the expectation value of the angular momentum operators is with respect to $|\psi(t)\rangle$. The first choice of state $|\phi\rangle$, say $|\phi_1\rangle$, is the m-qubit reduced state of the SCS localized in the direction $(\Theta_{\text{ev}}, \Phi_{\text{ev}})$, that is,

$$|\phi_1\rangle = \text{Tr}_{\text{N-m}}\, \text{SCS}|j; \Theta_{\text{ev}}, \Phi_{\text{ev}}\rangle \equiv |\Theta_{\text{ev}}, \Phi_{\text{ev}}\rangle^{\otimes m} \tag{4.8}$$

where $|\Theta_{\text{ev}}, \Phi_{\text{ev}}\rangle$ is the state of a qubit (2.24).

2. Consider the classical evolution of the initial state for time t which yields the classical state $(J_x(t), J_y(t), J_z(t))$. Let

$$(J_x(t), J_y(t), J_z(t)) = (j \sin\Theta_{\text{cl}} \cos\Phi_{\text{cl}}, j \sin\Theta_{\text{cl}} \sin\Phi_{\text{cl}}, j\cos\Theta_{\text{cl}})$$

The second choice of state $|\phi\rangle$, say $|\phi_2\rangle$, is the m-qubit reduced state of the SCS localized in the direction $(\Theta_{\text{cl}}, \Phi_{\text{cl}})$, that is,

$$|\phi_2\rangle = \text{Tr}_{\text{N-m}}\, \text{SCS}|j; \Theta_{\text{cl}}, \Phi_{\text{cl}}\rangle \equiv |\Theta_{\text{cl}}, \Phi_{\text{cl}}\rangle^{\otimes m}. \tag{4.9}$$

$|\phi_1\rangle$ and $|\phi_2\rangle$ are clearly product states and thus their von Neumann entropy is zero. Let $\rho_m(t)$ be the m-qubit reduced state of $|\psi(t)\rangle$, that is,

$$\rho_m(t) = \text{Tr}_{N-m}\, |\psi(t)\rangle. \tag{4.10}$$

Let D_{re} be the minimum of

(a) the trace distance between $\rho_m(t)$ and $|\phi_1\rangle\langle\phi_1|$,

(b) the trace distance between $\rho_m(t)$ and $|\phi_2\rangle\langle\phi_2|$,

that is,

$$D_{\text{re}} = \min(D(\rho_m(t), |\phi_1\rangle\langle\phi_1|), D(\rho_m(t), |\phi_2\rangle\langle\phi_2|)). \tag{4.11}$$

The entanglement in the m:$(N-m)$ bipartition of $|\psi(t)\rangle$ is given by $S(\rho_m(t))$. Using D_{re} in (4.7), we get an upper bound on $S(\rho_m(t))$,

$$S(\rho_m(t)) \leq D_{\text{re}} \log_2(d-1) + h(D_{\text{re}}). \tag{4.12}$$

Here, d is the dimension of $\rho_m(t)$ (which can be less than 2^m owing to the symmetries of the state). Furthermore, the trace distance is non-increasing under partial trace [33]. This implies that

(a) $D(\rho_m(t), |\phi_1\rangle\langle\phi_1|) \leq D(|\psi(t)\rangle, \mathrm{SCS}|j;\Theta_{\mathrm{ev}},\Phi_{\mathrm{ev}}\rangle) \equiv D_{\mathrm{ev}}$, and

(b) $D(\rho_m(t), |\phi_2\rangle\langle\phi_2|) \leq D(|\psi(t)\rangle, \mathrm{SCS}|j;\Theta_{\mathrm{cl}},\Phi_{\mathrm{cl}}\rangle) \equiv D_{\mathrm{cl}}$.

Also, the RHS in the inequality in (4.12) is a monotonically increasing function of D_{re} up to a critical value D_{cr} given by

$$D_{\mathrm{cr}} \leq 1 - 1/d. \tag{4.13}$$

Thus, for $D_{\mathrm{ev}} \leq (1 - 1/d)$, $D_{\mathrm{ev}}\log_2(d-1) + h(D_{\mathrm{ev}})$ will serve as a loose bound on entanglement in (4.12) in the bipartition $m{:}(N-m)$ for all possible values of m. Hence, our framework can be used to obtain a computationally efficient but loose bound to the entanglement. This loose bound is numerically inexpensive to calculate for any $m{:}(N-m)$ bipartition in comparison to the von Neumann entropy and the RHS bound in (4.12).

The bound on entanglement in (4.12) demonstrates that the generation of entanglement in any system depends on the trace distance between relevant states. When the state remains close to the minimum uncertainty classical-like SCS, the entanglement remains low. As the trace distance from these SCS grows, the second and higher-order cumulants in the evolving state grow, leading to a divergence from classicality. This illustrates how a divergence from classicality is associated with the generation of entanglement. In the case of chaotic systems, the states do not remain close to SCS, even in the semiclassical regime. Thus, the bound goes to a maximum for chaotic systems.

We can understand the physical motivation of choosing the two SCSs described above from the Ehrenfest correspondence principle, which examines when the expectation values of observables obey the classical equations of motion. Let us consider the initial state, $(X(0), Y(0), Z(0))$ and the corresponding $\mathrm{SCS}|j;\theta(0),\phi(0)\rangle$. The classical state $(X(0), Y(0), Z(0))$ evolves via the classical equation of motion to the state $(X(t), Y(t), Z(t))$ in a time t. The quantum state $\mathrm{SCS}|j;\theta(0),\phi(0)\rangle$ evolves to $|\psi(t)\rangle$ via the Schrodinger equation in a time t. According to the Ehrenfest correspondence principle,

$$(\langle X\rangle_{|\psi(t)\rangle}, \langle Y\rangle_{|\psi(t)\rangle}, \langle Z\rangle_{|\psi(t)\rangle}) \approx (X(t), Y(t), Z(t))$$

up to Ehrenfest's time scale. The first choice, $\mathrm{SCS}|j;\Theta_{\mathrm{ev}},\Phi_{\mathrm{ev}})$, is the quantum state localized in the direction $(\langle X\rangle_{|\psi(t)\rangle}, \langle Y\rangle_{|\psi(t)\rangle}, \langle Z\rangle_{|\psi(t)\rangle})$. The second choice, $\mathrm{SCS}|j;\Theta_{\mathrm{cl}},\Phi_{\mathrm{cl}}\rangle$, is the quantum state localized in the direction $(X(t), Y(t), Z(t))$.

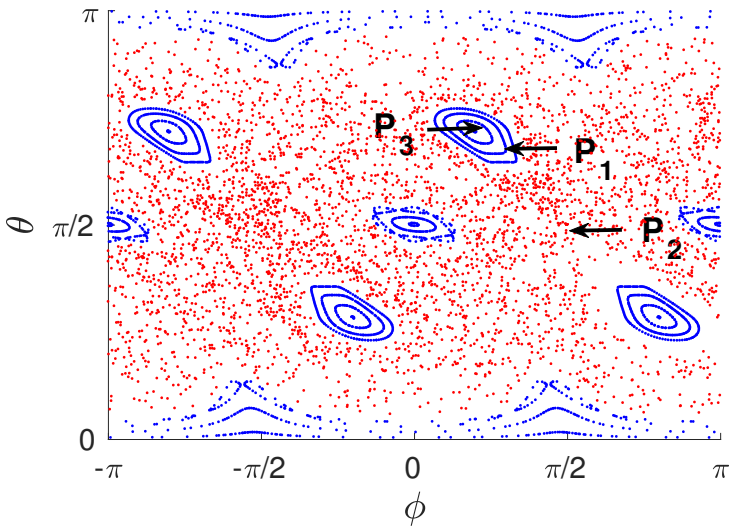

Figure 4.1: Classical stroboscopic map for the kicked top showing a mixed phase space of regular (blue) islands in a chaotic (red) sea. P_1, P_2 and P_3 are 3 points corresponding to $(\theta, \phi) = (2.1, 0.9), (1.5, 1.5)$ and $(2.25, 0.75)$ respectively. $\kappa = 3$, $p = \pi/2$, and $\tau = 1$.

4.3 Entanglement in the QKT

In this section, we apply the framework proposed in the previous section to the model QKT. We illustrate that the upper bound on entanglement given in (4.12) is a tight bound and hence a good estimator of entanglement in the QKT. Furthermore, we show how this framework is useful in resolving the debates in the literature about the relationship between entanglement and classical chaos.

We study 1:$(N-1)$ and 2:$(N-2)$ partition entanglement in the QKT (where $N = 2j$), measured by $S(\rho^A)$ and $S(\rho^{AA})$ respectively. Since the qubits are indistinguishable in the QKT, we use the notation ρ^{AA} for any two-qubit reduced state of the QKT. ρ^{AA} lies in the $j = 1$ symmetric subspace and thus has dimension $d = 3$ instead of 4. We consider the evolution of an initial SCS $|j; \theta, \phi\rangle$, and compute $S(\rho^A)$, $S(\rho^{AA})$, and the corresponding upper bounds using (4.12). We study this in the deep quantum regime as well as in the semiclassical regime for an initial state in the regular region (point P_1 in Fig. 4.1) and an initial state in the chaotic region (point P_2 in Fig. 4.1). Figure 4.2 shows the evolution for P_1, and Fig. 4.3 shows the evolution for P_2. In both the figures, we observe that the entanglement in the QKT almost saturates the upper bound on entanglement calculated

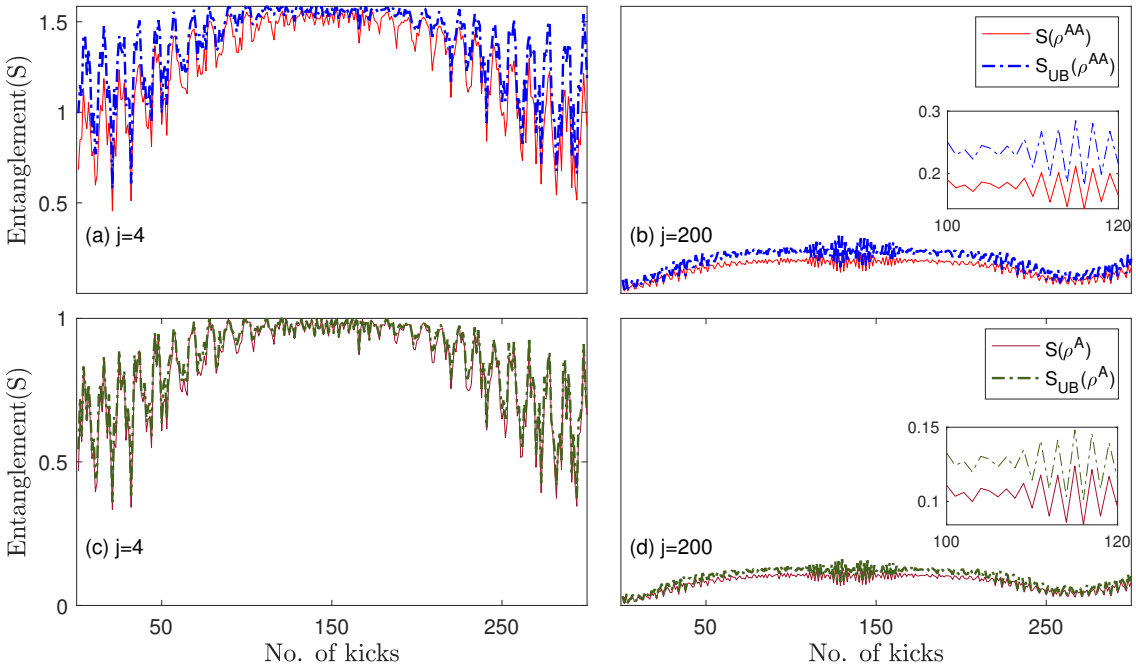

Figure 4.2: Evolution of QKT entanglement and the upper bound in (4.12) for an initial state in the regular region, P_1 in Fig. 4.1. (a) 2:$(N-2)$ entanglement for $j = 4$, (b) 2:$(N-2)$ entanglement for $j = 200$, (c) 1:$(N-1)$ entanglement for $j = 4$, and (d) 1:$(N-1)$ entanglement for $j = 200$. The upper bound on entanglement is almost saturated by the entanglement generated in the kicked top.

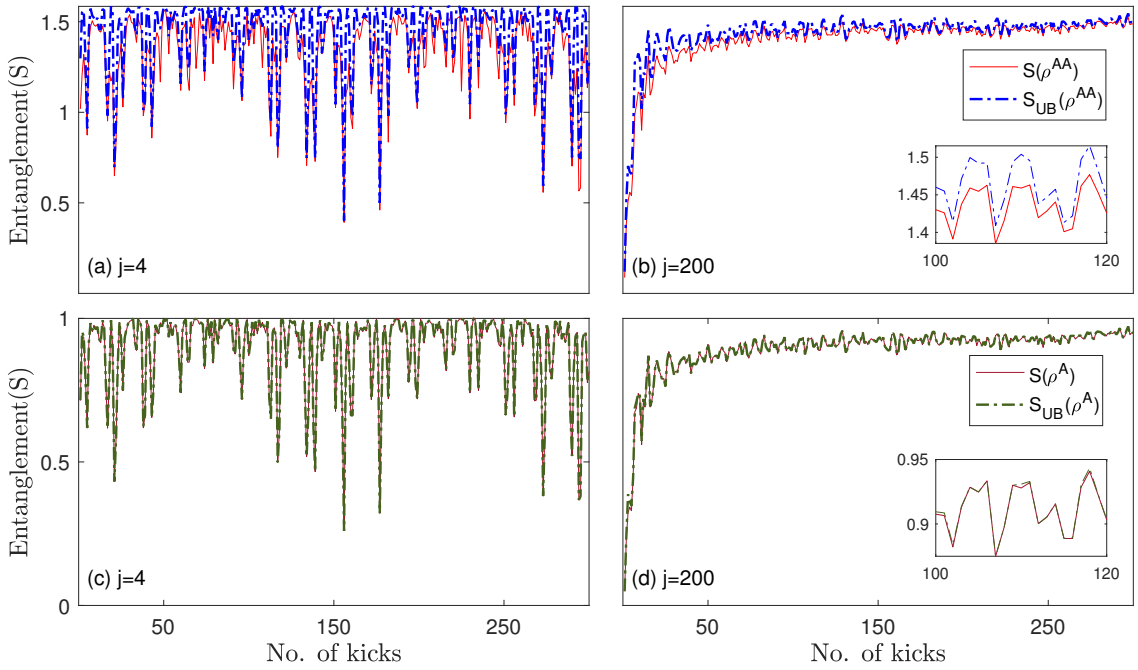

Figure 4.3: Evolution of QKT entanglement and the upper bound in (4.12) for an initial state in the chaotic region, P_2 in Fig. 4.1. (a) 2:$(N-2)$ entanglement for $j = 4$, (b) 2:$(N-2)$ entanglement for $j = 200$, (c) 1:$(N-1)$ entanglement for $j = 4$, and (d) 1:$(N-1)$ entanglement for $j = 200$. The upper bound on entanglement is almost saturated by the entanglement generated in the kicked top.

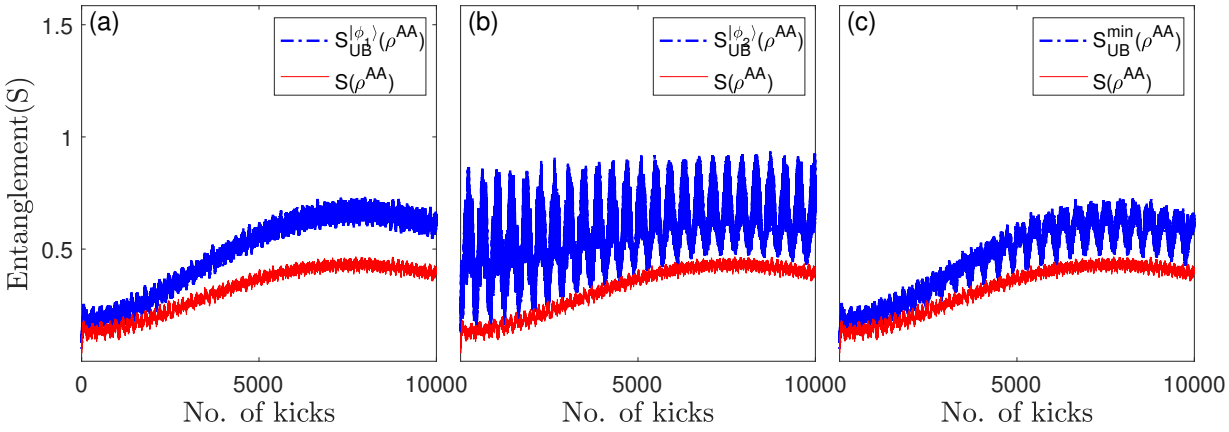

Figure 4.4: Comparison of the upper bounds on entanglement using $|\phi_1\rangle$ (4.8) and $|\phi_2\rangle$ (4.9) for $|\phi\rangle$ in (4.7) for an initial state in the regular region, P_3 in Fig. 4.1 for $j = 100$. (a) Left column: Evolution of exact 2:$(N-2)$ QKT entanglement versus the upper bound on entanglement using $|\phi_1\rangle$. (b) Middle column: Evolution of exact 2:$(N-2)$ QKT entanglement versus the upper bound on entanglement using $|\phi_2\rangle$. Right column: Evolution of exact 2:$(N-2)$ QKT entanglement versus the upper bound on entanglement in (4.12) using the state, $|\phi_1\rangle$ or $|\phi_2\rangle$, whichever has minimum trace distance with $\rho^{AA}(t)$. It also shows the long term evolution of QKT entanglement and the upper bound in (4.12).

using (4.12). Thus, our upper bound provides a very good estimate for the 1:$(N-1)$ and 2:$(N-2)$ partition entanglement in the QKT both in the deep quantum regime as well as the semiclassical regime irrespective of the underlying classical behavior (regular or chaotic).

Figure 4.4 shows the comparison of the upper bounds (for 2:$(N-2)$ entanglement) using both the choices of $|\phi\rangle$ in (4.7), that is $|\phi_1\rangle$ and $|\phi_2\rangle$, for the initial state P_3 in Fig. 4.1. We observe that the choice $|\phi_1\rangle$ generally provides a good upper bound, but combining both the choices indeed provides a better upper bound, which results in a good estimate of the actual entanglement in the QKT. The long-time evolution (Fig. 4.4(c)) results in a small deviation between the upper bound and the actual entanglement. Nevertheless, the deviation is not large, and the upper bound remains a good estimate of the entanglement.

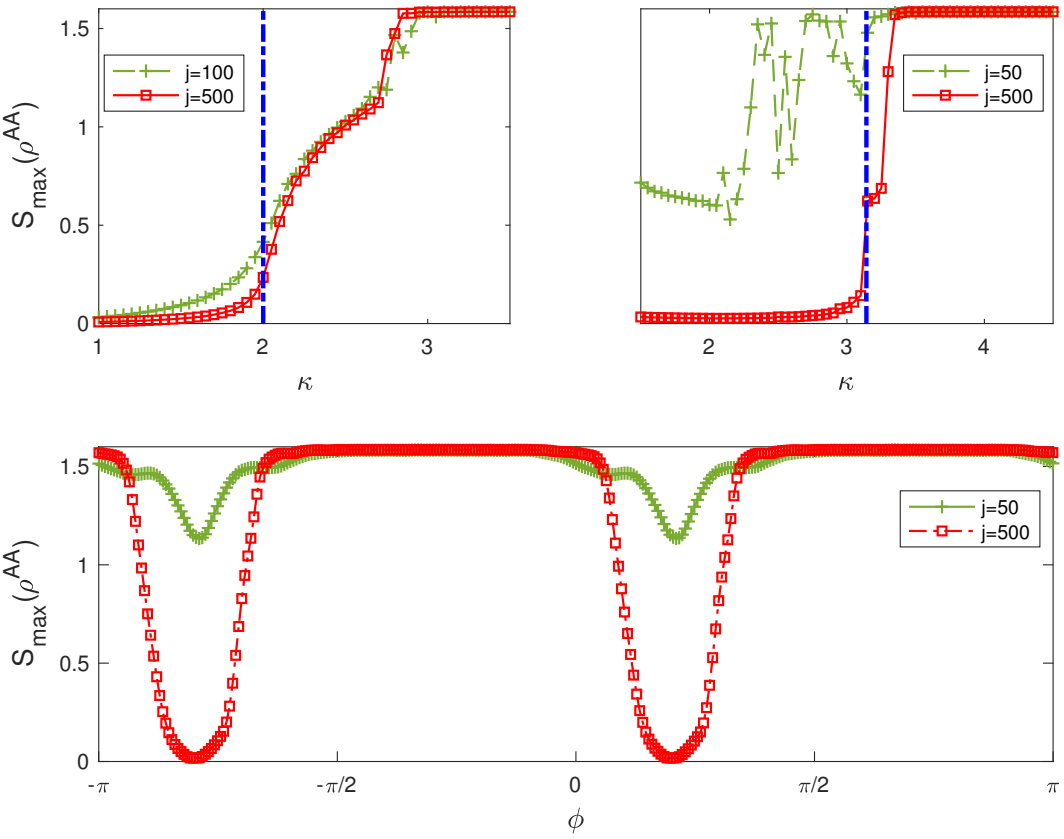

Figure 4.5: Maximum 2:$(N-2)$ partition entanglement over 5000 kicks in the kicked top (a) as a function of κ where the initial state is centered at fixed point, FP_1, which loses stability at $\kappa = 2$, (b) as a function of κ where the initial state is centered at a period-4 orbit, $P4$, which loses stability at $\kappa = \pi$, and (c) as a function of initial condition (θ, ϕ) where $\theta = 2.25$ is fixed and ϕ is varied, $\kappa = 3$. The vertical dotted dashed lines in panels (a) and (b) depicts the κ value at which bifurcation leads to loss of stability of these orbits.

Reconciling the debates in the literature

We now explore the connections between chaos and entanglement in periodically driven (Floquet) spin systems. Though several previous studies have explored whether entanglement exhibits signatures of chaos, there is a still a lack of consensus about this question, even in a specific model such as the QKT. In this model, entanglement was shown to display signatures of chaos in numerical and experimental studies even in a very deep quantum regime such as $j = 3/2, 3$ and, 4 [54, 55, 29, 30]. While these studies showed higher time-averaged entanglement in chaotic regions compared to regular regions, Lombardi *et.al.* [53, 62] found instances of initial states in regular regions that also led to generation of high entanglement. On the other hand, Ruebeck et. al [56] correlated classical regular dynamics with low or high time-averaged entanglement, and chaos with medium level of entanglement in the deepest possible quantum regime of the QKT, $j = 1$. These studies suggest that the relationship between entanglement and classical dynamics is largely debated in the regular regions. The effect of chaos on the generation of entanglement can be untangled only when the effect of regular dynamics on the generation of entanglement is well understood. Hence, we clarify the connection between entanglement and chaos by explaining the dynamics in the regular regions and then comparing it to the more well-studied chaotic case, in both quantum and semiclassical regimes. By considering the divergence of the quantum states from SCSs in regular versus chaotic regions, we resolve these seemingly conflicting studies.

Our analysis shows that in the deep quantum regime where j is small, the upper bound on the entanglement can be large in both regular and chaotic regions, whereas in a semiclassical regime with higher j, the bound on entanglement remains lower in regular regions near stable periodic orbits than in chaotic regions (see Figs. 2 and 3). We first discuss the deep quantum regime where j is very small. In Chapter 3, we presented criteria for determining the magnitude of the quantum number j at which quantum-classical correspondence will be observed near stable classical periodic orbits. The criteria require that the SCSs centered on all the points in a periodic orbit be almost orthogonal to each other (overlap of order roughly less than 10^{-10}) in order to observe a correspondence between the classical and the quantum dynamics near the periodic orbits on time scales sufficiently long compared to the dynamics. When these criteria are satisfied near stable classical periodic orbits, the evolved states remain close to the SCSs, and thus the bound on entanglement in (4.12) remains small.

However, in a deep quantum regime, our criteria for quantum-classical correspondence are typically violated. The states diverge from the SCSs and this results in a higher upper bound on entanglement in (4.12) in both regular and chaotic regions. For example, the

period-4 orbit, $P4$, violates the criteria for $j \lesssim 20$ (Sec. 3.2.1), where $P4$ is $(1,0,0) \to (0,0,-1) \to (-1,0,0) \to (0,0,1) \to (1,0,0)$ [$(\cdot,\cdot,\cdot)$ refers to the classical coordinates (X,Y,Z), refer Table 2.1]. Thus the states do not remain close to SCSs and entanglement can be large even close to the regular periodic orbit. In [56], the high entanglement regions identified in the QKT for $j = 1$ are precisely the regions in the vicinity of the period-4 orbit. Our discussion above explains why high entanglement in these regular regions of the kicked top was observed in a deep quantum regime in [56].

While large entanglement can be generated in both regular and chaotic regions in the deep quantum regime, the situation changes in the semiclassical regime of large j. In general, a regular region in Floquet systems consists of stable periodic orbits, while chaotic regions emerge around the unstable periodic orbits. The criteria for quantum and classical-like states to remain close are satisfied in regular regions but not in chaotic regions in the semiclassical regime. In the QKT, consider the fixed point, FP_1 $(0,1,0)$, and the period-4 orbit, $P4$, which lose stability at $\kappa = 2$ and π respectively 2.2.2. Figures 4.5(a) and 4.5(b) show that when these orbits are stable, they exhibit very low entanglement for high j values corresponding to the semiclassical limit. In Fig. 4.5(c), the maximum 2:$(N-2)$ entanglement over 5000 kicks is plotted for a range of initial conditions (θ,ϕ). The maximum entanglement remains very low in regular regions for $j = 500$ but not for $j = 50$, while chaotic regions always exhibit high entanglement. The same characteristics are seen in Figs. 4.2 and 4.3.

4.4 Summary

We have presented a general framework to obtain an upper bound on the entanglement in any bipartition of a spin system that preserves the collective angular momentum value j of any initial quantum state. Our framework shows that entanglement generation is associated with a divergence from minimum-uncertainty classical-like spin coherent states (SCSs) as measured by the trace distance. We illustrated in the quantum kicked top (QKT) model that our upper bound estimates the entanglement extremely well in regular as well as chaotic regions for j values in the deep quantum regime as well as the semiclassical regime. This demonstrates that the magnitude of entanglement generation can be inferred from the trace distance between the evolved state and the SCSs. This trace distance, in turn, can be inferred from the localized versus delocalized evolution of the system in the Husimi phase space. Our criteria in Chapter 3 for quantum-classical correspondence in periodically driven systems can be used to determine the quantum numbers for which the evolution is localized versus delocalized. Thus, our framework combined with the afore-

mentioned criteria provides a clear and more nuanced understanding of the relationship between entanglement generation and the underlying classical dynamics, compared to previous studies.

By relating entanglement to the trace distance, our work provides insight and intuition about the quantum-classical connection. It shows that entanglement, a purely quantum phenomenon, grows when the quantum evolution diverges from nearby classical evolution as measured by the trace distance. Thus as the distance between quantum and classical evolution grows, quantum properties like entanglement grow as one might expect. Our analysis makes this argument clear and more quantitative, and explains previous seemingly contradicting results about chaos and entanglement.

Our approach and framework has many interesting characteristics.

(a) This framework is very useful for systems with mixed phase space, which are in general difficult to deal with.

(b) Whereas past studies have often focused on the linear entropy, which is an approximation of the von Neumann entropy to measure entanglement, our bound applies directly to the von Neumann entropy.

(c) Our framework can be used to estimate the entanglement for any bipartition of the system.

(d) While any pure state of dimension d in place of ρ_m^{SCS} would provide an upper bound on the entanglement in the relevant bipartition, our chosen SCSs provide a very good estimate of the actual entanglement. These states are chosen without any optimization and with physical motivation from the Ehrenfest correspondence principle. The particular choice of SCS is not critical in chaotic regions since they generate near to maximal entanglement and hence a large upper bound. However, the choice of SCS is significant in regular regions to obtain a tight bound in order to tease out the differences between regular and chaotic behavior.

Our approach also provides a way to efficiently estimate a loose upper bound for entanglement in spin systems and is thus of interest for experiments, where entanglement is challenging to measure. Our results not only provide insights into the fundamental connections between chaos and entanglement, but are also relevant for applications in condensed matter and quantum computing.

Chapter 5

Nonlocal Correlations in the QKT

This chapter is based on Kumari, Ghose and Mann [106, 107].

In the previous chapters, we studied the quantum dynamics in the quantum kicked top (QKT) in comparison to its classical dynamics. Furthermore, we studied how classical dynamics affects the generation of quantum entanglement in the QKT. In this chapter, we study nonlocality in the QKT. The relationship between nonlocal correlations and the classical dynamics of any system has not received much attention in the literature, unlike quantum entanglement. Since nonlocality and entanglement are inequivalent quantum correlations [108], a separate study is required to understand the relationship between the classical dynamics of any collective spin system and the generation of nonlocality in that system. It is important to note here that only a multi-qubit QKT can generate nonlocal quantum states. A QKT with a single spin-j cannot be nonlocal because nonlocal correlations can only be defined with respect to different particles or subsystems. In this chapter, we study nonlocality in a multi-qubit QKT governed by the multi-qubit Hamiltonian (2.19). Since there is a correspondence between the multi-qubit representation for symmetric states and the collective spin representation, both of them have been used interchangeably in the text.

The Clauser-Horne-Shimony-Holt (CHSH) inequality and Svetlichny inequality are well known generalizations of Bell inequalities whose violation by any quantum state implies the existence of nonlocal correlations in that quantum state [32]. In this chapter, we first numerically investigate bipartite nonlocal correlations using the CHSH correlation function in

(a) 2-qubit pure states for $j = 1$ QKT, and

(b) 2-qubit reduced states of the QKT for $j \geq 3/2$.

Furthermore, we also study multipartite nonlocal correlations using Svetlichny correlation function in

(a) 3-qubit and 4-qubit pure states for $j = 3/2$ and $j = 2$ QKT respectively, and

(b) 3-qubit reduced states of the QKT for $j \geq 2$.

Our studies show that the pure states for $j = 1, 3/2$ and 2, the QKT often exhibit nonlocal correlations. On the other hand, we observe that the 2-qubit and 3-qubit reduced states of the QKT do not violate the CHSH inequality and Svetlichny inequality respectively. We also analytically prove that any 2-qubit reduced state of multiqubit symmetric pure states cannot violate the CHSH inequality. We further show that dynamical tunnelling in the QKT leads to generation of multiqubit Greenberger-Horne-Zeilinger (GHZ)-like states. These GHZ-like states belong to a general class of states that we refer to as N-qubit antipodal GHZ states. We analytically prove that these states violate the N-qubit Svetlichny's inequality maximally.

We numerically and analytically explore two aspects of nonlocality in this chapter - nonlocality in the reduced states, and nonlocality in the pure states of the QKT. First, we review the Bell inequalities, namely the CHSH inequality and Svetlichny inequality for $2-$qubit states and $N-$qubit states respectively in Sec. 5.1. We begin our analysis of nonlocality in the QKT in Sec. 5.2 where we numerically show that the pure states in the QKT often violate the Bell inequalities while the reduced states do not violate them. Sections 5.3 and 5.4 focuses on developing an analytical understanding of the numerical results in Sec. 5.2 for the reduced states of the QKT. In Sec. 5.3, we review symmetric extension of quantum states - a concept that is required for the next section, in which we formulate and prove two theorems related to the CHSH inequality. These theorems prove that any $2-$qubit mixed state which has a symmetric extension or a symmetric purification cannot violate the CHSH inequality, and hence explain the numerical results in section 5.2. Next, we pursue a better understanding of nonlocality in the pure states of the QKT in Secs. 5.5 and 5.6. In Sec. 5.5, we numerically show that dynamical tunnelling in the QKT can lead to generation of GHZ-like states. In Sec. 5.6, we show that these GHZ-like states belong to a larger class of states that we define as $N-$qubit antipodal GHZ states. We further analytically prove that this class of states exhibits maximal nonlocal correlations. In Sec. 5.7, we briefly summarize and discuss the results.

5.1 Bell Inequalities

Bell inequalities are the most famous identifier and quantifier of nonlocal correlations in quantum states [32]. Specifically, the CHSH (Clauser-Horne-Shimony-Holt) inequality is a Bell inequality for 2−qubit states [109]. Svetlichny inequalities generalize the CHSH inequality to $N-$qubit states for any $N > 2$ [110].

5.1.1 CHSH inequality

The CHSH correlation function for a 2-qubit quantum state, ρ, is written as:

$$\text{CHSH}(\rho) = \max_{A_1,A_2,B_1,B_2} \text{Tr}\left((A_1B_1 + A_1B_2 + A_2B_1 - A_2B_2)\rho\right) \tag{5.1}$$

where A_1 and A_2 are operators acting on the first qubit of ρ, and B_1 and B_2 are operators acting on the second qubit of ρ. These operators have eigenvalues $+1$ and -1. For any 2-qubit state ρ, the CHSH correlation function (5.1) can be written analytically [109] as

$$\text{CHSH}(\rho) = 2\sqrt{u+v} \tag{5.2}$$

where u and v are the largest and the second largest eigenvalues of the 3×3 matrix $\tilde{T} = T^T T$, whose entries are

$$T_{ij} = \text{Tr}\left((\sigma_i \otimes \sigma_j)\rho\right), \tag{5.3}$$

with σ_i, σ_j being the Pauli matrices. Note that (5.2) does not need any optimization over the set of operators. The CHSH inequality is given by

$$\text{CHSH}(\rho) \leq 2. \tag{5.4}$$

Violation of (5.4) by any 2-qubit state implies that it cannot be described by any local hidden variable (LHV) model and hence exhibits nonlocal correlations. The normalized CHSH correlation function is

$$\overline{\text{CHSH}}(\rho) = \sqrt{u+v} \tag{5.5}$$

and $\overline{\text{CHSH}}(\rho) > 1$ implies the existence of nonlocal correlations in ρ. Thus, the normalized CHSH inequality is given by

$$\overline{\text{CHSH}}(\rho) \leq 1. \tag{5.6}$$

5.1.2 Svetlichny inequality

Svetlichny inequality is a Bell-type inequality for multi-qubit states. Its violation by any quantum state implies the existence of genuine multipartite nonlocal correlations. For N-qubit states, the Svetlichny operator is given by [110, 111]

$$S_N = \sum_I \nu_{t(I)} A^{(1)}_{i_1} .....A^{(N)}_{i_N}, \tag{5.7}$$

where I is the sequence $\{i_1, i_2, ..., i_N\}$ (where $i_k \in \{1, 2\}$), $t(I)$ is the number of times 2 appears in the sequence I, $\nu_{t(I)}$ is the sequence $(-1)^{t(I)*(t(I)-1)/2}$, and A_{i_k}'s are dichotomic observables with eigenvalues $+1$ and -1. For instance, the Svetlichny operator for $3-$qubit and $4-$qubit states are respectively given by

$$\begin{aligned} S_3 \;=\; & A^{(1)}_1 A^{(2)}_1 A^{(3)}_1 + A^{(1)}_1 A^{(2)}_1 A^{(3)}_2 + A^{(1)}_1 A^{(2)}_2 A^{(3)}_1 - A^{(1)}_1 A^{(2)}_2 A^{(3)}_2 \\ & + A^{(1)}_2 A^{(2)}_1 A^{(3)}_1 - A^{(1)}_2 A^{(2)}_1 A^{(3)}_2 - A^{(1)}_2 A^{(2)}_2 A^{(3)}_1 - A^{(1)}_2 A^{(2)}_2 A^{(3)}_2 \end{aligned}$$

and

$$\begin{aligned} S_4 \;=\; & A^{(1)}_1 A^{(2)}_1 A^{(3)}_1 A^{(4)}_1 + A^{(1)}_1 A^{(2)}_1 A^{(3)}_1 A^{(4)}_2 + A^{(1)}_1 A^{(2)}_1 A^{(3)}_2 A^{(4)}_1 - A^{(1)}_1 A^{(2)}_1 A^{(3)}_2 A^{(4)}_2 \\ & + A^{(1)}_1 A^{(2)}_2 A^{(3)}_1 A^{(4)}_1 - A^{(1)}_1 A^{(2)}_2 A^{(3)}_1 A^{(4)}_2 - A^{(1)}_1 A^{(2)}_2 A^{(3)}_2 A^{(4)}_1 - A^{(1)}_1 A^{(2)}_2 A^{(3)}_2 A^{(4)}_2 \\ & + A^{(1)}_2 A^{(2)}_1 A^{(3)}_1 A^{(4)}_1 - A^{(1)}_2 A^{(2)}_1 A^{(3)}_1 A^{(4)}_2 - A^{(1)}_2 A^{(2)}_1 A^{(3)}_2 A^{(4)}_1 - A^{(1)}_2 A^{(2)}_1 A^{(3)}_2 A^{(4)}_2 \\ & - A^{(1)}_2 A^{(2)}_2 A^{(3)}_1 A^{(4)}_1 - A^{(1)}_2 A^{(2)}_2 A^{(3)}_1 A^{(4)}_2 - A^{(1)}_2 A^{(2)}_2 A^{(3)}_2 A^{(4)}_1 + A^{(1)}_2 A^{(2)}_2 A^{(3)}_2 A^{(4)}_2 \end{aligned}$$

where A^k is the dichotomic observable corresponding to the k^{th} qubit. For any quantum state $|\psi\rangle$, Svetlichny's inequality is given by

$$|\langle S_N \rangle_{|\psi\rangle}| \leq 2^{N-1}. \tag{5.8}$$

The normalized version of the Svetlichny operator (5.7) corresponds to

$$\bar{S}_N = \frac{1}{2^{N-1}} S_N \tag{5.9}$$

and so violation of the inequality

$$\max |\langle \bar{S}_N \rangle_{|\psi\rangle}| \leq 1, \tag{5.10}$$

by any N-qubit quantum state implies that it has genuine $N-$qubit nonlocality. The maximum possible violation $|\langle \bar{S}_N \rangle_{|\psi\rangle}| = \sqrt{2}$.

Unlike the CHSH inequality, an analytic formula for Svetlichny inequality is not known for general N-qubit states but only for a very few states [112, 113].

5.2 Nonlocality Generation in the QKT

In this section, we investigate numerically whether the states generated by the QKT Hamiltonian exhibit nonlocal correlations. We study this using the normalized Bell inequalities summarized in the previous section. If the value of the normalized Bell correlation function for any quantum state is greater than 1, then there exists nonlocal correlations in that quantum state.

First, we study the nonlocal correlations in the $2-$qubit reduced states for $j \geq 3/2$ QKT using the normalized CHSH correlation function (5.5). Our numerical study indicates there is no violation of the normalized CHSH inequality (5.6) by these states. As an example, we illustrate the evolution of the normalized CHSH correlation function for the $2-$qubit reduced states of $j = 10$ QKT in Figs. 5.1(a) and (b) for the SCS centered at the fixed point FP_1 (refer Table 2.1). Our results in Sec. 5.4 explains these numerical observations where we prove that any $2-$qubit state having a symmetric extension cannot violate the CHSH inequality. The notion of symmetric extension of quantum states is reviewed in 5.3.

We also study nonlocal correlations in the $3-$qubit reduced states for $j \geq 2$ QKT using the normalized Svetlichny correlation function (5.9). We do not observe any violation of the normalized Svetlichny inequality (5.10) by these states. In Figs. 5.1(c) and (d), we illustrate the evolution of the normalized Svetlichny correlation function for the $3-$qubit reduced states of $j = 10$ QKT for the SCS centered at the fixed point FP_1.

Next, we study the nonlocal correlations in the pure states evolving unitarily with the QKT Hamiltonian for $j = 1, 1.5$ and 2 (corresponding to $2-$qubit, $3-$qubit and $4-$qubit QKT respectively). Our study shows that these pure states often exhibit nonlocal correlations. In Fig. 5.2, we illustrate the results for an initial state corresponding to the SCS centered at FP_1. Recall from Sec. 2.2.2 that FP_1 is a fixed point which is stable for $\kappa \leq 2$ and unstable for $\kappa > 2$. Figures 5.2(b), (d) and (f) show that there are significant violations of the normalized Bell inequalities by the evolving states (though with a lot of fluctuations) when FP_1 is unstable. Hence, they exhibit significant nonlocal correlations (multipartite for $j = 1.5$ and 2) . Instability of the fixed point ensures chaos in its vicinity in the classical phase space. Thus, these results suggest that chaos may generate multipartite nonlocal correlations in spin systems.

Figures 5.2(a), (c) and (d) correspond to the evolution of stable FP_1. Stability of the fixed point ensures regular behavior in its vicinity in the classical phase space. As we have seen in chapter 4, the study of quantum correlations corresponding to regular classical dynamics is much more nuanced than the chaotic dynamics, especially in a deep quantum regime (which corresponds to small j values in the case of the QKT). The behavior of Bell

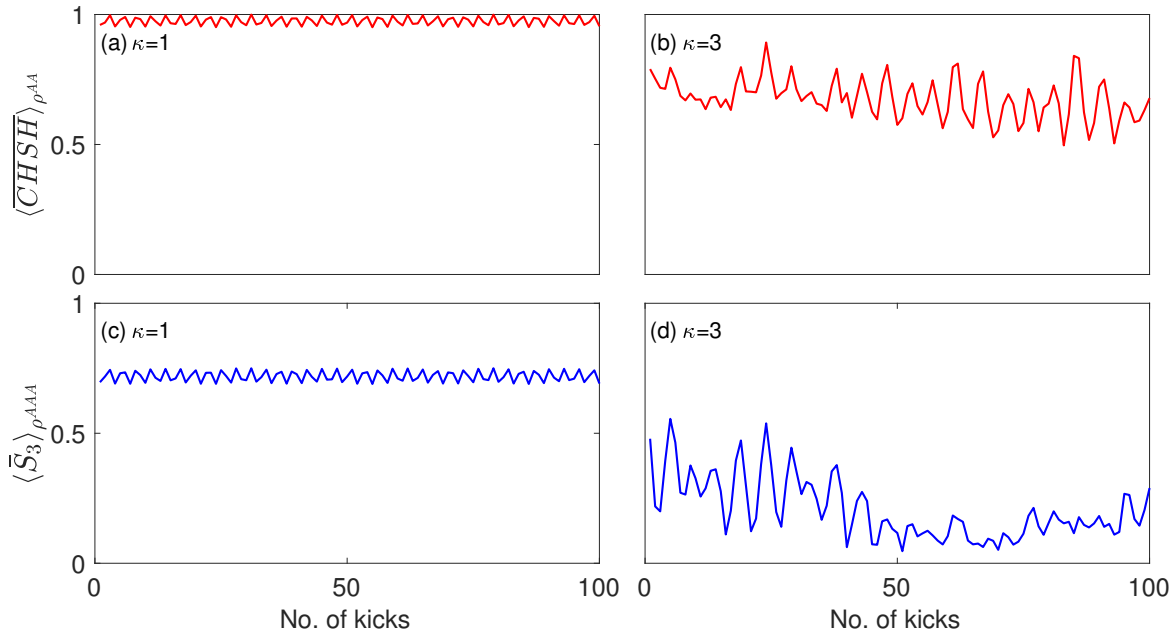

Figure 5.1: Evolution of normalized CHSH and Svetlichny correlation functions for 2−qubit and 3−qubit reduced states respectively for j=10 QKT for $\kappa = 1$ and 3. Initial state: SCS$|10; \frac{\pi}{2}, \frac{\pi}{2}\rangle$ (SCS corresponding to FP_1). FP_1 is stable for $\kappa = 1$ and unstable for $\kappa = 3$.

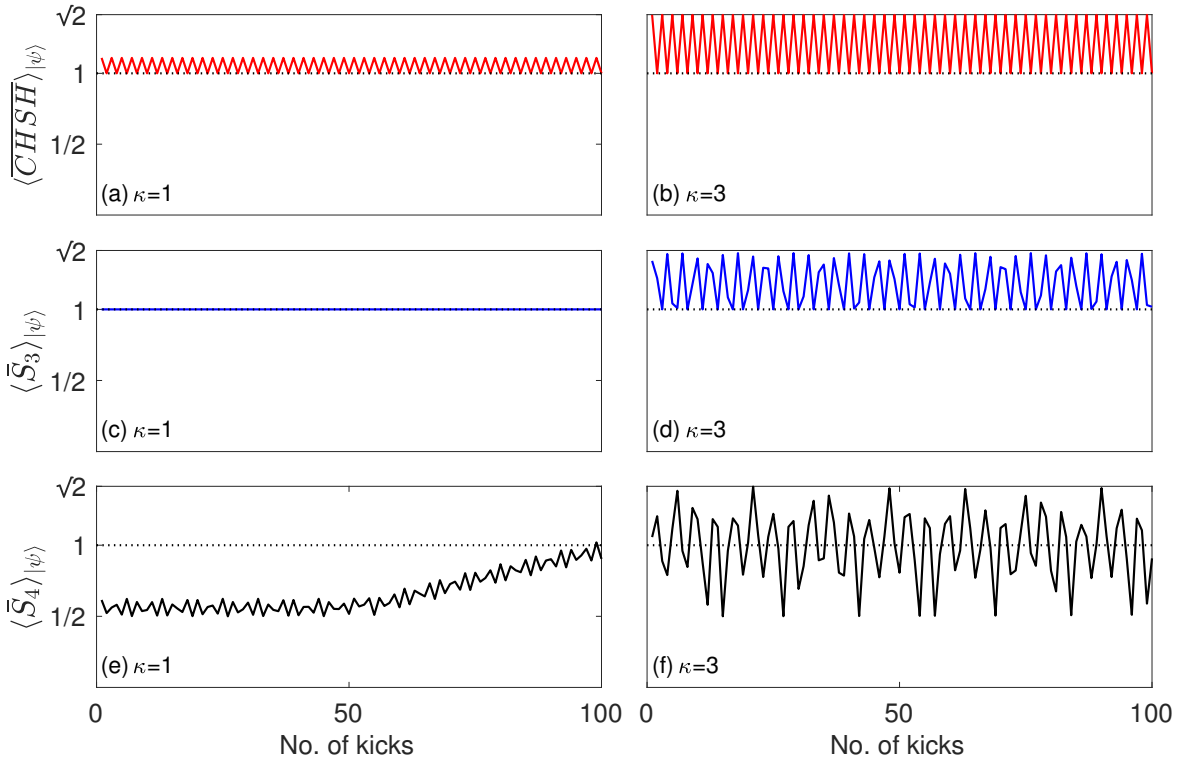

Figure 5.2: Evolution of normalized CHSH correlation function for $j = 1$ QKT, 3−qubit Svetlichny's correlation function for $j = 1.5$ QKT, and 4−qubit Svetlichny correlation functions for $j = 2$ QKT. Each of them plotted for $\kappa = 1$ and 3. Initial state: SCS$|j; \frac{\pi}{2}, \frac{\pi}{2}\rangle$ (SCS corresponding to FP_1). FP_1 is stable for $\kappa = 1$ and unstable for $\kappa = 3$.

correlation functions in Figs. 5.2(a), (c) and (d) can be better understood by analyzing the quantum dynamics of the initial state as done in Sec. 3.2.1. An SCS centered at stable FP_1 exhibits localized evolution for $j = 1$ and $j = 1.5$. Figure 5.2(a) shows that there is a small amount of nonlocal correlation in the $j = 1$ evolving state but no nonlocal correlations in the $j = 1.5$ evolving state. On the other hand, there is dynamical tunnelling between FP_1 and FP_2 for $j = 2$ (as shown in Fig. 3.1 in Sec. 3.2.1, and to be shown in Sec. 5.5). This leads to the evolution of the initial state to a GHZ-like state that exhibits maximal nonlocal correlations. Thus we see a growth of the $4-$qubit Svetlichny correlation function in Fig. 5.2(e) in a small time interval. Evolution for a longer time shows maximal violation for stable FP_1 for $j = 2$ (Fig. 5.4).

We illustrated in Fig. 5.2 that an initial SCS centered on FP_1 can lead to generation of nonlocal states. Furthermore, we show that evolution of any initial SCS, $|j;\theta,\phi\rangle$, typically leads to generation of nonlocal states in the QKT. We illustrate this for $j = 1$ (2-qubit) and $j = \frac{3}{2}$ (3-qubit) in Fig. 5.3 for two different values of the chaoticity parameter, κ. We plot the time-averaged nonlocal correlations as a function of initial conditions ($|j;\theta,\phi\rangle$) for $j = 1$ and $j = 3/2$. The time-averaged nonlocal correlations for the $j = 1$ QKT is measured using the normalized CHSH correlation function (5.5) and averaged over 500 kicks. We observe that all initial states generate nonlocal correlations on average for the $j = 1$ QKT (left column in Fig. 5.3). The time-averaged nonlocal correlations for the $j = 3/2$ QKT is measured using the normalized Svetlichny correlation function (5.9) for 3 qubits. We time-average over 25 kicks and observe that most of the initial states generate nonlocal correlations on average for the $j = 3/2$ QKT (middle column in Fig. 5.3). We also plot the classical stroboscopic phase space of the kicked top in the right column of Fig. 5.3. We observe a correspondence between the classical phase space structures and the time-averaged nonlocal correlation plots, similar to the time-averaged entanglement as shown in the literature [54, 30, 56]. Thus we conclude that the QKT is a generator of nonlocal correlations including genuine multipartite nonlocal correlations for the case of $j \geq 3/2$.

5.3 Symmetric Extension of Quantum States

Numerical results in the previous section suggest that the reduced states of the QKT cannot violate the CHSH and Svetlichny's inequalities. We prove this analytically for the CHSH inequality in the next section. Before doing so, in this section we review the concept of symmetric extension of quantum states which is required for the proof.

Any 2-qudit quantum state ρ_{AB} is said to have a symmetric extension if there exists

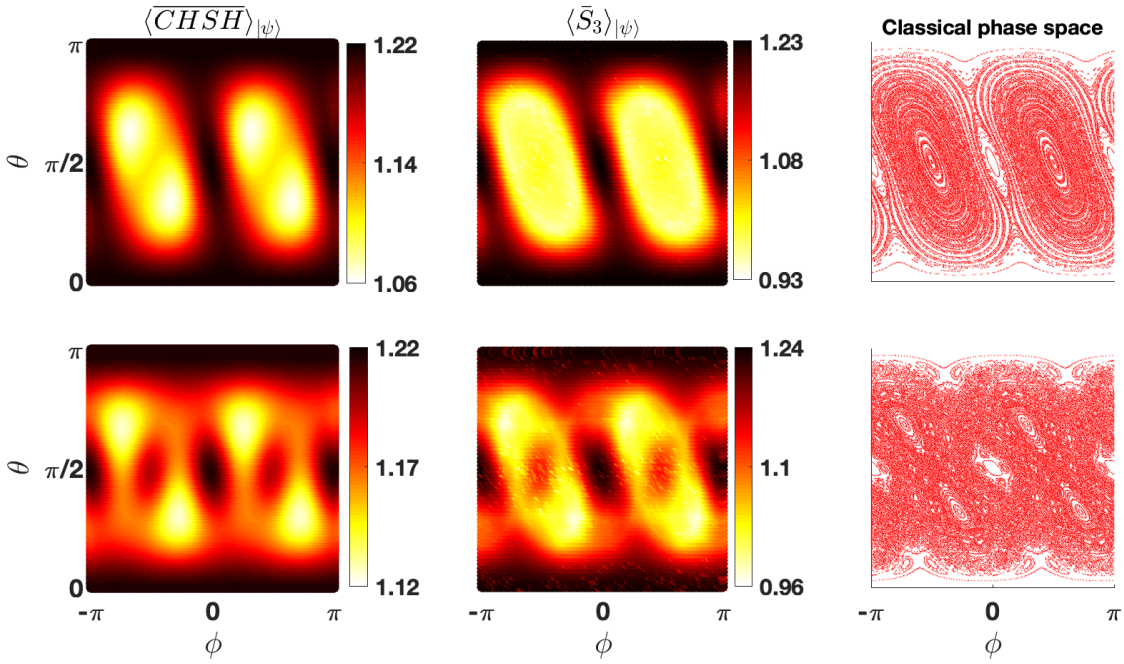

Figure 5.3: Top row: $\kappa = 1.5$, Bottom row: $\kappa = 2.6$. Left Column: Time-averaged nonlocal correlations, measured using normalized CHSH correlation function (5.5), as a function of initial conditions for $j = 1$ QKT. Middle column: Time-averaged nonlocal correlations, measured using the normalized Svetlichny correlation function (5.9), as a function of initial conditions for $j = 3/2$ QKT. Right column: Classical stroboscopic phase space of kicked top. The color value represents the time-averaged $\langle \overline{\text{CHSH}} \rangle_{|\psi\rangle}$ and the time-averaged $\langle \bar{S}_3 \rangle_{|\psi\rangle}$ in left and middle columns respectively.

a 3-qudit state $\rho_{ABB'}$ such that tracing over the qudit B or B$'$ yields the same quantum state [114], that is,

$$\rho_{AB} \equiv \rho_{AB'}. \tag{5.11}$$

Since the quantum states ρ_{AB} and $\rho_{AB'}$ belong to different Hilbert spaces, therefore we have an 'equivalent' sign in (5.11). Any 2-qubit state ρ_{AB} exhibits a symmetric extension if and only if the following condition holds for that quantum state

$$\mathrm{Tr}\,\rho_B^2 \geq \mathrm{Tr}\,\rho_{AB}^2 - 4\sqrt{\det(\rho_{AB})}, \tag{5.12}$$

where $\mathrm{Tr}_A\,\rho_{AB} = \rho_B$ [114].

Furthermore, a 2-qubit symmetric state ρ_{AA} is said to have a symmetric purification if there exists an $N-$qubit pure symmetric state $|\psi\rangle$ such that

$$\mathrm{Tr}_{N-2}(|\psi\rangle) = \rho_{AA}. \tag{5.13}$$

In the QKT, the qubits in the quantum states are indistinguishable (since the quantum states lie in the symmetric subspace of $N = 2j$ qubits). Thus, any 2-qubit reduced state of the QKT for $j \geq 3/2$ naturally has a symmetric purification (which is the pure state $|\psi\rangle$ from which $(N-2)$ qubits have been traced out to obtain the 2-qubit reduced state). Further, the 3-qubit reduced state of $|\psi\rangle$ is a symmetric extension of the 2-qubit reduced state of $|\psi\rangle$.

In the next section, we study the connections between Bell inequalities and symmetric extensions. Using the notion of symmetric extension and the symmetric extendibility criteria (5.12), we prove that any 2-qubit reduced states having a symmetric purification cannot violate the CHSH inequality.

5.4 Nonlocality of 2-qubit Reduced States of Multi-qubit Symmetric Pure States

In this section, we analytically prove that the 2-qubit reduced states of the QKT for $j \geq 3/2$ cannot violate the CHSH inequality (5.4). We prove this in two ways from the formulation of two different theorems.

In the first theorem, we prove that any 2-qubit symmetric state that has an N-qubit symmetric purification for $N \geq 3$ cannot violate the CHSH inequality. It is important to note here that in general, a 2-qubit symmetric state, ρ_{AA}, may not have a symmetric

purification. In this section, we denote by ϱ_{AA} those 2-qubit symmetric states that have a symmetric purification in order to distinguish these states from general 2-qubit symmetric states. Since symmetric purification guarantees the existence of symmetric extension, so ϱ_{AA} will satisfy the symmetric extendibility criterion in (5.12)

$$\mathrm{Tr}\,(\varrho_A^2) \geq \mathrm{Tr}\,(\varrho_{AA}^2) - 4\sqrt{\det(\varrho_{AA})}. \tag{5.14}$$

Since ϱ_{AA} belongs to the $j = 1$ subspace of 2-qubit states, they span only the 3-dimensional subspace of 2-qubit states. Thus, $\mathrm{rank}(\varrho_{AA}) \leq 3$, and hence

$$\det(\varrho_{AA}) = 0.$$

Consequently (5.14) becomes

$$\mathrm{Tr}\,(\varrho_A^2) \geq \mathrm{Tr}\,(\varrho_{AA}^2). \tag{5.15}$$

We briefly recapitulate the properties of ϱ_{AA} [115]. Any 2-qubit symmetric state ρ_{AA} takes the following form

$$\rho_{AA} = \begin{bmatrix} v_+ & x_+^* & x_+^* & u^* \\ x_+ & w & y^* & x_-^* \\ x_+ & y & w & x_-^* \\ u & x_- & x_- & v_- \end{bmatrix} \tag{5.16}$$

in the basis $\{|00\rangle, |01\rangle, |10\rangle, |11\rangle\}$. Now if ρ_{AA} has an N-qubit symmetric purification (for $N \geq 3$), that is, $\rho_{AA} \equiv \varrho_{AA}$, then the matrix components are written as

$$\begin{aligned} v_\pm &= \frac{N^2 - 2N + 4\langle J_z^2\rangle \pm 4\langle J_z\rangle(N-1)}{4N(N-1)}, \\ x_\pm &= \frac{(N-1)\langle J_+\rangle \pm \langle [J_+, J_z]_+\rangle}{2N(N-1)}, \\ w &= \frac{N^2 - 4\langle J_z^2\rangle}{4N(N-1)}, \\ y &= \frac{2\langle J_x^2 + J_y^2\rangle - N}{2N(N-1)} = \frac{N^2 - 4\langle J_z^2\rangle}{4N(N-1)} = w, \\ u &= \frac{\langle J_+^2\rangle}{N(N-1)} \end{aligned} \tag{5.17}$$

where the expectation values are with respect to the N-qubit pure state, which is the symmetric purification of ϱ_{AA}. We now demonstrate that ϱ_{AA} does not violate the CHSH

inequality (5.4).

Theorem 1: Any 2-qubit symmetric state having a symmetric purification does not violate the CHSH inequality, that is, $\mathrm{CHSH}(\varrho_{AA}) \leq 2$, where the matrix elements of ϱ_{AA} are defined in (5.16) and (5.17).

Proof : For the 2-qubit state in (5.16), the T matrix defined in (5.3) is

$$T = \begin{bmatrix} 2(w + \mathrm{Re}(u)) & 2\mathrm{Im}(u) & 2\mathrm{Re}(x_+ - x_-) \\ 2\mathrm{Im}(u) & 2(w - \mathrm{Re}(u)) & 2\mathrm{Im}(x_+ - x_-) \\ 2\mathrm{Re}(x_+ - x_-) & 2\mathrm{Im}(x_+ - x_-) & 1 - 4w \end{bmatrix} \tag{5.18}$$

It is clear that T is a symmetric matrix, and it is straightforward to show that its eigenvalues λ_1, λ_2 and λ_3 are real. Sorting them in order such that

$$\lambda_1^2 \leq \lambda_2^2 \leq \lambda_3^2, \tag{5.19}$$

we find that

$$\mathrm{CHSH}(\varrho_{AA}) = 2\sqrt{\lambda_2^2 + \lambda_3^2} \tag{5.20}$$

using the definition of $\mathrm{CHSH}(\rho)$ in (5.2). Furthermore T in (5.18) has unit trace and so

$$\lambda_1 + \lambda_2 + \lambda_3 = 1. \tag{5.21}$$

Squaring both sides of this equation yields, after some simplification

$$\lambda_1^2 + \lambda_2^2 + \lambda_3^2 = 1 - 2(\lambda_1\lambda_2 + \lambda_2\lambda_3 + \lambda_1\lambda_3). \tag{5.22}$$

From the properties of 3×3 matrices,

$$\begin{aligned} \lambda_1\lambda_2 + \lambda_2\lambda_3 + \lambda_1\lambda_3 &= \text{Sum of all } 2 \times 2 \text{ principal minors} \\ &= \begin{vmatrix} T_{11} & T_{12} \\ T_{21} & T_{22} \end{vmatrix} + \begin{vmatrix} T_{22} & T_{23} \\ T_{32} & T_{33} \end{vmatrix} + \begin{vmatrix} T_{11} & T_{13} \\ T_{31} & T_{33} \end{vmatrix}. \end{aligned} \tag{5.23}$$

Since T is a symmetric matrix for ϱ_{AA}, (5.23) becomes

$$\lambda_1\lambda_2 + \lambda_2\lambda_3 + \lambda_1\lambda_3 = T_{11}T_{22} + T_{22}T_{33} + T_{11}T_{33} - T_{12}^2 - T_{23}^2 - T_{13}^2. \tag{5.24}$$

Substituting matrix elements of T from (5.18) in (5.24), we get

$$\lambda_1\lambda_2 + \lambda_2\lambda_3 + \lambda_1\lambda_3 = 4(w - 3w^2 - |u|^2 - |x_+ - x_-|^2). \tag{5.25}$$

Using (5.15), we have

$$\mathrm{Tr}\,(\varrho_A^2) - \mathrm{Tr}\,(\varrho_{AA}^2) \geq 0. \tag{5.26}$$

Now,

$$\begin{aligned}
\mathrm{Tr}\,(\varrho_{AA}) &= 1 = v_+ + v_- + 2w, \\
\varrho_A &= \begin{bmatrix} v_+ + w & x_+^* + x_-^* \\ x_+ + x_- & v_- + w \end{bmatrix}, \\
\mathrm{Tr}\,(\varrho_{AA}^2) &= v_+^2 + v_-^2 + 2|u|^2 + 4(|x_+|^2 + |x_-|^2 + w^2), \\
\mathrm{Tr}\,(\varrho_A^2) &= (v_+ + w)^2 + (v_- + w)^2 + 2|x_+ + x_-|^2.
\end{aligned} \tag{5.27}$$

Using (5.27) in (5.26), we get

$$w(v_+ + v_-) - |x_+ - x_-|^2 - w^2 - |u|^2 \geq 0. \tag{5.28}$$

Equation (5.28) implies

$$\begin{aligned}
-w^2 - |u|^2 - |x_+ - x_-|^2 &\geq -w(v_+ + v_-) \\
\Rightarrow w - 3w^2 - |u|^2 - |x_+ - x_-|^2 &\geq w - 2w^2 - w(v_+ + v_-) \\
&= w(1 - v_+ - v_-) - 2w^2 \\
&= w \times 2w - 2w^2 = 0 \text{ (using } \mathrm{Tr}(\varrho_{AA}) = 1) \\
\Rightarrow w - 3w^2 - |u|^2 - |x_+ - x_-|^2 &\geq 0.
\end{aligned} \tag{5.29}$$

Using (5.29) in (5.25), we get

$$\lambda_1\lambda_2 + \lambda_2\lambda_3 + \lambda_1\lambda_3 \geq 0. \tag{5.30}$$

Using (5.30) in (5.22), we get

$$\lambda_1^2 + \lambda_2^2 + \lambda_3^2 = 1 - 2(\lambda_1\lambda_2 + \lambda_2\lambda_3 + \lambda_1\lambda_3) \leq 1. \tag{5.31}$$

Using (5.31) in (5.20) proves the result, namely $\mathrm{CHSH}(\varrho_{AA}) \leq 2$. ■

Since the 2-qubit reduced states of the QKT have a symmetric purification for sure, it follows directly from theorem 1 that they cannot violate the CHSH inequality (5.4).

The second theorem that we formulate and prove is a more general theorem that holds for any 2-qubit state. The CHSH correlation functions (5.1) have been proven to be

monogamous [116, 117]. Specifically, this monogamy property says that if ρ_{ABC} is any 3-qubit state such that ρ_{AB}, ρ_{BC} and ρ_{AC} are its three 2-qubit reduced density matrices, then at most only one of these can violate the CHSH inequality. For example,

$$\text{CHSH}(\rho_{AB}) > 2 \Rightarrow \text{CHSH}(\rho_{BC}) \leq 2 \text{ and } \text{CHSH}(\rho_{AC}) \leq 2. \tag{5.32}$$

Using this monogamy relation we prove the following theorem.

Theorem 2 : Any 2-qubit state that violates the CHSH inequality cannot possess a symmetric extension.

Proof : We will prove the theorem by contradiction. Let ρ_{AB} be any two-qubit state for which $\text{CHSH}(\rho_{AB}) > 2$.

Suppose there exists a symmetric extension of ρ_{AB}, which is ρ_{ABC}. Then either of the following holds true:

$$\rho_{BC} \equiv \text{Tr}_A\left(\rho_{ABC}\right) = \rho_{AB} \quad \text{or} \quad \rho_{AC} \equiv \text{Tr}_B\left(\rho_{ABC}\right) = \rho_{AB}, \tag{5.33}$$

and so if ρ_{AB} violates the CHSH inequality, either ρ_{BC} or ρ_{AC} will also violate it, in contradiction with the monogamy relation of (5.32). ■

Theorem 2 can be rephrased to conclude that any 2-qubit quantum state that has a symmetric extension cannot violate the CHSH inequality. Since the 2-qubit reduced states of the QKT have a symmetric extension (as explained in Sec. 5.3), they cannot violate the CHSH inequality.

5.5 Dynamical Tunnelling as a Generator of GHZ-like States

In this section, we explore another dynamical aspect of the QKT, that is, dynamical tunnelling. We show that dynamical tunnelling in the QKT leads to generation of $4-$qubit multipartite nonlocal states that violate the corresponding Svetlichny inequality (5.10). We also show that dynamical tunnelling in the QKT leads to the generation of $N-$qubit GHZ like states for even values of N. In the next section, we will analytically prove that

these $N-$qubit GHZ like states exhibits maximal violation of the corresponding N-qubit Svetlichny inequality.

Dynamical tunnelling is a quantum phenomenon in which quantum states tunnel between disconnected regions in the classical phase space between which classical dynamics is forbidden [100]. A chaotic sea may serve as a dynamical barrier for the classical evolution. Dynamical tunnelling in the QKT was first studied in [71] and was later experimentally observed [29].

Here we illustrate dynamical tunnelling between a few fixed points, and among different points of periodic orbits in the QKT. Our study shows that dynamical tunnelling can generate N-qubit GHZ states for appropriately chosen initial states and parameter values in the QKT Hamiltonian.

5.5.1 Fixed points

Let us consider the fixed points, FP_1 ($(X,Y,Z)=(0,1,0)$) and FP_2 ($(X,Y,Z)=(0,-1,0)$) listed in table 2.1. We had showed there that they are stable for $\kappa \leq 2$. In terms of (θ,ϕ), FP_1 corresponds to $(\frac{\pi}{2},\frac{\pi}{2})$, and FP_2 corresponds to $(\frac{\pi}{2},-\frac{\pi}{2})$.

Dynamical tunnelling between the SCS $|2;\frac{\pi}{2},\frac{\pi}{2}\rangle$ and the SCS $|2;\frac{\pi}{2},-\frac{\pi}{2}\rangle$ has been shown to occur for $\kappa_0 \ll 1$ on the timescale of $T_t \approx \frac{128\pi}{\kappa_0^3}$ via the 4-qubit GHZ-like state [58]

$$|\psi_4^y\rangle = \frac{1}{\sqrt{2}}\left(|+\rangle_y^{\otimes 4} - \mathrm{i}|-\rangle_y^{\otimes 4}\right), \tag{5.34}$$

where $|+\rangle_y$ and $|-\rangle_y$ are eigenstates of the Pauli matrix σ_y corresponding to the eigenvalues +1 and -1 respectively. For $\kappa = 0.1$ the tunnelling time $T_t \approx 402124$ kicks [58]. Here, we show that even for larger κ values, dynamical tunnelling takes place via states very close to the state in (5.34) on a very small timescale. The timescales for tunnelling for $\kappa \gtrsim 1$ are realizable in experiments. Thus, GHZ-like states exhibiting maximal multipartite nonlocality and entanglement can be generated using the QKT.

In Fig. 5.4, we illustrate dynamical tunnelling between FP_1 and FP_2 for four different values of κ. We find that the tunnelling time, T_t, corresponding to $\kappa = 1.25, 1.5, 1.75$ and 2 are 207, 113, 64 and 47 kicks respectively. We observe that the fidelity of the evolved state with the GHZ-like state in (5.34) (the blue curves in Fig. 5.4) is maximized after a number of kicks $\approx \frac{T_t}{2}$.

Given that dynamical tunnelling occurs between FP_1 and FP_2, we study genuine multipartite quantum correlations in the evolving state using the maximum violation of the

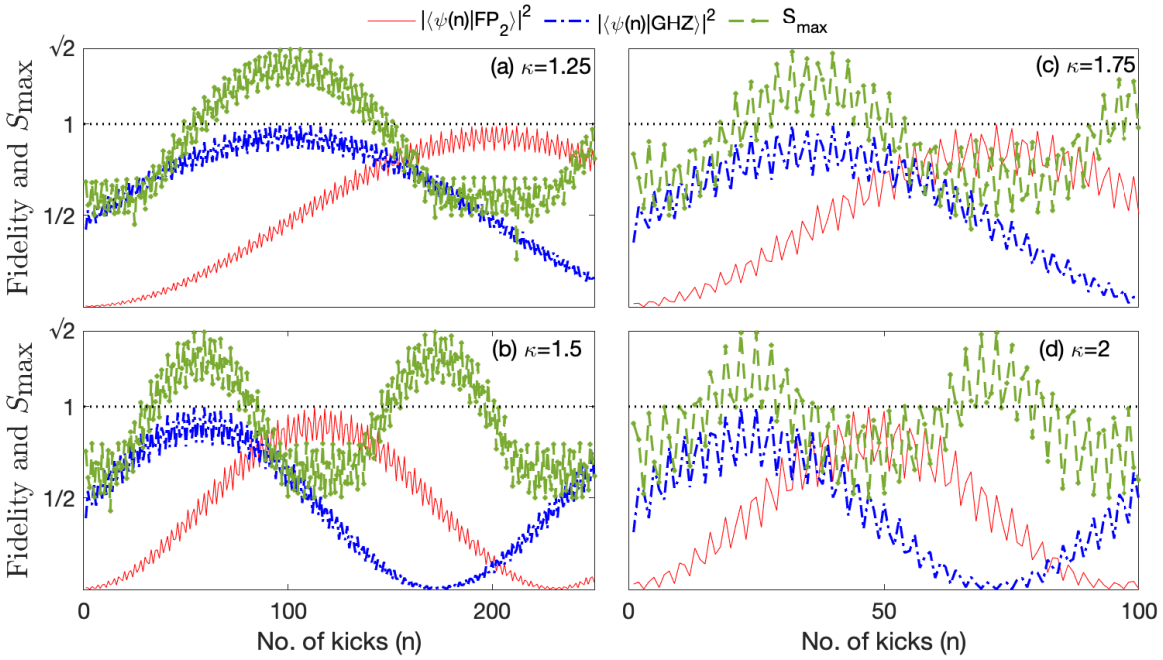

Figure 5.4: Illustration of dynamical tunnelling of the SCS $|2;\pi/2,\pi/2\rangle$ to the SCS $|2;\pi/2,-\pi/2\rangle$ via the GHZ-like state in (5.34) upon evolution with the QKT Hamiltonian for different κ values. The nonlocal correlations in the evolving state quantified using the normalized Svetlichny correlation function (5.9) are also plotted. (a) $\kappa = 1.25$ in top-left, (b) $\kappa = 1.5$ in bottom-left, (c) $\kappa = 1.75$ in top-right, and (d) $\kappa = 2$ in bottom-right.

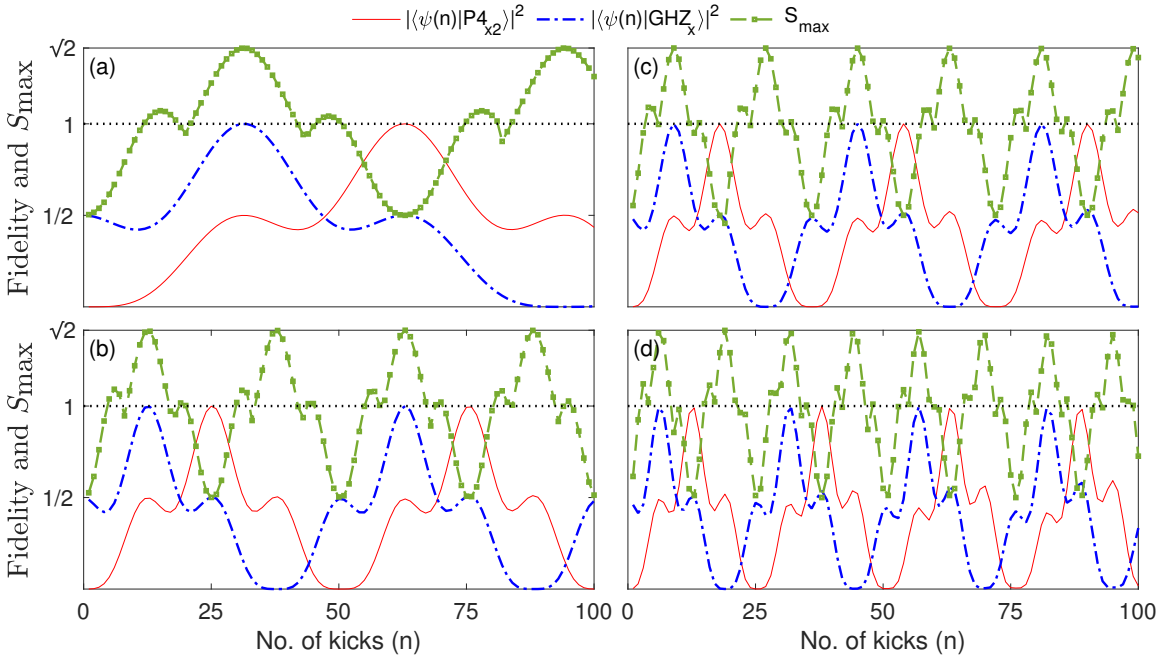

Figure 5.5: Illustration of dynamical tunnelling of the SCS $|2;\pi/2,0\rangle$ to the SCS $|2;\pi/2,\pi\rangle$ via the GHZ-like state in (5.35) upon evolution with the QKT Hamiltonian for different κ values. The number of kicks corresponds to the U^4 map. The nonlocal correlations in the evolving state quantified using the normalized Svetlichny correlation function (5.9) is also plotted. (a) $\kappa = 0.1$ in top-left, (b) $\kappa = 0.25$ in bottom-left, (c) $\kappa = 0.35$ in top-right, and (d) $\kappa = 0.5$ in bottom-right.

normalized Svetlichny correlation function (5.9) (the green curves in Fig. 5.4). We study the maximal violation by the evolved state numerically using optimization in Mathematica. In Fig. 5.4, we observe that the maximal violation during the evolution does correspond to a value very close to maximal nonlocal correlations (which is $\sqrt{2}$).

5.5.2 Period-4 orbit

As illustrated in previous chapters, the classical kicked top exhibits a period-4 orbit in the X-Z plane: $(1,0,0) \to (0,0,-1) \to (-1,0,0) \to (0,0,1) \to (1,0,0)$, where $(\cdot,\cdot,\cdot)$ refers to (X,Y,Z). These four points of the period-4 orbit will be fixed points of the fourth power of the classical kicked top evolution map. Quantum mechanically, we study the evolution

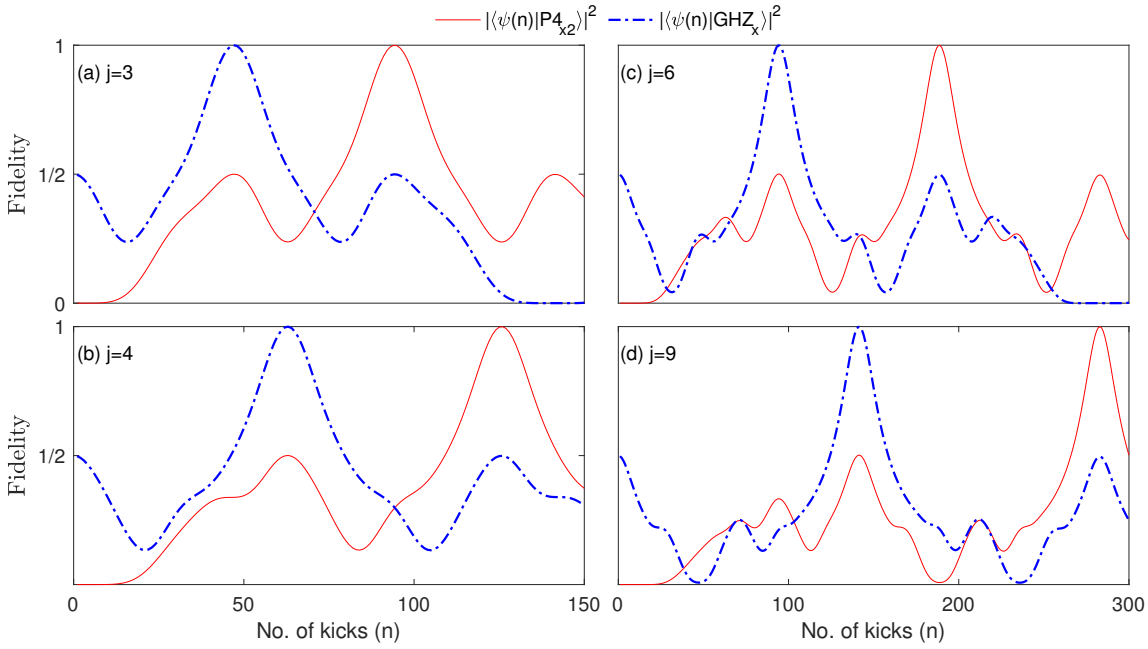

Figure 5.6: Illustration of dynamical tunnelling of the SCS $|j;\pi/2,0\rangle$ to the SCS $|j;\pi/2,\pi\rangle$ via the GHZ-like state in (5.35) upon evolution with the QKT Hamiltonian for different j values. $\kappa = 0.1$. The number of kicks corresponds to U^4 map. (a) $j = 3$ in top-left, (b) $j = 4$ in bottom-left, (c) $j = 6$ in top-right, and (d) $j = 9$ in bottom-right.

of the SCS corresponding to these points with the U^4 map, where U corresponds to the unitary operator in (2.3). We find that for small and positive values of the chaoticity parameter, κ, and positive integer j values, dynamical tunnelling occurs between (a) the SCS $|j;\pi/2,0\rangle$ and the SCS $|j;\pi/2,\pi\rangle$ if the initial state is either of these two SCSs, and (b) the SCS $|j;0,0\rangle$ and the SCS $|j;\pi,\pi\rangle$ if the initial state is either of these two SCSs.

The dynamical tunnelling between $|j;\pi/2,0\rangle$ $(\equiv |+\rangle_x^{\otimes 2j})$ and $|j;\pi/2,\pi\rangle$ $(\equiv |-\rangle_x^{\otimes 2j})$ happens via the $2j$-qubit GHZ-like state:

$$|\psi_{2j}^x\rangle = \frac{1}{\sqrt{2}}\left(|+\rangle_x^{\otimes 2j} - \mathrm{i}|-\rangle_x^{\otimes 2j}\right), \tag{5.35}$$

where $|+\rangle_x$ and $|-\rangle_x$ are eigenstates of the Pauli matrix σ_x corresponding to the eigenvalues +1 and -1 respectively. Likewise the dynamical tunnelling between $|j;0,0\rangle$ and $|j;\pi,\pi\rangle$ happens via the $2j$-qubit GHZ-like state:

$$|\psi_{2j}^z\rangle = \frac{1}{\sqrt{2}}\left(|0\rangle^{\otimes 2j} - \mathrm{i}|1\rangle^{\otimes 2j}\right). \tag{5.36}$$

This dynamical tunnelling is predominant up to j values approximately equal to 20 for $\kappa = 0.1$. Thus, one can generate GHZ-like states of even numbers of qubits (up to a significant number) from product states using the QKT Hamiltonian and its period-4 orbit.

In Fig. 5.5, we illustrate the dynamical tunnelling between $(1,0,0)$ (which we refer to as $P4_{x1}$) and $(-1,0,0)$ (which we refer to as $P4_{x2}$) for $j=2$ and four different values of κ. We see that the tunnelling times $\frac{T_t}{2}$ to the GHZ-like state (5.35) (the blue curves in Fig. 5.5) for $j=2$ are $31, 13, 9$ and 6 kicks for $\kappa = 0.1, 0.25, 0.35$ and 0.5 respectively. The fidelity of the state at $\frac{T_t}{2}$ with the GHZ-like state (5.35) is very close to 1 but not equal to 1. We also observe that the normalized nonlocal correlation value (the green curves in Fig. 5.5) is close to $\sqrt{2}$ but not exactly equal to $\sqrt{2}$ for these states. They are $1.4132, 1.4086, 1.4141$ and 1.3995 respectively for these κ values.

Further, we illustrate dynamical tunnelling between the SCS $|j;\pi/2,0\rangle$ and the SCS $|j;\pi/2,\pi\rangle$ for higher j values in Fig. 5.6. We observe that at half the tunnelling time, $\frac{T_t}{2}$, the fidelity of the evolved state with the GHZ-like state in (5.35) is very close to 1. Dynamical tunnelling seems to be a smoother process for smaller values of κ as compared to larger ones. This can be seen by comparing Fig. 5.4 with Figs. 5.5 and 5.6, and may be due to the fact that the phase space of the QKT is predominantly regular for small values of κ.

In the next section, we analytically prove that the GHZ-like states in (5.35) belong to a class of N-qubit antipodal GHZ states which exhibit maximal nonlocal correlation for

all integer values of $N \geq 2$. Thus, we can generate GHZ-like states for any even number of qubits, which exhibit maximal nonlocal correlations, using the QKT Hamiltonian and specific initial product states.

5.6 Maximal Nonlocal Correlations in N-qubit Antipodal GHZ States

In [110], it was shown that the N-qubit GHZ states,

$$\mathrm{GHZ}|\psi_N\rangle = \frac{1}{\sqrt{2}}\left(|0\rangle^{\otimes N} + |1\rangle^{\otimes N}\right) \tag{5.37}$$

violate Svetlichny's inequality maximally, that is,

$$\max|\langle \bar{S}_N\rangle_{\mathrm{GHZ}|\psi^N\rangle}| = \sqrt{2}. \tag{5.38}$$

In subsection 5.6.1, we prove that nonlocal correlations in the quantum state (5.37) remain invariant with an arbitrary relative phase difference between the two terms in that state. In subsection 5.6.2, we prove that a coherent superposition of $N-$qubit antipodal states, $|\theta,\phi\rangle^N$ and $|\pi-\theta,\pi+\phi\rangle^N$, with equal probabilities also exhibit maximal nonlocal correlations analogous to the N-qubit GHZ states.

5.6.1 Nonlocal correlations in GHZ states with a relative phase difference

Let us consider an N-qubit GHZ state with a relative phase difference, γ, between the two terms.

$$|\psi_N^\gamma\rangle = \frac{1}{\sqrt{2}}\left(|0\rangle^{\otimes N} + \exp(\mathrm{i}\gamma)|1\rangle^{\otimes N}\right). \tag{5.39}$$

Here, we analytically prove that the relative phase difference does not affect nonlocal correlations. We prove this by showing that there exists a set of measurement operators that violate the Svetlichny's inequality maximally for states in (5.39) ($\forall\gamma$ and $N \geq 2$). The proof follows along the same lines as for $\gamma = 0$ [110]. Our aim is to compute $\max|\langle\psi_N^\gamma|S_N|\psi_N^\gamma\rangle|$ where S_N is given in (5.7). For this, let us first compute $\langle\psi_N^\gamma|A_{i_1}^{(1)}.....A_{i_N}^{(N)}|\psi_N^\gamma\rangle$, where $A_l^k = \sin\beta_l^k\cos\alpha_l^k\sigma_x + \sin\beta_l^k\sin\alpha_l^k\sigma_y + \cos\beta_l^k\sigma_z$.

Using (5.7), we get

$$\langle\psi_N^\gamma|S_N|\psi_N^\gamma\rangle = \sum_I \nu_{t(I)}\langle\psi_N^\gamma|A_{i_1}^{(1)}.....A_{i_N}^{(N)}|\psi_N^\gamma\rangle. \tag{5.40}$$

Since

$$\begin{aligned} A_l^k|0\rangle &= \cos\beta_l^k|0\rangle + \sin\beta_l^k \exp(\mathrm{i}\alpha_l^k)|1\rangle \\ A_l^k|1\rangle &= \sin\beta_l^k \exp(-\mathrm{i}\alpha_l^k)|0\rangle - \cos\beta_l^k|1\rangle, \end{aligned}$$

this respectively implies

$$\begin{aligned} A_{i_1}^{(1)}.....A_{i_N}^{(N)}|0\rangle^{\otimes N} &= \overset{N}{\underset{k=1}{\otimes}}\left(\cos\beta_{i_k}^k|0\rangle + \sin\beta_{i_k}^k \exp(\mathrm{i}\alpha_{i_k}^k)|1\rangle\right) \\ &= \prod_{k=1}^N\left(\cos\beta_{i_k}^k\right)|0\rangle^{\otimes N} + \prod_{k=1}^N\left(\sin\beta_{i_k}^k\right)\exp(\mathrm{i}\sum_{l=1}^N\alpha_{i_l}^l)|1\rangle^{\otimes N} \\ &\quad +...(\text{cross terms})... \end{aligned}$$

and

$$\begin{aligned} A_{i_1}^{(1)}.....A_{i_N}^{(N)}|1\rangle^{\otimes N} &= \overset{N}{\underset{k=1}{\otimes}}\left(\sin\beta_{i_k}^k \exp(-\mathrm{i}\alpha_{i_k}^k)|0\rangle - \cos\beta_{i_k}^k|1\rangle\right) \\ &= \prod_{k=1}^N\left(\sin\beta_{i_k}^k\right)\exp(-\mathrm{i}\sum_{l=1}^N\alpha_{i_l}^l)|0\rangle^{\otimes N} - \prod_{k=1}^N\left(\cos\beta_{i_k}^k\right)|1\rangle^{\otimes N} \\ &\quad +...(\text{cross terms})... \end{aligned}$$

Noting that all cross terms are orthogonal to $|\psi_N^\gamma\rangle$ we obtain

$$\begin{aligned} \langle\psi_N^\gamma|A_{i_1}^{(1)}.....A_{i_N}^{(N)}|\psi_N^\gamma\rangle &= \frac{1}{2}\exp(\mathrm{i}\gamma)\exp(-\mathrm{i}\sum_{l=1}^N\alpha_{i_l}^l)\prod_{k=1}^N\left(\sin\beta_{i_k}^k\right) \\ &\quad +\frac{1}{2}\exp(-\mathrm{i}\gamma)\exp(\mathrm{i}\sum_{l=1}^N\alpha_{i_l}^l)\prod_{k=1}^N\left(\sin\beta_{i_k}^k\right) \\ &= \cos\left(-\gamma+\sum_{k=1}^N\alpha_{i_k}^k\right)\prod_{l=1}^N\sin\beta_{i_l}^l. \end{aligned}$$

This straightforward calculation yields

$$\langle\psi_N^\gamma|A_{i_1}^{(1)}....A_{i_N}^{(N)}|\psi_N^\gamma\rangle = \cos\left(-\gamma+\sum_{k=1}^N\alpha_{i_k}^k\right)\prod_{l=1}^N\sin\beta_{i_l}^l \tag{5.41}$$

and so $|\psi_N^\gamma\rangle$ will exhibit maximum violation of the $N-$qubit Svetlichny inequality if there exists a choice of measurement angles, $\alpha_{i_l}^l$ and $\beta_{i_l}^l$, such that the value of $\langle\psi_N^\gamma|A_{i_1}^{(1)}....A_{i_N}^{(N)}|\psi_N^\gamma\rangle$ for all possible $\{i_1, i_2, ..., i_N\}$ is $\nu_{t(I)}/\sqrt{2}$, where $\nu_{t(I)}$ (a sequence consisting of $+1$ and -1) is defined above in Sec. 5.1.2. There are 2^N possibilities of the sequence $\{i_1, i_2, ..., i_N\}$ which will then yield the sum in the Svetlichny correlation function (5.7) as $2^{N-1}\sqrt{2}$ (implying maximal violation of Svetlichny's inequality in (5.8)).

We now illustrate that such a choice of measurement angles exists. Choosing $\beta_{i_l}^l = \frac{\pi}{2}$ for all possible values of i and l, we get

$$\langle\psi_N^\gamma|A_{i_1}^{(1)}....A_{i_N}^{(N)}|\psi_N^\gamma\rangle = \cos\left(-\gamma + \sum_{k=1}^{N}\alpha_{i_k}^k\right). \tag{5.42}$$

For the following choice of the measurement angles, $\alpha_{i_k}^k$:

$$\begin{aligned} \alpha_1^1 = \ & -\tfrac{\pi}{4} + \gamma, \quad \alpha_2^1 = \frac{\pi}{4} + \gamma, \\ \alpha_1^k = \ & 0, \text{ and } \quad \alpha_2^k = \frac{\pi}{2} \qquad \forall k \in \{2, 3, ..., N\}. \end{aligned} \tag{5.43}$$

we obtain

$$\begin{aligned} \langle\psi_N^\gamma|S_N|\psi_N^\gamma\rangle &= \sum_I \nu_{t(I)}\langle\psi_N^\gamma|A_{i_1}^{(1)}.....A_{i_N}^{(N)}|\psi_N^\gamma\rangle \\ &= \sum_I \nu_{t(I)}\cos\left(-\frac{\pi}{4} + t(I)\frac{\pi}{2}\right) \\ &= \sum_I \nu_{t(I)}\left(\frac{\nu_{t(I)}}{\sqrt{2}}\right) \\ &= 2^{N-1}\sqrt{2}. \end{aligned} \tag{5.44}$$

demonstrating that $|\psi_N^\gamma\rangle$ violates Svetlichny's inequality (5.8) maximally. One specific choice of measurement operators that yields maximum violation is:

$$A_{i_k}^k = \cos\alpha_{i_k}^k\sigma_x + \sin\alpha_{i_k}^k\sigma_y,$$

where $\alpha_{i_k}^k$'s are as in (5.43).

5.6.2 Nonlocal correlations in N-qubit antipodal GHZ states

The $N-$qubit GHZ state is a superposition of $|0\rangle^{\otimes N}$ and $|1\rangle^{\otimes N}$. In the Dicke basis, $|0\rangle^{\otimes N} = |N/2, N/2\rangle \equiv \mathrm{SCS}|N/2; 0, 0\rangle$ and $|1\rangle^{\otimes N} = |N/2, -N/2\rangle \equiv \mathrm{SCS}|N/2; \pi, \pi\rangle$. The direction vectors $(0, 0)$ and (π, π) are antipodal to each other. Generalizing the $N-$qubit GHZ state to a superposition of two SCSs localized in arbitrary antipodal directions, we get

$$|\psi_N^{\theta\phi}\rangle = \frac{1}{\sqrt{2}}\left(|\theta, \phi\rangle^{\otimes N} + \exp\left(\mathrm{i}\gamma\right)|\pi - \theta, \pi + \phi\rangle^{\otimes N}\right) \tag{5.45}$$

where $|\theta, \phi\rangle$ is the representation of a qubit (2.24) on the Bloch sphere. We define these states as $N-$qubit antipodal GHZ states. The GHZ-like states generated from dynamical tunnelling in the QKT (mentioned in (5.34) and (5.35)) belong to this class of states for specific values of N and (θ, ϕ). In this subsection, we prove that these states violate Svetlichny's inequality (5.8) maximally, and thus exhibit maximal multipartite nonlocal correlations.

The Bloch representation of the qubit can be written as

$$|\theta, \phi\rangle = \exp\left(\frac{\mathrm{i}\theta}{2}\left(\sigma_x \sin\phi - \sigma_y \cos\phi\right)\right)|0\rangle \equiv V|0\rangle, \tag{5.46}$$

where V is the unitary operator corresponding to one qubit

$$V = \exp\left(\frac{\mathrm{i}\theta}{2}\left(\sigma_x \sin\phi - \sigma_y \cos\phi\right)\right). \tag{5.47}$$

Moreover

$$\begin{aligned} V|1\rangle &= -\exp\left(-\mathrm{i}\phi\right)|\pi - \theta, \pi + \phi\rangle \\ \Rightarrow |\pi - \theta, \pi + \phi\rangle &= \exp\left(\mathrm{i}(\pi + \phi)\right)V|1\rangle \end{aligned} \tag{5.48}$$

and so

$$\begin{aligned} |\psi_N^{\theta\phi}\rangle &= \frac{1}{\sqrt{2}}\left(|\theta, \phi\rangle^{\otimes N} + \exp\left(\mathrm{i}\gamma\right)|\pi - \theta, \pi + \phi\rangle^{\otimes N}\right) \\ &= V^{\otimes N}\frac{1}{\sqrt{2}}\left(|0\rangle^{\otimes N} + \exp\left(\mathrm{i}\left(\gamma + N\left(\pi + \phi\right)\right)\right)|1\rangle^{\otimes N}\right) \\ &= V^{\otimes N}|\psi_N^{\gamma + N(\pi+\phi)}\rangle. \end{aligned} \tag{5.49}$$

Thus, the state $|\psi_N^{\theta\phi}\rangle$ (5.45) can be obtained by applying local unitary transformations, V, on each of the qubit in the $N-$qubit GHZ state with a relative phase difference $(\gamma +$

$N(\pi+\phi)$) in (5.39). Now, we proved in Sec. 5.6.1 that $N-$qubit GHZ states with arbitrary relative phase difference violate Svetlichny's inequality maximally. Thus,

$$\begin{aligned}
2^{N-1}\sqrt{2} &= \max\langle\psi_N^{\gamma+N(\pi+\phi)}|S_N|\psi_N^{\gamma+N(\pi+\phi)}\rangle \\
&= \max\langle\psi_N^{\theta\phi}|V^{\otimes N}S_N\left(V^\dagger\right)^{\otimes N}|\psi_N^{\theta\phi}\rangle \\
&= \max\sum_I \nu_{t(I)}\langle\psi_N^{\theta\phi}|V^{\otimes N}\left(A_{i_1}^{(1)}.....A_{i_N}^{(N)}\right)\left(V^\dagger\right)^{\otimes N}|\psi_N^{\theta\phi}\rangle \\
&= \max\sum_I \nu_{t(I)}\langle\psi_N^{\theta\phi}|\bigotimes_{k=1}^{N} VA_{i_k}^{(k)}V^\dagger|\psi_N^{\theta\phi}\rangle \\
&= \max\sum_I \nu_{t(I)}\langle\psi_N^{\theta\phi}|\bigotimes_{k=1}^{N} A_{i_k}^{\prime(k)}|\psi_N^{\theta\phi}\rangle \\
&= \max\langle\psi_N^{\theta\phi}|S_N|\psi_N^{\theta\phi}\rangle. \qquad (5.50)
\end{aligned}$$

This proves that the $N-$qubit antipodal GHZ states, $|\psi_N^{\theta\phi}\rangle$, violate Svetlichny's inequality maximally for measurement operators $A_{i_k}^{\prime(k)} = VA_{i_k}^{(k)}V^\dagger = \cos\alpha_{i_k}^k V\sigma_x V^\dagger + \sin\alpha_{i_k}^k V\sigma_y V^\dagger$ (where $\alpha_{i_k}^k$'s are as in (5.43)). Thus, we have identified a class of states that exhibit maximal multipartite nonlocal correlations analogous to GHZ states. We have also identified the measurement operators that will lead to a maximal violation of the Svetlichny's inequality by these states.

Through the calculations in (5.50), we have essentially shown that the maximum value of Svetlichny's correlation function for any quantum state remains invariant under local unitary transformation of individual qubits. Furthermore, the GHZ-like state in (5.39) with a relative phase difference can be obtained from the GHZ state in (5.37) by applying a local unitary operator equivalent to a phase gate with phase γ to any of the qubits in the GHZ state. Hence, maximal violation of Svetlichny's inequality by GHZ-like states in (5.39) follows in a straightforward manner using invariance of $\max\langle S_N\rangle$ under local unitary transformations. However, the detailed proof in Sec. 5.6.1 helps us to easily identify the measurement operators for these states that leads to maximal violation of Svetlichny inequality.

5.7 Summary

We have explored the nonlocal quantum correlations in the quantum kicked top model using Bell inequalities. Our numerical analysis showed that while the 2-qubit and 3-qubit reduced

states of the kicked top do not exhibit any nonlocal correlation, the pure states obtained from unitary evolution exhibit multipartite nonlocal correlations. Furthermore, we have analytically proved that any 2-qubit mixed state which has a symmetric purification cannot violate the CHSH inequality. We have also proved that any 2-qubit state that has a symmetric extension cannot violate the CHSH inequality. These theorems provide an analytical understanding of the numerical results related to the 2-qubit reduced states in the QKT.

Next we showed that dynamical tunnelling in the quantum kicked top between classical fixed points and periodic orbits of the kicked top leads to generation of nonlocal correlations and $N-$qubit GHZ-like states for even values of N. We have further showed that these GHZ-like states belong to a larger class of states that we refer to as $N-$qubit antipodal GHZ states. We have analytically proven that these states exhibit maximal nonlocal correlations analogous to the GHZ states itself. We have also identified the set of measurement operators that lead to maximal violation of Svetlichny's inequality for these states.

Our results indicate that classically chaotic dynamics can generate multipartite nonlocal correlations in addition to multipartite entanglement. The QKT provides a deterministic method for the preparation of nonlocal states. This may be helpful in devising schemes to prepare quantum states with nonlocal correlations for tasks in quantum information processing. Our numerical results suggest that a delocalized evolution of the pure state, either due to chaos or quantum effects like dynamical tunnelling, plays a critical role in the generation of nonlocality. Developing an analytical understanding for this, analogous to the methods we developed for understanding entanglement, would be a fruitful area for future work. Our methods in analytical proofs may further be used to find classes of states that exhibit maximal nonlocal correlations. Our work shows that the distinct concepts of nonlocality and symmetric extensions are intrinsically linked and provides motivation for future studies of monogamy of nonlocality.

Chapter 6

Summary and Outlook

This thesis aimed at understanding the relationship between the quantum properties of a system and its underlying regular versus chaotic classical dynamics. Specifically, the goals of this thesis were twofold. The first goal was to understand and resolve the debates in the literature regarding the relationship between classical chaos and quantum entanglement. The second goal was to study the relationship between classical chaos and nonlocal correlations. We summarize here our results that helped us achieve the two goals individually, providing an outlook to our work as well as future directions.

Classical chaos and quantum entanglement

We have provided a new and systematic approach to solve the long-standing debates regarding the relationship between chaos and entanglement in spin systems. By proposing a framework to find an upper bound on entanglement, we have shown that entanglement generation is directly related to the trace distance of a system from classical-like spin coherent states. This helps us to explain why the behaviour of entanglement is different for regular versus chaotic systems in semiclassical and deep quantum regimes. To calculate the relevant trace distance in the proposed framework, one needs to track the quantum evolution of the system and compare it to classical-like spin coherent states. We have shown three different possibilities. If the system is chaotic, then the trace distance between the states typically grows quickly in both quantum and semiclassical regimes leading to the generation of large entanglement. If the system is regular and in the semiclassical regime, then the trace distance can remain small for long times which restricts the growth of entanglement to large values. If the system is regular and in the deep quantum regime, then

the trace distance can also grow quickly implying the possibility of generation of large entanglement.

By focusing on regular dynamics rather than the more widely studied chaotic dynamics, we gained new insight into correspondence in both regular and chaotic regimes. A deeper analysis of the regular systems in a deep quantum regime led us to design a set of criteria for quantifying the well-known Bohr correspondence principle for periodically driven systems. These criteria can be used to calculate the quantum numbers for which the quantum evolution tracks the classical trajectory at stable periodic orbits. It provides a simple quantitative method to figure out the conditions when the quantum and classical-like states remain close, thus limiting the entanglement generated to low values. These criteria are satisfied by regular systems in a semiclassical regime but typically not in a deep quantum regime. This justifies the magnitude of entanglement generated in the corresponding regimes. Thus, our framework for finding an upper bound on entanglement together with these criteria helped us understand and resolve the existing debates in the literature regarding the connections between entanglement and chaos. Moreover, our criteria for the quantification of Bohr correspondence principle helped us identify new quantum signatures of classical bifurcations even in a deep quantum regime. We have illustrated all our aforementioned results in an experimentally realized, textbook model of quantum chaos - the quantum kicked top (QKT).

Our approaches are general and widely applicable, and give deep insights into the mechanism of generation of entanglement in spin systems. By shifting the question of understanding the generation of entanglement to the evolution of trace distance, our work provides insight and intuition about the fundamental question of quantum-classical connection that is of general interest to the community. This may also be useful in experiments where trace distance can be measured rather than entanglement. These methods provide a new approach to analyzing quantum chaos and designing systems that can efficiently generate entanglement. Thus, our work is relevant for applications in quantum information processing and condensed matter physics.

Classical chaos and nonlocality

We have presented the first study to show that a chaotic system can generate bipartite and genuine multipartite nonlocality. Though the relationship between entanglement and chaos has received significant attention in the literature, the relationship between nonlocality and chaos has remained largely unexplored. Since entanglement and nonlocality are inequivalent quantum resources, an explicit study of nonlocality in chaotic systems is

worth exploring to understand the connections between chaos and nonlocality. In order to investigate this connection, we performed a detailed investigation of nonlocal correlations in the QKT model using well-known generalizations of Bell inequalities - the Clauser-Horne-Shimony-Holt (CHSH) inequality for 2-qubit states, and Svetlichny's inequality for N-qubit states. While the reduced states of the QKT did not show any violation, the pure states did exhibit significant violation for $2-$qubit, $3-$qubit and $4-$qubit QKT. This implies generation of genuine multipartite nonlocality in the $3-$qubit and $4-$qubit QKT. A deeper analysis of the numerical results for the reduced states led us to formulate general theorems that showcase fundamental connections between Bell inequalities and symmetric extensions of quantum states.

Our study of the relationship between entanglement and chaos provided us with a guide to choosing the appropriate quantum states for the study of quantum-classical connection in a deep quantum regime. With the appropriate choice of initial states, we observed that localized evolution either led to no violation or small amounts of violation of the Bell inequalities by the pure states of the QKT. On the other hand, delocalized evolution, either due to chaos or quantum phenomena like dynamical tunnelling, led to significant violation of the Bell inequalities. These observations raise important questions about the role of delocalized evolution in the generation of nonlocality. Moreover, we have identified dynamical tunnelling between fixed points and periodic orbits of the kicked top as a generator of maximally nonlocal GHZ-like states for even number of qubits. Thus our investigation of nonlocality in the chaotic model, the QKT, indicates that chaos can generate multipartite nonlocal correlations in addition to multipartite entanglement.

The results we have obtained for nonlocality in a chaotic system have laid the groundwork for future research into the connections between classical chaos and nonlocality. We have presented preliminary evidence that chaotic maps generate significant multipartite nonlocality. A natural progression of our work is to analyze nonlocal correlations in the eigenstates of random matrices since they are excellent statistical tools to study the properties of chaotic maps. Moreover, insights into the important question regarding the role of delocalized evolution in the generation of nonlocality can be gained by first exploring inequalities for Bell correlation functions analogous to the Fannes-type inequality for von Neumann entropy. These inequalities can be further used to develop a framework analogous to the one we have formulated for the case of entanglement in order to find an upper or lower bound on nonlocality. These studies would establish quantum chaos as a generator of nonlocal correlations in addition to quantum entanglement, and thus a potential resource for quantum computing. The work in this thesis thus opens up new avenues for theoretical and experimental studies of quantum chaos that can lead to fundamental insights as well as practical applications in the future.

References

[1] L. Reichl. *The Transition to Chaos: Conservative Classical Systems and Quantum Manifestations*. Institute for Nonlinear Science. Springer, 2004.

[2] Edward Ott. *Chaos in dynamical systems*. Cambridge university press, 2002.

[3] Marie Lucy Cartwright and John Edensor Littlewood. On non-linear differential equations of the second order: I. the equation $\ddot{y} - k(1 - y^2)\dot{y} + y = b\lambda k \cos(\lambda t + a)$, k large. *Journal of the London Mathematical Society*, 1(3):180–189, 1945.

[4] Robert C Hilborn et al. *Chaos and nonlinear dynamics: an introduction for scientists and engineers*. Oxford University Press on Demand, 2000.

[5] Troy Shinbrot, Celso Grebogi, Jack Wisdom, and James A. Yorke. Chaos in a double pendulum. *American Journal of Physics*, 60(6):491–499, 1992.

[6] Yakov Borisovich Pesin. Ljapunov characteristic exponents and ergodic properties of smooth dynamical systems with an invariant measure. In *Doklady Akademii Nauk*, volume 226, pages 774–777. Russian Academy of Sciences, 1976.

[7] Kenneth S Krane. *Modern Physics*. Wiley, 1995.

[8] Leslie E Ballentine. *Quantum mechanics: a modern development*. World Scientific Publishing Company, 1998.

[9] Shohini Ghose, Paul Alsing, Ivan Deutsch, Tanmoy Bhattacharya, and Salman Habib. Transition to classical chaos in a coupled quantum system through continuous measurement. *Phys. Rev. A*, 69:052116, May 2004.

[10] Shohini Ghose, Paul Alsing, Ivan Deutsch, Tanmoy Bhattacharya, Salman Habib, and Kurt Jacobs. Recovering classical dynamics from coupled quantum systems through continuous measurement. *Phys. Rev. A*, 67:052102, May 2003.

[11] Ian Percival. *Quantum state diffusion*. Cambridge University Press, 1998.

[12] Albert Messiah. *Quantum Mechanics*. Wiley, New York, 1961.

[13] Wojciech Hubert Zurek and Juan Pablo Paz. *Why We Don't Need Quantum Planetary Dynamics: Decoherence and the Correspondence Principle for Chaotic Systems*, pages 167–177. Springer Netherlands, Dordrecht, 1999.

[14] Jack Wisdom. Urey prize lecture: Chaotic dynamics in the solar system. *Icarus*, 72(2):241–275, 1987.

[15] Fritz Haake. *Quantum signatures of chaos*, volume 54. Springer Science & Business Media, 2013.

[16] Asher Peres. Stability of quantum motion in chaotic and regular systems. *Physical Review A*, 30(4):1610, 1984.

[17] Joseph Emerson, Yaakov S Weinstein, Seth Lloyd, and DG Cory. Fidelity decay as an efficient indicator of quantum chaos. *Physical review letters*, 89(28):284102, 2002.

[18] Rüdiger Schack, Giacomo M. D'Ariano, and Carlton M. Caves. Hypersensitivity to perturbation in the quantum kicked top. *Phys. Rev. E*, 50:972–987, Aug 1994.

[19] Eric J. Heller. Bound-state eigenfunctions of classically chaotic hamiltonian systems: Scars of periodic orbits. *Phys. Rev. Lett.*, 53:1515–1518, Oct 1984.

[20] Juan Maldacena, Stephen H. Shenker, and Douglas Stanford. A bound on chaos. *Journal of High Energy Physics*, 2016(8):106, Aug 2016.

[21] Akira Shudo and Yasushi Shimizu. Extensive numerical study of spectral statistics for rational and irrational polygonal billiards. *Phys. Rev. E*, 47:54–62, Jan 1993.

[22] Jan Wiersig. Spectral properties of quantized barrier billiards. *Phys. Rev. E*, 65:046217, Apr 2002.

[23] Toma ž Prosen. General relation between quantum ergodicity and fidelity of quantum dynamics. *Phys. Rev. E*, 65:036208, Feb 2002.

[24] M. F. Andersen, A. Kaplan, T. Grünzweig, and N. Davidson. Decay of quantum correlations in atom optics billiards with chaotic and mixed dynamics. *Phys. Rev. Lett.*, 97:104102, Sep 2006.

[25] Brian Swingle and Debanjan Chowdhury. Slow scrambling in disordered quantum systems. *Phys. Rev. B*, 95:060201, Feb 2017.

[26] Efim B. Rozenbaum, Sriram Ganeshan, and Victor Galitski. Lyapunov exponent and out-of-time-ordered correlator's growth rate in a chaotic system. *Phys. Rev. Lett.*, 118:086801, Feb 2017.

[27] Efim B Rozenbaum, Leonid A Bunimovich, and Victor Galitski. Quantum chaos in classically non-chaotic systems. *arXiv preprint arXiv:1902.05466*, 2019.

[28] Ph. Jacquod. Semiclassical time evolution of the reduced density matrix and dynamically assisted generation of entanglement for bipartite quantum systems. *Phys. Rev. Lett.*, 92:150403, Apr 2004.

[29] S Chaudhury, A Smith, BE Anderson, S Ghose, and PS Jessen. Quantum signatures of chaos in a kicked top. *Nature*, 461(7265):768, 2009.

[30] C Neill, P Roushan, M Fang, Y Chen, M Kolodrubetz, Z Chen, A Megrant, R Barends, B Campbell, B Chiaro, et al. Ergodic dynamics and thermalization in an isolated quantum system. *Nature Physics*, 12(11):1037–1041, 2016.

[31] Ryszard Horodecki, Paweł Horodecki, Michał Horodecki, and Karol Horodecki. Quantum entanglement. *Rev. Mod. Phys.*, 81:865–942, Jun 2009.

[32] Nicolas Brunner, Daniel Cavalcanti, Stefano Pironio, Valerio Scarani, and Stephanie Wehner. Bell nonlocality. *Rev. Mod. Phys.*, 86:419–478, Apr 2014.

[33] Michael A Nielsen and Isaac L Chuang. *Quantum computation and quantum information*. Cambridge university press, 2010.

[34] Charles H. Bennett, Herbert J. Bernstein, Sandu Popescu, and Benjamin Schumacher. Concentrating partial entanglement by local operations. *Phys. Rev. A*, 53:2046–2052, Apr 1996.

[35] K. Furuya, M. C. Nemes, and G. Q. Pellegrino. Quantum dynamical manifestation of chaotic behavior in the process of entanglement. *Phys. Rev. Lett.*, 80:5524–5527, Jun 1998.

[36] Wojciech Hubert Zurek and Juan Pablo Paz. Decoherence, chaos, and the second law. *Phys. Rev. Lett.*, 72:2508–2511, Apr 1994.

[37] R. M. Angelo, K. Furuya, M. C. Nemes, and G. Q. Pellegrino. Rapid decoherence in integrable systems: A border effect. *Phys. Rev. E*, 60:5407–5411, Nov 1999.

[38] R. M. Angelo, K. Furuya, M. C. Nemes, and G. Q. Pellegrino. Recoherence in the entanglement dynamics and classical orbits in the n-atom jaynes-cummings model. *Phys. Rev. A*, 64:043801, Sep 2001.

[39] Paul A. Miller and Sarben Sarkar. Signatures of chaos in the entanglement of two coupled quantum kicked tops. *Phys. Rev. E*, 60:1542–1550, Aug 1999.

[40] Jayendra N. Bandyopadhyay and Arul Lakshminarayan. Testing statistical bounds on entanglement using quantum chaos. *Phys. Rev. Lett.*, 89:060402, Jul 2002.

[41] Jayendra N. Bandyopadhyay and Arul Lakshminarayan. Entanglement production in coupled chaotic systems: Case of the kicked tops. *Phys. Rev. E*, 69:016201, Jan 2004.

[42] Rafał Demkowicz-Dobrzański and Marek Kuś. Global entangling properties of the coupled kicked tops. *Phys. Rev. E*, 70:066216, Dec 2004.

[43] Collin M. Trail, Vaibhav Madhok, and Ivan H. Deutsch. Entanglement and the generation of random states in the quantum chaotic dynamics of kicked coupled tops. *Phys. Rev. E*, 78:046211, Oct 2008.

[44] Arul Lakshminarayan. Entangling power of quantized chaotic systems. *Phys. Rev. E*, 64:036207, Aug 2001.

[45] M J Everitt, T D Clark, P B Stiffell, J F Ralph, A R Bulsara, and C J Harland. Persistent entanglement in the classical limit. *New Journal of Physics*, 7:64–64, Feb 2005.

[46] Arul Lakshminarayan and V. Subrahmanyam. Entanglement sharing in one-particle states. *Phys. Rev. A*, 67:052304, May 2003.

[47] Xi-Wen Hou and Bambi Hu. Decoherence, entanglement, and chaos in the dicke model. *Phys. Rev. A*, 69:042110, Apr 2004.

[48] N. N. Chung and L. Y. Chew. Dependence of entanglement dynamics on the global classical dynamical regime. *Phys. Rev. E*, 80:016204, Jul 2009.

[49] Fumihiro Matsui, Hiroaki S. Yamada, and Kensuke S. Ikeda. Relation between irreversibility and entanglement in classically chaotic quantum kicked rotors. *Europhys. Lett.*, 114(6):60010, Jun 2016.

[50] Hiroto Kubotani, Satoshi Adachi, and Mikito Toda. Exact formula of the distribution of schmidt eigenvalues for dynamical formation of entanglement in quantum chaos. *Phys. Rev. Lett.*, 100:240501, Jun 2008.

[51] Lev Vidmar and Marcos Rigol. Entanglement entropy of eigenstates of quantum chaotic hamiltonians. *Phys. Rev. Lett.*, 119:220603, Nov 2017.

[52] Don N. Page. Average entropy of a subsystem. *Phys. Rev. Lett.*, 71:1291–1294, Aug 1993.

[53] M. Lombardi and A. Matzkin. Entanglement and chaos in the kicked top. *Phys. Rev. E*, 83:016207, Jan 2011.

[54] Xiaoguang Wang, Shohini Ghose, Barry C. Sanders, and Bambi Hu. Entanglement as a signature of quantum chaos. *Phys. Rev. E*, 70:016217, Jul 2004.

[55] Shohini Ghose, Rene Stock, Poul Jessen, Roshan Lal, and Andrew Silberfarb. Chaos, entanglement, and decoherence in the quantum kicked top. *Phys. Rev. A*, 78:042318, Oct 2008.

[56] Joshua B. Ruebeck, Jie Lin, and Arjendu K. Pattanayak. Entanglement and its relationship to classical dynamics. *Phys. Rev. E*, 95:062222, Jun 2017.

[57] Udaysinh T. Bhosale and M. S. Santhanam. Periodicity of quantum correlations in the quantum kicked top. *Phys. Rev. E*, 98:052228, Nov 2018.

[58] Shruti Dogra, Vaibhav Madhok, and Arul Lakshminarayan. Quantum chaos, thermalization and tunneling in an exactly solvable few body system. *arXiv preprint arXiv:1808.07741*, 2018.

[59] Angelo Piga, Maciej Lewenstein, and James Q. Quach. Quantum chaos and entanglement in ergodic and nonergodic systems. *Phys. Rev. E*, 99:032213, Mar 2019.

[60] V. R. Krithika, V. S. Anjusha, Udaysinh T. Bhosale, and T. S. Mahesh. Nmr studies of quantum chaos in a two-qubit kicked top. *Phys. Rev. E*, 99:032219, Mar 2019.

[61] Vaibhav Madhok. Comment on "entanglement and chaos in the kicked top". *Phys. Rev. E*, 92:036901, Sep 2015.

[62] M. Lombardi and A. Matzkin. Reply to "comment on 'entanglement and chaos in the kicked top' ". *Phys. Rev. E*, 92:036902, Sep 2015.

[63] Vaibhav Madhok, Shruti Dogra, and Arul Lakshminarayan. Quantum correlations as probes of chaos and ergodicity. *Optics Communications*, 420:189 – 193, 2018.

[64] Radu Ionicioiu, Robert B. Mann, and Daniel R. Terno. Determinism, independence, and objectivity are incompatible. *Phys. Rev. Lett.*, 114:060405, Feb 2015.

[65] Raymond Y Chiao and John C Garrison. Realism or locality: Which should we abandon? *Foundations of Physics*, 29(4):553–560, 1999.

[66] A. Einstein, B. Podolsky, and N. Rosen. Can quantum-mechanical description of physical reality be considered complete? *Phys. Rev.*, 47:777–780, May 1935.

[67] J. S. Bell. On the einstein podolsky rosen paradox. *Physics Physique Fizika*, 1:195–200, Nov 1964.

[68] B. Hensen, H. Bernien, A. E. Dréau, A. Reiserer, N. Kalb, M. S. Blok, J. Ruitenberg, R. F. L. Vermeulen, R. N. Schouten, C. Abellán, W. Amaya, V. Pruneri, M. W. Mitchell, M. Markham, D. J. Twitchen, D. Elkouss, S. Wehner, T. H. Taminiau, and R. Hanson. Loophole-free bell inequality violation using electron spins separated by 1.3 kilometres. *Nature*, 526:682–6, Oct 2015.

[69] Meenu Kumari and Shohini Ghose. Quantum-classical correspondence in the vicinity of periodic orbits. *Phys. Rev. E*, 97:052209, May 2018.

[70] Fritz Haake, M Kuś, and Rainer Scharf. Classical and quantum chaos for a kicked top. *Zeitschrift für Physik B Condensed Matter*, 65(3):381–395, 1987.

[71] B. C. Sanders and G. J. Milburn. The effect of measurement on the quantum features of a chaotic system. *Zeitschrift für Physik B Condensed Matter*, 77(3):497–510, Oct 1989.

[72] Marek Kus, Fritz Haake, and Bruno Eckhardt. Quantum effects of periodic orbits for the kicked top. *Zeitschrift für Physik B Condensed Matter*, 92(2):221–233, Jun 1993.

[73] Hiroshi Fujisaki, Takayuki Miyadera, and Atushi Tanaka. Dynamical aspects of quantum entanglement for weakly coupled kicked tops. *Phys. Rev. E*, 67:066201, Jun 2003.

[74] George Stamatiou and Demetris PK Ghikas. Quantum entanglement dependence on bifurcations and scars in non-autonomous systems. the case of quantum kicked top. *Physics Letters A*, 368(3):206–214, 2007.

[75] Vaibhav Madhok, Vibhu Gupta, Denis-Alexandre Trottier, and Shohini Ghose. Signatures of chaos in the dynamics of quantum discord. *Phys. Rev. E*, 91:032906, Mar 2015.

[76] Ernest Teng Siang Ong and Lock Yue Chew. The effect of spin squeezing on the entanglement entropy of kicked tops. *Entropy*, 18(116), 2016.

[77] Udaysinh T. Bhosale and M. S. Santhanam. Signatures of bifurcation on quantum correlations: Case of the quantum kicked top. *Phys. Rev. E*, 95:012216, Jan 2017.

[78] Eric J Meier, Jackson Ang'ong'a, Fangzhao Alex An, and Bryce Gadway. Exploring quantum signatures of chaos on a floquet synthetic lattice. *arXiv preprint arXiv:1705.06714*, 2017.

[79] Joseph Emerson. Quantum chaos and quantum-classical correspondence. *arXiv preprint quant-ph/0211035*, 2002.

[80] Hernán G Solari, Mario A Natiello, and Gabriel B Mindlin. *Nonlinear dynamics: a two-way trip from physics to math*. CRC Press, 1996.

[81] Gerard J Milburn. Simulating nonlinear spin models in an ion trap. *arXiv preprint quant-ph/9908037*, 1999.

[82] Akshay Seshadri, Vaibhav Madhok, and Arul Lakshminarayan. Tripartite mutual information, entanglement, and scrambling in permutation symmetric systems with an application to quantum chaos. *Phys. Rev. E*, 98:052205, Nov 2018.

[83] Wei-Min Zhang, Da Hsuan Feng, and Robert Gilmore. Coherent states: Theory and some applications. *Rev. Mod. Phys.*, 62:867–927, Oct 1990.

[84] J M Radcliffe. Some properties of coherent spin states. *Journal of Physics A: General Physics*, 4(3):313–323, May 1971.

[85] F. T. Arecchi, Eric Courtens, Robert Gilmore, and Harry Thomas. Atomic coherent states in quantum optics. *Phys. Rev. A*, 6:2211–2237, Dec 1972.

[86] Jian Ma, Xiaoguang Wang, C.P. Sun, and Franco Nori. Quantum spin squeezing. *Physics Reports*, 509(2):89 – 165, 2011.

[87] G. S. Agarwal. Relation between atomic coherent-state representation, state multipoles, and generalized phase-space distributions. *Phys. Rev. A*, 24:2889–2896, Dec 1981.

[88] Hai-Woong Lee. Theory and application of the quantum phase-space distribution functions. *Physics Reports*, 259(3):147 – 211, 1995.

[89] J Rud Nielsen. *The correspondence principle (1918-1923)*, volume 3. Elsevier, 2013.

[90] P. Ehrenfest. Bemerkung über die angenäherte gültigkeit der klassischen mechanik innerhalb der quantenmechanik. *Zeitschrift für Physik*, 45(7):455–457, Jul 1927.

[91] Joshua Wilkie and Paul Brumer. Quantum-classical correspondence via liouville dynamics. i. integrable systems and the chaotic spectral decomposition. *Phys. Rev. A*, 55:27–42, Jan 1997.

[92] Joshua Wilkie and Paul Brumer. Quantum-classical correspondence via liouville dynamics. ii. correspondence for chaotic hamiltonian systems. *Phys. Rev. A*, 55:43–61, Jan 1997.

[93] L. E. Ballentine, Yumin Yang, and J. P. Zibin. Inadequacy of ehrenfest's theorem to characterize the classical regime. *Phys. Rev. A*, 50:2854–2859, Oct 1994.

[94] Bo Gao. Breakdown of bohr's correspondence principle. *Phys. Rev. Lett.*, 83:4225–4228, Nov 1999.

[95] Adam J. Makowski and Katarzyna J. Górska. Bohr's correspondence principle: The cases for which it is exact. *Phys. Rev. A*, 66:062103, Dec 2002.

[96] Gennady P Berman and George M Zaslavsky. Condition of stochasticity in quantum nonlinear systems. *Physica A: Statistical Mechanics and its Applications*, 91(3-4):450–460, 1978.

[97] Wojciech Hubert Zurek and Juan Pablo Paz. Quantum chaos: a decoherent definition. *Physica D: Nonlinear Phenomena*, 83(1):300 – 308, 1995. Quantum Complexity in Mesoscopic Systems.

[98] Herbert Goldstein, Charles Poole, and John Safko. *Classical mechanics*. AAPT, 2002.

[99] Michael J Davis and Eric J Heller. Quantum dynamical tunneling in bound states. *The Journal of Chemical Physics*, 75(1):246–254, 1981.

[100] Srihari Keshavamurthy and Peter Schlagheck. *Dynamical tunneling: theory and experiment*. CRC Press, 2011.

[101] Meenu Kumari and Shohini Ghose. Untangling entanglement and chaos. *Phys. Rev. A*, 99:042311, Apr 2019.

[102] M. Fannes. A continuity property of the entropy density for spin lattice systems. *Communications in Mathematical Physics*, 31(4):291–294, Dec 1973.

[103] Koenraad MR Audenaert. A sharp continuity estimate for the von neumann entropy. *Journal of Physics A: Mathematical and Theoretical*, 40(28):8127, 2007.

[104] H.J. Lipkin, N. Meshkov, and A.J. Glick. Validity of many-body approximation methods for a solvable model: (i). exact solutions and perturbation theory. *Nuclear Physics*, 62(2):188 – 198, 1965.

[105] Sébastien Dusuel and Julien Vidal. Finite-size scaling exponents of the lipkin-meshkov-glick model. *Phys. Rev. Lett.*, 93:237204, Dec 2004.

[106] Meenu Kumari, Shohini Ghose, and Robert B. Mann. Sufficient condition for nonexistence of symmetric extension of qudits using bell inequalities. *Phys. Rev. A*, 96:012128, Jul 2017.

[107] Meenu Kumari, Shohini Ghose, and Robert B. Mann. Quantum kicked top as a generator of nonlocality. *in preparation*.

[108] R. Augusiak, M. Demianowicz, J. Tura, and A. Acín. Entanglement and nonlocality are inequivalent for any number of parties. *Phys. Rev. Lett.*, 115:030404, Jul 2015.

[109] R. Horodecki, P. Horodecki, and M. Horodecki. Violating bell inequality by mixed spin-12 states: necessary and sufficient condition. *Physics Letters A*, 200(5):340 – 344, 1995.

[110] Michael Seevinck and George Svetlichny. Bell-type inequalities for partial separability in n-particle systems and quantum mechanical violations. *Phys. Rev. Lett.*, 89:060401, Jul 2002.

[111] George Svetlichny. Distinguishing three-body from two-body nonseparability by a bell-type inequality. *Phys. Rev. D*, 35:3066–3069, May 1987.

[112] S. Ghose, N. Sinclair, S. Debnath, P. Rungta, and R. Stock. Tripartite entanglement versus tripartite nonlocality in three-qubit greenberger-horne-zeilinger-class states. *Phys. Rev. Lett.*, 102:250404, Jun 2009.

[113] S Ghose, S Debnath, N Sinclair, A Kabra, and R Stock. Multiqubit nonlocality in families of 3- and 4-qubit entangled states. *Journal of Physics A: Mathematical and Theoretical*, 43(44):445301, Oct 2010.

[114] Jianxin Chen, Zhengfeng Ji, David Kribs, Norbert Lütkenhaus, and Bei Zeng. Symmetric extension of two-qubit states. *Phys. Rev. A*, 90:032318, Sep 2014.

[115] X. Wang and K. Mølmer. Pairwise entanglement in symmetric multi-qubit systems. *The European Physical Journal D - Atomic, Molecular, Optical and Plasma Physics*, 18(3):385–391, 2002.

[116] Valerio Scarani and Nicolas Gisin. Quantum communication between N partners and bell's inequalities. *Phys. Rev. Lett.*, 87:117901, Aug 2001.

[117] Ben Toner. Monogamy of nonlocal quantum correlations. *Proceedings of the Royal Society of London A: Mathematical, Physical and Engineering Sciences*, 465(2101):59–69, 2009.